MULTIDISCIPLINARY CENTER FOR EARTHQUAKE ENGINEERING RESEARCH
A National Center of Excellence in Advanced Technology Applications

Assessment of Advanced Technologies for Loss Estimation

by

David M. Tralli[1]

Publication Date: December 21, 2000
Submittal Date: March 31, 2000

MCEER-00-SP02

Task Number 01-3033

NSF Master Contract Number EEC 9701471

1 Consultant, 290 Oakhurst Lane, Suite B, Arcadia, California 91007

MULTIDISCIPLINARY CENTER FOR EARTHQUAKE ENGINEERING RESEARCH
University at Buffalo, State University of New York
Red Jacket Quadrangle, Buffalo, NY 14261

Abstract

This document provides an assessment of the current state of advanced airborne and spaceborne remote sensing and ground-based technologies applicable to the analysis of seismic risk and vulnerability of buildings and lifeline systems. Continuous Global Positioning System (GPS) ground deformation monitoring and seismological networks provide critical measurements for understanding the earthquake process. Real-time seismological systems used for early warning and rapid response rely on the ability to perform real-time waveform inversions to provide earthquake parameters during the actual rupture process. Integration of GPS network data with seismic data helps distinguish the effects of wave propagation from those of earthquake rupture. However, the growth of remote sensing systems has created arguably the most significant opportunity for improving loss estimation methodologies. Maps and information products derived from remotely sensed imagery increasingly support seismic information. Imaging man-made structures and lifelines with remote sensing is an emergent capability. Developing an inventory of structures and lifelines is a critical element in loss estimation methodologies. No one is currently developing quantitative databases of the built environment by extracting information from remote sensing imagery. There is a need for a multidisciplinary approach to the theoretical and practical integration of remote sensing with dense seismographic and GPS networks.

Acknowledgment

The author would like to thank members of the MCEER Project Team of which this task is one element. This report would not have been possible without the leadership shown by Ron Eguchi of ImageCat, Inc., the many discussions with Bijan Houshmand of the University of California, Los Angeles, the research perspectives provided by Masanobu Shinozuka of the University of Southern California, and the support and opportunities for professional interactions provided by MCEER.

Executive Summary

This document provides an assessment of the current state of advanced remote sensing and ground-based technologies that are applicable to the analysis of seismic risk and its impact on the vulnerability of buildings and lifeline systems in loss estimation methodologies. Advanced technologies as categorized herein refer to sensors, instruments and their platforms (i.e. aircraft, unmanned aerial vehicles and satellites), data, data storage and delivery systems, image processing, visualization, display capabilities and telecommunications.

Benefits that could be derived from the application and adoption of new technological capabilities suggest the development of:

- Innovative procedures for assessing the seismic hazard potential of large urban regions;
- Alternative approaches for developing regional damage or vulnerability models for buildings and lifelines;
- Cost-effective procedures for creating building and lifeline inventories;
- Rapid loss estimation and model calibration methodologies for post-earthquake damage assessment.

Ground-based technologies such as continuous Global Positioning System (GPS) ground deformation monitoring networks and seismological systems for real-time response provide critical measurements for understanding the earthquake process and its impact on the built environment. The operational objectives of continuous GPS arrays include:

- Providing regional coverage for estimating earthquake potential;
- Identifying active blind faults and testing models of tectonics;
- Measuring local variations in strain rate that might reveal the mechanical properties of earthquake faults;
- Measuring permanent crustal deformation not detectable seismically, as well as measuring the response of major faults to the regional change in strain.

It is now possible to identify transient inter-seismic deformations. The continued densification of GPS networks allows measurement of fault slip rate patterns, in order to infer aseismic slip distribution at depth, determine the source time history of slow earthquakes, and compare the pattern of aseismic slip before and after large earthquakes. The amount of three-dimensional positions that are generated by dense networks points to a practical need to develop automated data inversion methods. Continued development of GPS monitoring networks is expected to lead to:

- Better definition of off-fault surface deformation;
- Timely detection of diagnostic changes in the fault environment;

- Constraints on the extent of surficial fault creep and its significance to potentially significant earthquakes;
- Accurate estimates of the distribution of potentially damaging ground motions from such earthquakes to enable ground motion modeling, structural design planning and risk assessment.

However, the ability of geodetic data to resolve variations in slip pattern diminishes greatly with slip depth. **The relationship of surface strain to earthquake occurrence must be understood if GPS networks are going to contribute significantly to loss estimation methodologies.**

Real-time seismological monitoring systems can be used to calculate the likelihood of probabilistically related events. Seismological networks that are used for early warning and rapid response rely on the ability to perform real-time waveform inversions in order to provide earthquake parameters during the actual rupture process. These networks also contribute to the reduction of recovery times after a major earthquake, and help to allow a more rapid determination of the resources that will be needed for post-disaster rebuilding and recovery.

The emergence of remote sensing systems, from optical to microwave bands, has created arguably the most significant opportunity for improving loss estimation methodologies. When fully operational for natural hazards risk management and disaster response applications sometime over the next decade, these systems and attendant data visualization technologies will provide enhanced measurement accuracy, near-real-time capability, greater geographic coverage while holding the promise of reduced operational cost.

Digital maps and information products derived from remotely sensed imagery and integrated into a geographic information system (GIS) will increasingly support seismic information. Such map products can provide regularly updated information on regional geomorphology, urban topography, structures, roadway networks, land uses and land covers. However, preferred directions of ground motion can occur in areas with no surface topographic effects. Significant variations in site response can exist over short distances, up to a factor of two over 200 meters, that are not explained by differences in surficial geology but rather by the influence of geologic structures such as folds and buried basins up to a few kilometers in depth. *Remote sensing is only a complementary layer in a multidisciplinary approach to understanding risk and its impact on the vulnerability of the built environment.*

The capability to image man-made structures and lifelines with remote sensing is beginning to be addressed. This information layer can be superimposed on the various layers that characterize the terrain. In so doing, in GIS architecture, surficial effects could be integrated into the vulnerability models of structures and lifelines and for developing map-based loss estimates with granularities, or geospatial grid resolutions (i.e. counties, zip codes, census tracts, blocks) required by disaster management and insurance and financial applications.

The integration of GPS network data with seismic data helps distinguish the effects of wave propagation from those of earthquake rupture. Geodetic and seismic data are necessary in order to understand the source-rupture process and thus infer the resultant patterns of damage.

The correlation of seismicity with regional tectonics is an important element of the overall seismic hazard assessment. Three advantages of joint inversion include the following:

- Since GPS and waveform stations do not cover a geographic area uniformly in the near-source region, a combined data set enhances the spatial sampling.
- Frequencies sampled are from the range of DC to about 1.0 Hz. Slip models thus can be compared that sample only the coseismic slip (waveform data) with those that include slip from aftershocks and any aseismic contributions.
- The slip pattern determined from geodetic data is independent of rupture timing. Imposing a model requirement that the final slip in the waveform inversion fit the static data provides an independent constraint on *a priori* timing assumptions made in the waveform inversion. Band-limited inversions otherwise experience a trade-off between rupture timing and slip location.

Prediction of strong motion velocities from geodetic data alone offers limited spectral response, and thus is a poor replacement for actual strong motion recordings that are critical to earthquake engineering. Strong motion data typically necessitate more heterogeneous slip distribution in order to yield the variation observed in velocity amplitude, frequency content and waveform complexity. On the other hand, a smooth slip pattern is often sufficient to model geodetic data.

There is a clear need for a multidisciplinary approach to the theoretical and practical integration of remote sensing data products with measurements provided by dense seismographic and GPS networks. The geospatial information that can be extracted from remotely sensed imagery is relevant not only to assessing the potential of risk, but towards better defining the overall state of vulnerability (i.e. including the characterization of the ground surface), and thus the exposure to loss, within a given geographic region. Capabilities exist for broad land use characterization. Based on relative building heights and their spatial distribution, regional land use classifications can be segmented into distinct regional structure classes. Land use is a key link between image interpretation and physically characterizing risk. For example, development of automated interferometric synthetic aperture radar (InSAR) and multispectral processors for urban land use classification would help to:

- Improve the information content of databases for inferring aggregate valuation of building inventories;
- Assess the exposure of the built environment to natural hazards.

Technical objectives that would have to be addressed include:

- Advancing electromagnetic scattering model capabilities to improve building height measurements;
- Developing building height information extraction algorithms from InSAR data;
- Using multispectral data to improve radar-based characterization of the urban environment;
- Developing building material classification layers from remotely sensed multispectral data.

Existing satellite-based InSAR systems lack the spatial and height resolution for urban applications, although their capabilities for ground deformation monitoring have been demonstrated. Sources of airborne InSAR data are marginally adequate for assessing their capabilities for urban applications. InSAR has demonstrated significant potential to map crustal strain. However, the small movements involved (e.g. 1-2 mm/year) are often outside the system's spatial or displacement resolution. Recent research in remote sensing of urban areas points out the need for multi-band data registration and fusion using various sensors and ancillary data sources, such as census data and thematic maps. Spatial resolution of less than 5 meters is required for the extraction of urban geometrical patterns. Aircraft imagery of damage at Kobe, acquired at 1-m resolution and degraded step-wise to 10 m indicates that 2-m or better resolution is generally needed to reliably detect major damage with single acquisitions. The increasing utilization of high-resolution lidar systems offers another exciting avenue for urban applications.

Developing an inventory of structures and lifelines is a critical element in loss estimation methodologies, and one that high-resolution three-dimensional remote sensing imaging is able to address. No one is currently developing quantitative databases of the built environment by extracting information from remote sensing imagery. The robustness of generating an inventory remotely must be assessed through continued research and validation studies that rely on ground truth data to assess the accuracy and efficacy of a remote sensing methodology. Trade-off in cost and uncertainty must be considered. Furthermore, the error budget in loss estimation must be understood in order to evaluate the marginal benefits that would be attributable to the adoption of geospatial technologies.

Research efforts are increasing in the joint analysis of GPS and InSAR measurements. InSAR and GPS integration was first attempted fairly recently, wherein InSAR, GPS and results of dislocation modeling of the 1992 Landers earthquake were superimposed. GPS measurements and InSAR images can be combined to help constrain significant postseismic rebound in both horizontal and vertical directions. Both data types can be used to study whether rebound is due to continuous time-dependent afterslip at depth or due to viscoelastic flow below seismogenic depths. Not knowing the extent of creep and locked portions of a fault yields uncertainty about the potential for future earthquakes, their magnitudes and probabilities. Significant challenges need to be overcome before reliable deformation measurements can be made on a routine or operational basis with InSAR.

The application of remote sensing technology to real-time damage assessment will require a comprehensive research program. Several issues must be addressed; the most important of which is how to model remote sensing data to quantitatively separate the effects of surface displacement from building or infrastructure damage. The 1995 Hyogoken-Nanbu earthquake provides a good first published study. Detection of damaged built-up areas using SAR intensity images was reported. Spectral characteristics of the area damaged by the earthquake were investigated using Landsat and SPOT satellite optical images taken before and after the earthquake. Multispectral characteristics were different between images of the liquefied areas and burned areas taken by airborne remote sensing just after the earthquake occurred. The difference before and after the earthquake is considered to reflect the changes to the land cover. The correlation image and the difference image were compared with the damage to buildings evaluated from

field survey data in a GIS. The results show that the difference of the back-scattering coefficients becomes high and negative and the correlation coefficient becomes low in the area of a high severe damage. On the other hand, in the area of a low severe damage ratio, the difference of the back-scattering coefficients becomes high and positive and the correlation coefficient becomes high. However, uncertainties are still quite large in this published study. *An augmented approach may be to rely on remote sensing as the primary data source, but to add independent data such as GPS observations and ground motions from real-time earthquake monitoring networks in order to separate decorrelation due to damage to the built environment from that due to ground displacements***.** While this is theoretically sound, the reduction to practice is subject to data availability and sampling limitations.

Remote sensing will become an increasingly utilized contributor to catastrophic risk modeling and emergency management. Decisions made in the minutes and hours following a major event are based on limited field reconnaissance. Necessary parameters include:

- Accurate and reliable data on earthquake magnitude and location;
- Distribution maps for peak accelerations and shaking intensity;
- Loss estimates inferred from damage and population distributions;
- Remote sensing images and data of disaster stricken areas for transmission to relevant organizations on a global basis.

The improving capabilities of catastrophe modeling to provide estimates of potential losses, quantify these losses by geographic regions, and provide scenarios for managing risk from natural disasters have placed modeling in a critical role in the issuance of catastrophe bonds and the development of other risk transfer mechanisms. Originally used for gauging an insurance company's probable maximum loss from natural hazards, catastrophe modeling is now a critical tool for the development of pricing, underwriting, and risk-transfer strategies leading to overall portfolio optimization and integrated risk management. As the insurance and capital markets continue to merge, catastrophe modeling will play an increasingly important role in these new alternatives to traditional reinsurance.

Databases of variable resolution maps would be created for post-disaster use, to identify areas of highest multi-hazard risk. Broadband seismic network data and the increasing utilization of permanent GPS geodetic networks would be integral elements of such a system. Recommendations for such use of earth observation technology, from a study that is described in http://www.ceos.noaa.gov include:

- Expand existing global database of seismic risk zones, and coincide with population distribution, seismic history, relevant geology, known strain (i.e. as from GPS networks), estimated InSAR coherence level and optical very-high resolution base maps.
- Begin to develop an archived database of multi-year InSAR-derived strain over seismic regions.
- Support research efforts into "point sample" InSAR (i.e. differencing signal phase against point targets).

High-resolution data, such as SPOT panchromatic and very-high resolution optical data (i.e. IKONOS-2 panchromatic and multispectral) data could play a significant role in base-mapping regions in the developing world that are in zones of high seismic risk. Non-near-real-time damage mapping using image differencing is operational. However, near-real-time damage mapping is still in a developmental stage.

Contents

Illustrations

Illustrations, Continued

Tables

1. Introduction

There is a growing global need for developing, validating, demonstrating and implementing advanced technologies that will enable the routine assessment of the vulnerability of the built environment to natural hazards. This need is driven by the continually increasing exposure, on human and economic terms, of the built environment to natural and man-made (e.g. technological) risk. Consider that about 74% of the world's population in developed and developing countries live in urbanized regions that are tectonically active, near the coast or within river flood plains. In the United States, for example, the population in areas exposed to hurricanes and earthquakes rose 24.5% from 1970 to 1990, while the populations of other areas of the country rose only 20.7%. Based on demographic projections provided by NPA Data Services, Inc., the population of areas exposed to natural catastrophes will rise another 36.6% from 1990 to 2025 [1].

Natural hazards risk management decisions, in the engineering and financial communities, have enormous economic impact. This impact is measured in both casualties and property losses, and even indirect economic measures such as losses due to business interruption. Risk management decisions rely increasingly on improved models and an understanding of the underlying geophysical processes that lead to the occurrence of catastrophic events. The need for advanced risk assessment and mitigation planning tools on a worldwide basis represents an enormous challenge and opportunity for the application of advanced technologies.

Fig. 1. Aerial photo of building damage in the city of Gölcük due to the Izmit Earthquake, Turkey, August 18, 1999. [Courtesy: Website, Department of Earth and Atmospheric Sciences, St. Louis University].

1.1 Advanced Technologies

In this document, advanced technologies refer to sensors, instruments and their platforms (i.e. aircraft, unmanned aerial vehicles (UAVs) and satellites), data storage and delivery systems, image processing, visualization, display capabilities and telecommunications. These technologies, once integrated and fully operational through government agencies or commercial enterprises, will provide enhanced measurement accuracy, near-real-time capability, greater geographic coverage and hold the promise of reduced operational cost. Furthermore, advanced technologies will enable significant enhancements in earthquake science and engineering.

The emergence of remote sensing technologies, such as airborne and spaceborne (e.g. satellite-based) optical, near and thermal infrared, laser and radar sensor systems, has created significant opportunities for improving loss estimation methodologies from research through development and into operational capacity. These methodologies, with the input of such remote sensing and other geospatial information, have a growing role in both pre-event (i.e. mitigation planning) and near-real-time post-event (i.e. response planning) scenarios, in addition to long-term monitoring of risk and reconstruction. (For a review of the implications of natural disaster risk in pre-disaster preparation, response planning and recovery for developing countries, and the potential role for remote sensing, see [2]).

Advances in seismological instrumentation, and continuous or permanent Global Positioning System (GPS) ground deformation monitoring networks (i.e. wherein geodetic monuments are continuously instrumented rather than operated at discrete measurement epochs) are providing large amounts of spectrally rich data. An increasingly capable data processing and global telecommunications infrastructure is enabling the dissemination of these and other geospatial data to users and adopters, analysts and decision-makers worldwide. These and other attendant technologies, initially developed and validated primarily under government-sponsored programs in federal laboratories and universities, are transitioning to varying degrees into commercial and operational agency capacity for routine and broadened utilization.

This report is a step towards increasing the awareness of advanced technologies in the risk management communities, particularly those served by the **Multidisciplinary Center for Earthquake Engineering Research (MCEER),** http://mceer.buffalo.edu, and its government-funded sponsor, the **National Science Foundation (NSF).** The NSF is recognized as a significant sponsor of the diverse research and applications represented in this document, and as a leader in identifying new research needs and directions [3].

Dissemination of the types of geospatial data and information products yielded by application of advanced technologies will be supported by the emerging development of a global information network that relies heavily on rapid advances in telecommunications technologies. Specific areas that will benefit from these new capabilities include:

- Alternative procedures for assessing the seismic hazard potential of large urban regions;

- Alternative approaches for developing regional damage or vulnerability models for buildings and lifelines;
- Cost-effective procedures for creating building and lifeline inventories;
- Rapid calibration procedures for post-earthquake damage assessment.

Each of these application areas is addressed in this document and the attendant research project [4].

Fig. 2. Image of Taipei, Taiwan collected January 3, 2000 by Space Imaging Corp. IKONOS satellite. Buildings, roadways and bridges are discernible with the systems 1-m panchromatic resolution.

It is anticipated that real-time or near-real-time information from anywhere in the world will be used by the engineering, insurance and financial communities, and emergency management professionals, to model and assess risk and to mitigate losses using traditional and innovative methodologies and software tools. Information and supporting image data will be of increasingly broader bandwidth, transmitted to portable ground stations in the field and to centralized processing and information dissemination facilities.

The critical factor for achieving widespread utilization will be the growth of user-driven information products derived from the image data. The sensors, platforms, acquisition,

storage and image processing requirements must become "transparent" to the end-user of the information products, while these products must provide solutions to end-user problems in an effective and readily adaptable manner.

1.2 Technology Assessment

This document provides an assessment of the current state of advanced remote sensing and ground-based technologies that are applicable to the quantification of risk and to the analysis of the corresponding vulnerability of buildings and lifeline systems to seismic hazard. The assessment is segmented by applications for estimating or quantifying actual (i.e. post-event) losses and for estimating or predicting potential (i.e. pre-event) losses due to natural hazards. The focus is earthquake peril, although the extension to other significant natural hazards such as severe wind, hurricane and flood, for example, is straightforward in certain cases.

The challenge for the hazards risk management and disaster response communities is to demonstrate how the adoption and integration of these technologies can be of value and provide marginal and measurable benefit (i.e. in a cost/benefit sense with corresponding case studies) to the use of ground-based elements alone. The specific applications considered are risk assessment, vulnerability analyses, loss estimation, mitigation and response planning, and the monitoring of reconstruction efforts.

The validation, verification, demonstration and subsequent adoption of advanced technologies in new applications pose unique challenges to instrument and data suppliers, value-added companies, users and decision-makers in both the private and public sectors. While some of these technologies may or may not have yet gone through a validation stage in their development, many have not been demonstrated necessarily in a risk assessment and loss estimation environment (i.e. in operational settings that are constrained by spatial and temporal requirements). Innovative applications require the collaboration of public and private entities to encourage further technology development, and to stimulate applied research focused on particular themes and broad user needs.

Recognizing and quantifying the maturity level of a technology is a necessary step in any assessment process or methodology. Such formalism is directly related to managing the risk associated with the adoption of an innovative technology. Throughout this document, earth observation capability will be categorized as follows:

- *Operational*: Science is proven and technology, systems and processes exist to provide a continuing operational service (but not necessarily everywhere).
- *Developmental*: Methodology and technology have been validated and are in the process of being implemented operationally.
- *Research*: Results are still uncertain or only form the basis for ongoing research and understanding, and thus are not at a stage where their utilization by practitioners can be expected.

Marketing innovative technologies requires deliberately addressing the transition from developmental capabilities to operational utilization. Education of the supplier and user

communities therefore is a critical first step towards the acceptance and adoption of products and services that are enabled by new technologies, thus building capacity and higher technology utilization rates.

The demonstration of advanced technologies in novel applications is necessary in evaluating their potential for routine use (i.e. in an operational environment). The relative, and marginal, benefits of advanced technology applications in loss estimation are based on diverse technical, operational and scientific performance criteria, such as:

- Cost reduction;
- Geographic coverage;
- Routine availability;
- Accuracy of extracted parameters;
- Ease of integration with complementary and ancillary data;
- Ease of input into existing GIS-based loss estimation methodologies.

Trade-offs can be established between various technologies as to their effectiveness and practicality for a given application [5], such as on elements of performance and operational cost.

Existing commercial loss estimation methodologies and software tools are reviewed as testbeds for the import, integration and application of the above technologies for real-time damage assessment, and for advancing the state of loss estimation in general. Evaluation criteria are suggested that help identify the strengths and weaknesses of each technology from the standpoint of hazard analysis, inventory development, model development and loss calibration, in addition to the practical issues of implementation and operational utilization.

1.3 Data Sources and Document Organization

A comprehensive review of the recent scientific and engineering research literature was performed. Trade literature in the commercial remote sensing industry was used to identify current and future systems and market applications. In addition to this secondary research, the assessment draws primarily upon the author's experience in the area of advanced technologies, applied research, industrial economic assessments, and technology marketing or transfer that concerns the development and adoption of innovative technologies to address user needs.

In Section 2, ground-based technologies – integrated Global Positioning System (GPS) and broadband seismic networks – that are commanding a growing place in loss estimation tools and civil engineering applications are reviewed and evaluated. A technical overview of GPS also is provided.

Diverse remote sensing sensor systems are reviewed in Section 3, ranging from optical through infrared, radar and laser systems. Much of the information in this Section comes from ongoing research and development efforts in the academic and public sectors of the remote sensing community.

Section 4 addresses the use of remote sensing in the urban environment. This, a focus for loss estimation, includes the most recent results from the remote sensing community and discusses some of the technical challenges for extracting loss parameters.

Integration of remote sensing and GPS data is discussed in Section 5. GPS networks afford remote sensing a means of calibration and differentiating image correlation differences over time due to ground displacements and changes in the urban environment.

Section 6 describes the application of remote sensing to loss estimation methodology. Of particular interest are the prospects for deriving building and lifeline inventories from remote sensing imagery. This would contribute to real-time or near-real-time loss estimation and decision support systems on a global basis and at reduced cost.

Finally, recommendations and directions for further research, development and technology demonstration are offered in Section 7.

2. Ground-Based Measurements

Earthquake prediction efforts are intimately related to generating an increased understanding of the fundamental dynamics of major faults. Fault segment definition leads to a better description of the expected details of earthquake faulting and ruptures. This improved knowledge guides two aspects of hazard mitigation: prediction technology, and ground and structure response mapping.

In this section, advances due to continuous or permanent Global Positioning System (GPS) networks and seismological systems for real-time response are reviewed. Both technologies provide critical measurements for understanding the earthquake process and its impact on the built environment.

Loss estimation consists of three principal elements: (1) the assessment of the risks associated with the occurrence of natural hazards; (2) the characterization of the vulnerability of the built environment to this risk; and (3) the quantification of financial exposure of structures and lives on property and casualty liability bases, respectively.

Ground-based and remotely sensed measurements of ground motion and land change have direct bearing on our understanding of geophysical processes and evaluating the likelihood of occurrence of natural hazards. Measurements and mathematical modeling of ground displacements are used to estimate the potential impact on structures and lifelines. Financial and economic impacts then are estimated from the geophysical models and the presumed interaction of ground motion with the built environment, for a given scenario event or series of events, and structural engineering characteristics and occupancies.

2.1. Global Positioning System

The Global Positioning System (GPS) is a navigation and positioning system funded, controlled and operated by the U.S. Department of Defense (DoD). Originally designed for military operation, the civil and research usage of GPS is significant and the number of applications is increasing accordingly (for example, see http://www.trimble.com for a representation of available commercial products and the GPS trade organization at http://www.gpsworld.com for innovative applications).

GPS is part of a satellite-based navigation system developed by the DoD under its Navigation Signal Timing and Ranging (NAVSTAR) satellite program. The GPS satellites themselves comprise what is known as the *space segment* of the system. These space vehicles, or SVs as they are known, transmit specially coded radio signals that can be processed in a GPS receiver to determine the receiver's position in three dimensions and a time offset in the receiver clock. The nominal GPS Operational Constellation consists of 24 satellites approximately uniformly dispersed around six circular orbits of four satellites each, with the orbits inclined at an angle of 55 degrees relative to the earth's equatorial plane and separated from each other by multiples of 60 degrees longitude.

The satellite orbits have radii of 26,560 kilometers and are approximately circular. The orbits are non-geosynchronous, with 0.5 sidereal day (11.967 hours) orbital time intervals, so that the satellites move with time relative to the Earth below, with a 4-minute precessional advance each day. Theoretically, three or more GPS satellites are visible from most points on the Earth's surface, and visual access to two or more satellites is used to determine an observer's position anywhere on the Earth's surface, 24 hours per day. Each satellite carries a cesium or rubidium atomic clock to provide timing information for the signals transmitted by the satellites. Internal clock correction is provided for each satellite clock.

Fig. 3. The GPS constellation is designed and operated as a 24-satellite system, consisting of six orbital planes, with a minimum of four satellites per plane.

The GPS Master Control facility is located at Schriever (formerly Falcon) Air Force Base in Colorado. The system of tracking stations located around the globe is known as the GPS *control segment*. Signals from the SVs are monitored and incorporated into orbital models for each satellite in order to compute precision ephemeris and clock corrections. These corrections are uploaded to the SVs that then, in turn, send subsets of these data to GPS receivers in the user community over radio signals. The receivers and user community comprises what is known as the *user segment*.

Each GPS satellite transmits two spread spectrum, L-band carrier signals: an L1 signal having a frequency f_1=1575.42 MHz and an L2 signal having a frequency f_2=1227.6 MHz. These two frequencies are integral multiples of a base frequency of 1.023 MHz: 1540 for f_1 and 1200 for f_2. The L1 signal from each satellite is a binary phase shift key (BPSK) modulated by two pseudo-random noise (PRN) codes in phase quadrature, designated as the C/A-code and P-code. The L2 signal from each satellite is BPSK modulated by only the P-code. The nature of these PRN codes is described below.

One motivation for use of the two carrier signals L1 and L2 is to allow partial compensation for the propagation delay of such a signals through the ionosphere; this delay varies approximately as the inverse square of the signal frequency. When the transit time delay through the ionosphere is determined, a phase delay associated with a given carrier signal can be determined.

PRN codes allow use of a plurality of GPS satellite signals for determining an observer's position and for providing navigation information. A signal transmitted by a particular GPS satellite is selected by generating and matching, or correlating, the PRN code for that particular satellite. All PRN codes are known and are generated or stored in GPS satellite signal receivers carried by ground observers.

A first PRN code for each GPS satellite, sometimes referred to as a precision code or P-code, is a relatively long, fine-grained code having an associated clock or chip rate of 10.23 MHz. A second PRN code for each GPS satellite, sometimes referred to as a clear/acquisition code or C/A-code, is intended to facilitate rapid satellite signal acquisition and hand-over to the P-code and is a relatively short, coarser-grained code having a clock or chip rate of 1.023 MHz.

The C/A-code for any GPS satellite has a length of 1023 chips or time increments before this code repeats. The full P-code has a length of 259 days, with each satellite transmitting a unique portion of the full P-code. The portion of P-code used for a given GPS satellite has a length of precisely a week (7.000 days) before this code portion repeats [6].

The GPS satellite bit stream includes navigational information on the ephemeris (orbit) of the transmitting GPS satellite and an almanac for all GPS satellites. Additionally, it contains parameters providing corrections for ionospheric signal propagation delays suitable for single frequency receivers and for an offset time between satellite clock time and true GPS time. The navigational information is transmitted at a rate of 50 baud [7].

The U.S. Department of Transportation Civil GPS Service has designated the National Oceanographic and Atmospheric Administration (NOAA) to be the federal agency responsible for providing accurate and timely GPS satellite ephemerides to the general public. The GPS precise orbits are derived using 24-hour data segments from the global GPS network coordinated by the International Geodynamics GPS Service (IGS). The reference frame used in the computation is the International Earth Rotation Service Terrestrial Reference Frame (ITRF).

A second configuration for global positioning is the Global Orbiting Navigation Satellite System (GLONASS), placed in orbit by the former Soviet Union and now maintained by the Russian Republic. GLONASS also uses 24 satellites, distributed approximately uniformly in three orbital planes of eight satellites each. Each orbital plane has a nominal inclination of 64.8 degrees relative to the equator, and the three orbital planes are separated from each other by multiples of 120 degrees longitude. The GLONASS circular orbits have smaller radii, about 25,510 kilometers, and a satellite period of revolution of 8/17 of a sidereal day (11.26 hours). A GLONASS satellite and a GPS satellite will thus complete 17 and 16 revolutions, respectively, around the Earth every 8 days.

The GLONASS system uses two carrier signals, L1 and L2, with frequencies of f_1 equal to (1.602+9k/16) GHz and f_2 equal to (1.246+7k/16) GHz, where the index k = (0, 1, 2, . . ., 23) is the channel or satellite number. These frequencies lie in two bands at 1.597-1.617 GHz (L1) and 1,240-1,260 GHz (L2). The L1 code is modulated by a C/A-code (chip rate equal to 0.511 MHz) and by a P-code (chip rate equal to 5.11 MHz). The L2 code is presently modulated only by the P-code. The GLONASS satellites also transmit navigational data at a rate of 50 Baud. Because the channel frequencies are distinguishable from each other, the P-code is the same, and the C/A-code is the same, for each satellite. The methods for receiving and analyzing the GLONASS signals are similar to the methods used for the GPS signals.

Table 1. GPS approaches based on signal types and with respective estimated accuracy.

Approach	Accuracy Estimate	L1 C/A Code	L1 P-Code	L1 Carrier	L2 P-Code	L2 Y-Code
SPS Navigation	100 m	X				
SPS Differential > 30 km	10 m	X				
SPS Differential < 30 km	1 m	X				
PPS Navigation	10 m	X	X		X	
Anti-Spoofing Navigation	10 m	X	X	X	X	X
L1 Carrier Phase Survey	0.1 m	X		X		
L1 L2 Carrier Phase Survey	0.01 m	X	X	X		

In summary, a Satellite Positioning System (SATPS), such as GPS or GLONASS, uses transmission of coded radio signals, with the structure described above, from a plurality of Earth-orbiting satellites. A single passive receiver of such signals is capable of determining receiver absolute position in an Earth-centered, Earth-fixed coordinate reference system utilized by the SATPS.

GPS receivers convert SV signals into position, velocity and time estimates. Observation of four satellites is required to compute the four dimensions of X, Y, Z position and time. A configuration of two or more receivers can be used to accurately determine the relative positions between the receivers or stations. Precision positioning using GPS relies on reference stations that provide corrections and relative positioning data for remote receivers. This method, known as differential positioning, is far more accurate than absolute positioning, provided that the distances between these stations are substantially less than the distances from these stations to the satellites, which is the usual case. Differential positioning can be used for survey or construction work in the field, providing location coordinates and distances that are accurate to within a few centimeters.

In differential position determination, many of the errors in the SATPS that compromise the accuracy of absolute position determination are similar in magnitude for stations that are physically close. A process of partial error cancellation therefore substantially reduces the effect of these errors on the accuracy of differential position determination.

A SATPS antenna receives SATPS signals from a plurality (preferably four or more) of SATPS satellites and passes these signals to an SATPS signal receiver/processor, which:

- Identifies the SATPS satellite source for each SATPS signal,
- Determines the time at which each identified SATPS signal arrives at the antenna,
- Determines the present location of the SATPS antenna from this information and from information on the ephemerides for each identified SATPS satellite.

Authorized users with cryptographic equipment and keys and specially equipped GPS receivers use what is known as the Precise Positioning System (PPS). Examples of such users include the U.S. and Allied military, certain U.S. government agencies, and selected civil users approved by the U.S. Government. The predictable accuracy of PPS is 22 meters in the horizontal dimension, 27.7 meters in the vertical and 100 nanoseconds in time. The P- or Y-Code is the basis for PPS [8].

Civil users use the Standard Positioning Service (SPS), with predictable accuracy of 100-meter horizontal, 156-meter vertical and 340 nanoseconds in time. This degraded accuracy is the result of the Department of Defense usage of Selective Availability, and represents 95% (two standard deviations or error) figures. The C/A modulated L1 carrier is the basis for the civil SPS.

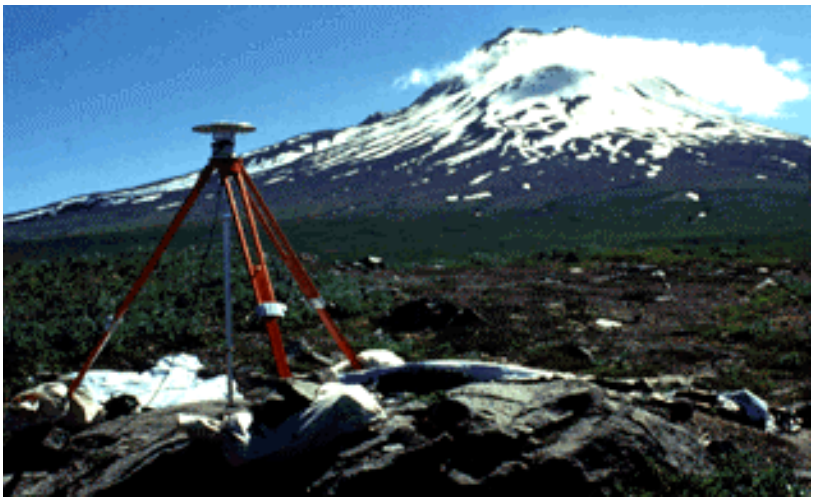

Fig. 4. GPS ground receiver with antenna set up on a tripod on the flank of Augustine Volcano, Cook Inlet, Alaska (Photograph Courtesy: Jerry Svarc, USGS).

2.1.1 Code Phase Tracking

The C/A Code modulates the L1 carrier phase. The P-Code modulates both L1 and L2 carrier phases. In the Anti-Spoofing (AS) mode of operation, the P-Code is encrypted into the Y-Code. The encrypted Y-Code requires a classified AS Module for each receiver channel. The Navigation Message also modulates the L1-C/A code signal. This message is a 50 Hz signal consisting of data bits that describe the GPS ephemerides, clock corrections and other system parameters.

A GPS receiver produces replicas of the C/A and/or P (Y)-Code. The C/A code sequence is specific to a given SV. The C/A code generator produces a different 1023 chip sequence for each phase tap setting. In modern receivers, the pre-computed C/A code chip is stored in memory. In a shift register implementation, the code chips are shifted in time by slewing the clock that controls the shift registers. the C/A code generator repeats the same 1023-chip PRN code sequence every millisecond. The receiver slides a replica of the code in time until there is correlation with the SV code, and some signal power is detected. As the SV and receiver codes line up completely, the spread-spectrum carrier signal is de-spread and full signal power is detected. The receiver PRN code start position at the time of full correlation is the time of arrival of the SV PRN at the receiver. This time of arrival is a measure of the range to the SV, offset by the amount to which the receiver clock is offset from GPS time, and is referred to as pseudo-range.

2.1.2 Pseudo-Range Navigation

The position of the receiver is where the pseudo-ranges from a set of SVs intersect at a single measurement epoch. The pseudo range measurements are used together with SV position estimates based on the precise ephemeris data to yield three position dimensions and time in an earth-centered, earth-fixed coordinate frame. This position is converted to geodetic latitude, longitude and height above a reference ellipsoid (i.e. WGS-84).

2.1.3 Carrier Phase Tracking

The L1 and/or L2 carrier signals are used in carrier phase surveying, providing range measurements with relative accuracy of as small as millimeters. Tracking the carrier phase signal provides the time of transmission information. The carrier signals, although modulated with time tagged binary codes, carry no time-tags that distinguish one phase cycle from another. Thus, the measurements used in carrier phase tracking are differences in carrier phase cycles and fractions of cycles over time. All carrier phase tracking is differential, requiring both a reference and remote receiver tracking carrier phases at the same time. L1-L2 differences can be used to measure ionospheric delays, such that the relative positions of fixed states can be determined over baselines of hundreds of kilometers.

Post-processed static carrier-phase surveying can provide 1-5 cm relative positioning within 30 km of the reference receiver with measurement time of 15 minutes for short baselines (10 km) and one hour for long baselines (30 km). Rapid static or fast static surveying can provide 4-10 cm accuracy with 1-km baselines and 15 minutes of recording time. Real-time kinematic (RTK) surveying techniques can provide centimeter measure-

ments in real time over 10 km baselines tracking five or more SVs and real-time radio links between the reference and remote receivers.

2.1.4 Differential GPS (DGPS)

Differential positioning is based on correcting bias errors at one location with measured bias errors at a known position. Since individual pseudo-ranges must be corrected priori to the formation of a navigation solution, DGPS implementations require software in the reference receiver that can track all SVs in view and form individual pseudo-range corrections for each SV. These corrections are passed to the remote, or rover, receiver that must be able to applying the individual pseudo-range corrections to each SV in the navigation solution.

Differential corrections may be used in real-time or in post-processing. Real-time corrections are transmitted by radio link. The U.S. Coast Guard maintains a network of differential monitors and transmits DGPS corrections over radio beacons. Private DGPS services use leased FM sub-carrier broadcasts, satellite links, or private radio beacons for real-time applications. To remove Selective Availability (SA) and other bias errors, differential corrections should be computed at the reference station and applied at the remote receiver at an update rate that is less than the correlation time of SA (suggested update rates are usually less than twenty seconds). Since DGPS removes common-mode errors (for receivers that are close together, e.g. less than 100 km apart). DGPS accuracy of 1-10 km is possible based on C/A code SPS signals.

The various applications of GPS are based on accuracy requirements that can be summarized as follows (see Table 1):

- Low-cost, single receiver SPS (100-m accuracy);
- Medium-cost, differential SPS code positioning (1-10 m accuracy);
- High-cost, single receiver PPS (20-m accuracy);
- High-cost, differential carrier phase (1-mm to 1-cm accuracy).

The latter is the basis of high-resolution geodetic crustal strain monitoring with repeated epoch measurements or with continuous or permanent GPS networks.

2.1.5 GPS Monitoring Networks

The increasing number of large permanent GPS arrays is made possible by the decreasing cost of GPS instrumentation and continued advances in telecommunications infrastructure and data storage. These arrays include:

- Southern California Integrated GPS Network (SCIGN) [9, 10];
- San Francisco Bay Area Regional Deformation (BARD) network [11];
- GPS Regional Array for Precise Surveying (GRAPES) in Japan [see 13];
- Continuous Strain Monitoring System (COSMOS) [12, 13].

The horizontal positioning capability of high-precision GPS approaches if not exceeds that of conventional surveying methods. The significant benefits of continuous GPS lie in the higher temporal resolution and nearly unattended continuous operation.

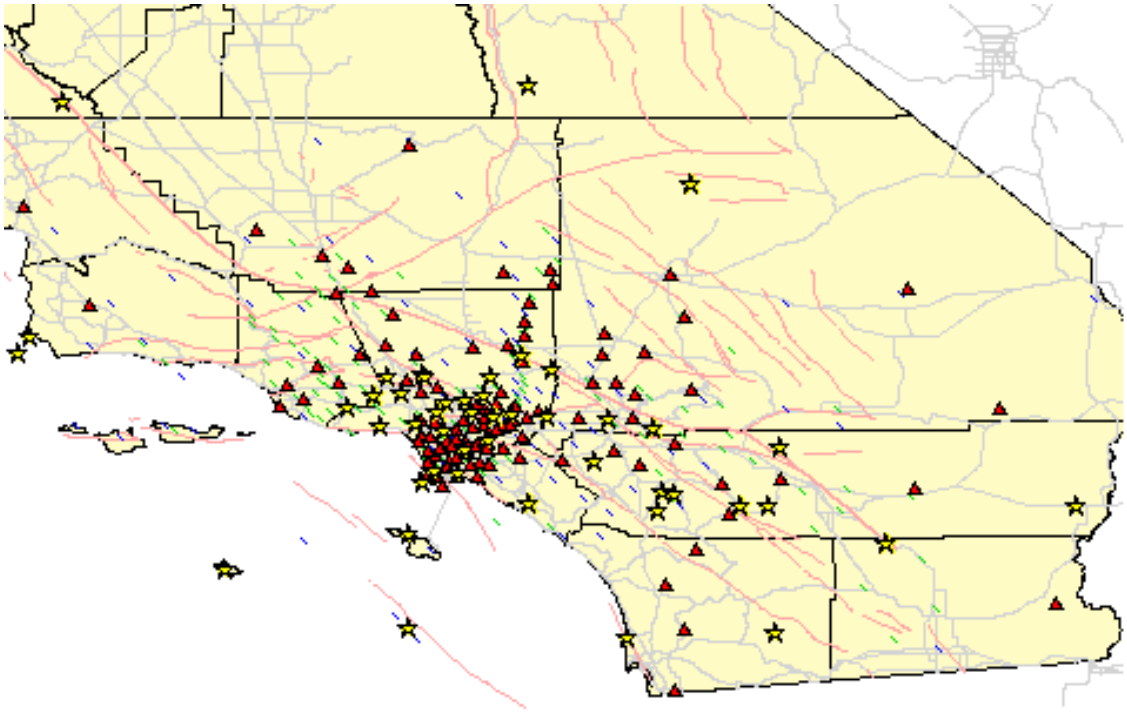

Fig. 5. Regional map of the sites of the Southern California Integrated GPS Network (SCIGN). Yellow stars denote operational site and red triangles denote planned sites. (See http://www.scign.org)

Primary objectives of SCIGN (see Fig. 5), for example, are:

- To provide regional coverage for estimating earthquake potential throughout Southern California;
- To identify active blind thrust faults and test models of compressional tectonics in the Los Angeles region (Fig. 6);
- To measure local variations in strain rate that might reveal the mechanical properties of earthquake faults;
- In the event of an earthquake, to measure permanent crustal deformation not detectable by seismographs, as well as the response of major faults to the regional change in strain.

SCIGN is organized under the auspices of the Southern California Earthquake Center (SCEC, http://www.scec.org). Major infrastructure funding comes from W.M. Keck Foundation, National Aeronautics and Space Administration, United States Geological Survey, and the National Science Foundation.

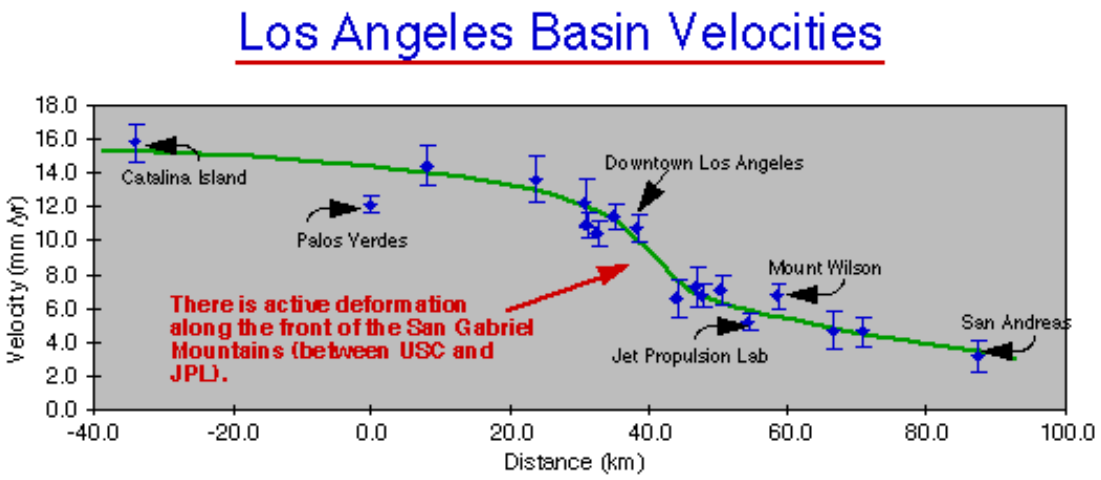

Fig. 6. This velocity graph is a result of GPS data gathered in the Los Angeles basin. GPS measurements indicate that the LA basin is being compressed in the northern, rather than southern, portion of the basin (e.g. the distance between basin stations moving in the same direction (north) at different velocities is getting smaller, implying compression (or shortening). The area and corresponding faults where most of this movement is occurring can be determined from this graph. If the line connecting the sites on this map were straight it would imply that all the faults in the entire basin were contributing to the movement equally. However, the line is steeper between Downtown LA and JPL. This shows that most of the compression is actually occurring in one area and is the result of movements on particular faults.

GPS, as a commercially available satellite-based surveying, point positioning and navigation tool, is demonstrating an ever-increasing utilization in public, private, military and civilian sectors. GPS monitoring networks in operation in the U.S. and Japan are yielding sub-centimeter level resolution of displacements and crustal strains of the order of 10^{-8}.

Recent advances in computer networking and database management are making it more feasible to place critical ground displacement data, virtually in real time, in the hands of those responsible for decision-making at the time of an emergency. In Japan, for example, there are about 1,000 GPS continuous observation facilities, installed as part by the Geographical Survey Institute and Science and Technology Agency; included in the plan is the installation of a further network with standard spatial internals of between 20 to 25 km [14].

Ground deformation measurements with GPS afford an areal coverage and temporal resolution that is not possible strictly with ground-based techniques. High-accuracy geodetic measurements with GPS can help to map strain changes at various distances from a fault, and help constrain the depth of creep or aseismic events and the extent of fault rupture. *GPS provides sufficient spatial and temporal resolutions to yield three-dimensional strain changes that may be diagnostic of a potential seismic event*. Once the most hazardous segments of potentially dangerous faults are described or assessed in terms of risk, priorities can be set for a systematic remediation program.

It is now possible to begin to identify transient inter-seismic deformations. The planned continued densification of these GPS networks allows measurement of fault slip rate patterns, in order to infer aseismic slip distribution at depth, determine the source time his-

tory of slow earthquakes, and compare the pattern of aseismic slip before and after large earthquakes [15]. The amount of three-dimensional positions that are generated by these networks clearly points to the practical need to develop automated inversion methods.

GPS geodetic network surveys measure surface strain accumulation with the expectation that some future earthquake or series of earthquakes will release such strain. Earthquake potential, however, is measured by accumulated seismic moment. Savage and Simpson [16] discuss that the correspondence of a scalar seismic moment rate with a given surface strain accumulation rate is not unique. This is due to approximating the strain rate in the entire seismogenic layer with that derived from surface geodetic observations. Further, since a moment-rate tensor cannot be uniquely resolved into two or more double-couple solutions, except under special cases, the scalar moment accumulation rate is ambiguous (a double-couple mechanism can be represented by a scalar moment accumulation rate).

A systematic seismic hazard remediation program involves a progressive approach to the highest risk areas, where both modern seismic and geodetic monitoring systems, and focused engineering studies, can be implemented. Continued deployment of permanent GPS monitoring networks will lead to:

- Better definition of off-fault surface deformation;
- Timely detection of diagnostic changes in the fault environment;
- Constraints on the extent of surficial fault creep and its significance to potentially significant earthquakes;
- Accurate estimates of the distribution of potentially damaging ground motions from such earthquakes to enable ground motion modeling, structural design planning and risk assessment.

Risk assessment and rapid response are critical elements if losses to life and property are to be minimized, and if they are to have direct impact on long-term planning of emergency services, transportation systems and public utilities. A high-precision geodetic monitoring network may provide longer-term warning, of the order of several hours to days depending on the nature of the surface deformation - in terms of temporal and spatial characteristics of potential precursory phenomena and signal magnitude. However, the relationship of surface strain to earthquake occurrence must be understood if GPS networks are going to contribute significantly to loss estimation methodologies.

2.2 Seismological Networks

Seismological networks that are used for early warning and rapid response rely on the ability to perform real-time waveform inversions in order to provide earthquake parameters during the actual rupture process [17]. Warning times, based on the strategic placement of seismic instrumentation relative to the rupturing fault, can range from a few seconds to at most one to two minutes. Kanamori et al. [18] review systems that currently are in operation in Japan, Mexico, Taiwan and the United States. Each system shares the intent of contributing to the reduction of recovery times after a major earthquake, and

helping to allow a more rapid determination of the resources that will be needed for post-disaster rebuilding and recovery.

The results of real-time seismological monitoring systems can be used to calculate the likelihood of subsequent, probabilistically related events at longer time intervals ranging from minutes to weeks. While wave propagation effects do not vary significantly for earthquakes in the same location, fault rupture characteristics, however, may lead to a greater diversity of effects. This clearly and directly impacts the ability to estimate potential losses for a given exposure. Additional layers of information are required for improved loss estimation. Information on seismicity and seismic networks is available at http://earthquakes.usgs.gov/ and http://neic.usgs.gov.

The 1999 earthquakes in Taiwan and Turkey produced surface faulting that caused ruptures through urban and industrial areas. Engineering structures were subjected to large strike-slip fault displacements (up to 5 meters in Turkey) and reverse faulting (up to several meters of vertical displacements and warping in Taiwan). Surface deformations associated with large fault ruptures can be difficult to predict, especially in fault step-overs and on the hanging wall adjacent to the primary fault traces.

Rupture directivity effects were less pronounced than suggested by current models that are intended to represent moderate high-frequency near-fault ground motions. Broadband digital recording provide the first reliable data on long period (greater than 3 seconds) ground motions close to a large earthquake [19].

The 1999 Turkey and Taiwan earthquakes were characterized by very large near-fault long period ground motions and static fault displacements that are unprecedented and may suggest major revisions in current near-fault ground motion models and in building codes.

Maps and information products derived from remotely sensed imagery that are integrated into a geographic information system (GIS) will increasingly support seismic information. Such map products can provide regularly updated information on regional geomorphology, urban topography, structures, roadway networks and vegetation. However, maps of surficial features must be considered within the specific framework of the risk. For example, preferred directions of ground motion can occur in areas with no surface topographic effects [20]. Furthermore, significant variations in site response can exist over short distances, up to a factor of two over 200 meters, that are not explained by differences in surficial geology but rather by the influence of structures such as folds and buried basins up to a few kilometers in depth.

With support from the Federal Emergency Management Agency (FEMA), California's Seismic Hazard Mapping Program has completed a three-year project in areas of Los Angeles, Ventura and Orange counties. DTED Level-II (i.e. 10 meter) digital elevation

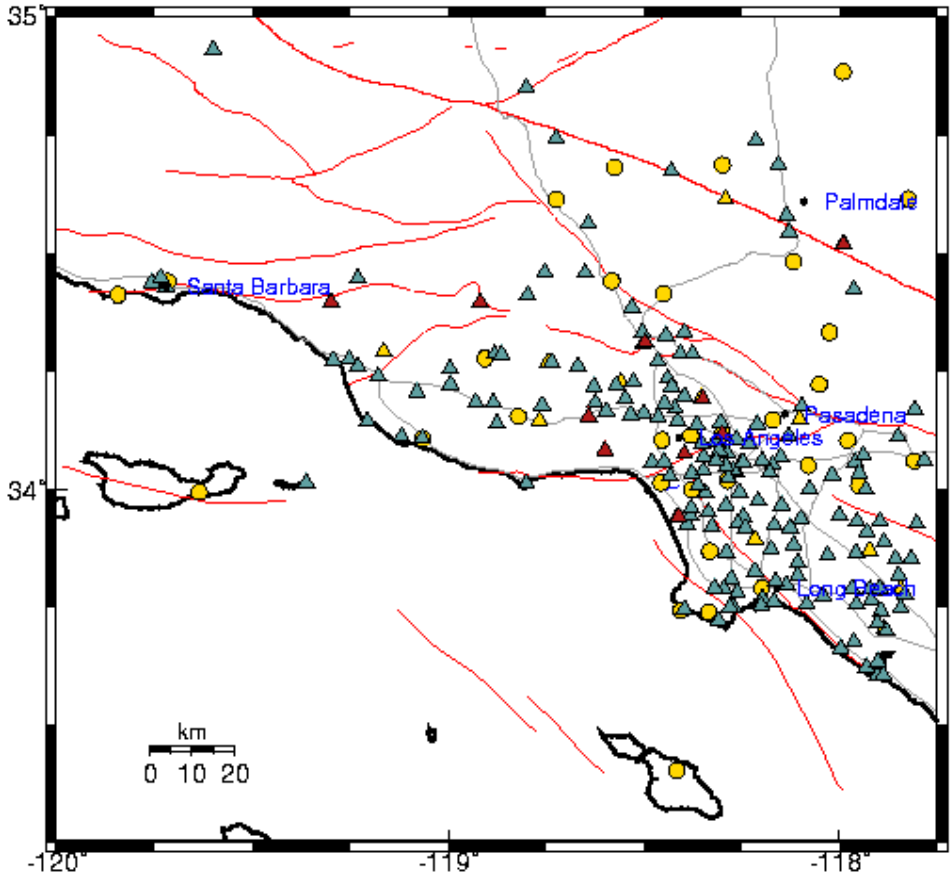

Fig. 7. Southern California seismic networks with instrument types. SCSN: Southern California Seismic Network. CSMIP: California Strong Motion Implementation Program – Department of Conservation. NSMP: USGS National Strong Motion Program.

models (DEMs) were obtained from the U.S. Geological Survey. These were updated to show modern topography in urbanized regions using both photogrammetric techniques

and synthetic aperture radar (SAR) derived elevation measurements provided by the NASA Jet Propulsion Laboratory, California Institute of Technology (Caltech), Pasadena, CA. Topography is an important element that affects ground shaking and liquefaction potential. This is due to the potential focusing of seismic wave propagation and the influence on hydrology.

The increasing capability to image man-made structures and lifelines with remote sensing is addressed is Section 4. This information layer then can be superimposed on the various layers that characterize the terrain. In so doing, in GIS architecture, surficial effects could be integrated into the vulnerability models of structures and lifelines and for developing map-based loss estimates with granularities, or geospatial grid resolutions (i.e. counties, zip codes, blocks) required by disaster management and insurance and financial applications.

The Southern California Seismic Network (SCSN), for example, is a cooperative project of the U.S. Geological Survey Pasadena office and the Caltech Seismological Laboratory (see Fig. 7). It is also part of the TriNet cooperative project between the USGS, Caltech, and the California Division of Mines and Geology [see http://www.trinet.org]. The SCSN is one of the largest and most automated seismic networks in the world. It consists of more than 350 analog and digital seismographs operated by multiple sources which relay both continuous and triggered seismic data back to a central computer facility in the Seismology Laboratory on the Caltech campus. After the seismic data are processed, they are archived and can be accessed from the Southern California Earthquake Center Data Center.

The automatically broadcast information and other data are also used by scientists to assess the status of seismic activity on a daily basis. Statistical studies of earthquake foreshock and aftershock sequences have used the catalog to determine the probabilities of any earthquake being a foreshock and the likelihood of the occurrence of damaging aftershocks following a mainshock. These probabilities are the basis of public advisories issued by the State of California.

TriNet products include the pilot Seismic Computerized Alert Network. This alert network is an emerging technology that will provide the capability to recognize and send notification that an earthquake is in progress before shaking from that event arrives at a distant site. Such alerts may provide a lead-time of seconds to several tens of seconds before the most damaging shaking arrives. Some potential uses for computerized alerts are stopping trains, protecting fragile facilities, interrupting the handling of toxic chemicals, and securing power supplies and databases. The network is a technology prototype.

Similarly, the Caltech US Geological Survey Broadcast of Earthquakes (CUBE) is a collaborative research project between Caltech, the United States Geological Survey, and Earthquake Research Affiliates members. CUBE has three goals:

- Provide near real-time locations, magnitudes, and ground motions for earthquakes.

- Develop a system to warn of imminent ground shaking while the earthquake is in progress.
- Develop strategies to use the information to respond efficiently to earthquakes.

Currently the CUBE system is being used by over thirty entities throughout the United States. These include major communication, public safety, transportation, and utility companies as well as several media organizations. Further information can be obtained through http://www.gps.caltech.edu/.

2.3 Integration of GPS and Seismic Network Data

GPS regional strain data provide valuable constraints on seismic hazard assessment. Seismic hazard analyses intend to assess the probability that ground motion at a site will exceed a certain value in a given period of time. A seismic source zone is defined as a seismically homogeneous area wherein each point has an equal epicentral probability. Delineation of seismic source zones requires understanding the geology, tectonics, and paleoseismic and neotectonic features of the region. The correlation of seismicity with regional tectonics is an important element of the overall seismic hazard assessment. An attendant seismicity model describes the geographical distribution of potential sources and the corresponding potential magnitudes, while an attenuation model describes the effect at a given site as a function of magnitude and distance from the source.

The integration of GPS network data with seismic data helps distinguish the effects of wave propagation from those of earthquake rupture. Both data types provide information on the potential for seismic risk and contribute critical inputs towards assessing the vulnerability of structures and lifelines. For example, in September 1995, Pacoima Dam, in the San Gabriel Mountains north of Los Angeles, CA, was instrumented with three continuously operating GPS receivers to test the feasibility of applying GPS to the field of structural monitoring [21].

The application of GPS for real-time structural motion sensing and control is in a research stage. Recent studies [22, 23] have shown 20 Hz differential carrier phase measurements with about 5 mm relative position accuracy on a test structure. Carrier phase tracking provides a valuable observable for measuring the elastic motions of a structure that exhibits vibrations within the bandwidth and deflection sensitivity limits of available GPS receivers. For example, by mounting an array of GPS antennas and GPS-like signal transmitters (i.e. pseudolites) on a flexible body, relative motion may be sensed and tested for applicability for real-time feedback control.

One benefit of mathematically inverting multiple datasets is to examine the resolving power of each. For example, the GPS and leveling geodetic displacements can be predicted with the dislocation model determined from waveform data. Conversely, the geodetic displacements can be used to infer an appropriate slip model that can be checked with the waveform data. Teleseismic data can be used to predict the nearer-field strong motions. Regional seismic data, as would be collected with portable instruments after a main shock, can be used to constrain regional velocity structure models.

All these types of data are necessary in order to understand the source-rupture process and thus infer the resultant patterns of damage [24]. Three advantages are:

- Since GPS and waveform stations do not cover a geographic area uniformly in the near-source region, a combined data set enhances the spatial sampling.
- Frequencies sampled are from the range of DC to about 1.0 Hz. Slip models thus can be compared that sample only the coseismic slip (waveform data) with those that include slip from aftershocks and any aseismic contributions.
- The slip pattern determined from geodetic data is independent of rupture timing. Imposing a model requirement that the final slip in the waveform inversion fit the static data provides an independent constraint on a priori timing assumptions made in the waveform inversion. Band-limited inversions otherwise experience a trade-off between rupture timing and slip location.

Resolving rupture characteristics depends on the rupture dimensions and source duration. The accelerations are more sensitive to wave propagation effects and site response. The longer-period waveforms are more sensitive to rupture directivity and radiation pattern. In the absence of near-source ground motion and geodetic displacement data, source slip patterns and ground motion estimates can be made using teleseismic data. Teleseismic data often yields the overall slip and degree of heterogeneity, the resolution is typically insufficient to constrain the slip pattern and reproduce the static displacements.

The ability of geodetic data to resolve variations in slip pattern diminishes greatly with slip depth. For example, the greater average depth of the slip in the Northridge earthquake did reduce the effective resolution of the geodetic data.

Prediction of strong motion velocities from geodetic data alone offers limited spectral response, and thus is a poor replacement for actual strong motion recordings that are critical to earthquake engineering. Strong motion data necessitate more heterogeneous slip distribution in order to yield the variation observed in velocity amplitude, frequency content and waveform complexity. On the other hand, a smooth slip pattern is often sufficient to model geodetic data.

GPS network station data over extended periods of time must be corrected by using secular velocity estimates. Other necessary corrections for inferring the coseismic displacement are:

- Permanent displacements due to aftershocks;
- Subsidence resulting from fluid withdrawal;
- Movement of monuments due to intense shaking.

Furthermore, motions induced by human activity must be distinguished from those due to tectonic deformation. This is a necessary calibration step for the interpretation of geodetic measurements. As noted in the Southern California Earthquake Center 1998 Annual Report, for example, observed vertical motion in the Los Angeles basin that is attributed to pumping and withdrawal of fluids from petroleum reservoirs and hydrologic

aquifers is 1 to 4 mm/yr. Horizontal displacements associated with this movement are up to 1 mm/yr in some areas.

The broad spectrum of ground displacement signatures that are measurable by GPS and seismic networks is subject to one major liability – the sampling is discrete. While there are increasing efforts to establish dense networks, economic constraints limit the deployment of these networks. The use of remote sensing imagery is considered in the next Section as a means to provide more spatially continuous information of both the geologic landscape and of the built environment. Combined with ground network data, remote sensing enables a better understanding of displacements, and validation of slip models that are cast in a regional setting of tectonic strain.

3. Remote Sensing

There is a need for a multidisciplinary approach to the theoretical and practical integration of remote sensing data and geospatial information products, with ground-based measurements provided by dense seismographic and GPS networks. The information that can be extracted from remotely sensed imagery is relevant not only to assessing the potential of risk, but towards better defining the state of vulnerability, and thus the exposure to loss, within a given geographic region. It is the ability to extract information from imagery that provides value to decision-making, and this should be distinguished from simply providing visual records.

Remote sensing technologies refer to all forms of airborne, including unmanned aerial vehicle (UAV), and spaceborne platforms with sensors that enable the active and passive measurement of the earth's surface properties and features. (Information on UAV platforms for remote sensing is obtainable, for example, at http://www.aerovironment.com/ and http://www.amtech-usa.org/).

Passive systems include optical and infrared sensors, while active systems consist typically of lidar (e.g. laser systems) and radar. For active systems, the platform has both a signal transmitter and receiver. The physical and chemical properties that are remotely measured by each sensor can be integrated to provide a better understanding of the surface and to infer natural and anthropogenic causes of changes detected over a given period of time. Monitoring land use and land cover changes is an important element of risk assessment, loss estimation and reconstruction monitoring.

3.1 Geographic Information Systems

A Geographic Information System (GIS) is a computer software system capable of assembling, storing, manipulating, and displaying geographically referenced information (i.e. data identified according to their locations). The manner in which maps and other data are stored or filed as layers of information in a GIS makes it possible to perform complex analyses. GIS and related technology help greatly in the management and analysis of large volumes of data, allowing for better understanding of terrestrial processes and supporting decision-making. The websites of leading GIS firms are http://www.esri.com, http://www.erdas.com, http://www.ermapper.com, http://www.intergraph.com and http://www.mapinfo.com.

Remote sensing data from satellite and airborne sensors will continue to fuel the growth of GIS use. According to a recent Frost & Sullivan report (reports can be reviewed in http://www.frost.com), the total market for remote sensing data and GIS software was $2.28 billion in 1998 with a growth rate of 10%. The evolutionary, yet steady growth is representative of increasing adoption among new commercial users and the expanding use of imagery and GIS software within existent user groups. The compound annual growth rate for this market is 10.1%.

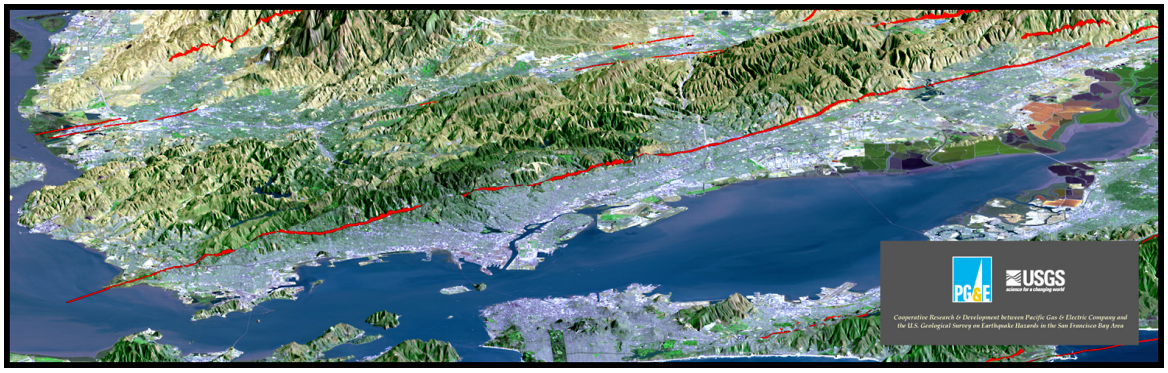

Fig. 8. Developed by Robert E. Crippen (JPL) and Ross Stein (USGS) these images drape Landsat TM satellite imagery over Digital Elevation Models to show the San Francisco Bay area. The vertical exaggeration in the oblique views is three times; the view angle is 20 degrees below the horizontal. Active faults (which slipped during the past 10,000 years) are from C.W Jennings, Fault Activity Map of California (1994). The offshore portion of the San Gregorio fault is modified after M.L. Zoback et al. [25]. (See also http://www.sfbayquakes.org).

The world commercial satellite imaging market grew at 16% in 1998, and is forecast to grow at a compound rate of 17.1% through the year 2005. This growth reflects the integration of high-resolution panchromatic data and the greater availability of multispectral and SAR data. Among the major drivers for market growth are:

- Continued commercialization of satellite data;
- Better temporal resolution than airborne platforms;
- Greater area coverage at comparable resolution to airborne platforms;
- Steady and recession-proof demand for surveillance and change monitoring;
- Increasing number of worldwide ground stations;
- Falling component and launch costs.

Factors that have hindered commercial satellite remote sensing industry growth include:

- Launch slippages and failures;
- Distributions channels not fully prepared for satellite data;
- Data format incompatibilities between several systems;
- Government-imposed imaging restrictions.

The compound annual growth rate of the airborne segment is projected to be 9.6% through 2005. Major drivers of this growth include the following:

- Urban growth creates greater needs for updated information (in applications such as urban planning, infrastructure, environmental impact assessment and transportation);
- Falling data costs enable current users to purchase more frequently (although there are still concerns over data rights, licensing and data sharing);

- Demand for 1-meter and higher resolution is growing (as is the realization that problem- or user-driven solutions dictate the integration of different spectral bands);
- Established aviation infrastructure aids growth;
- Aerial platform flexibility enables new imagery at increased intervals (recognizing the users must consider the trade-offs in performance, cost and delivery between airborne and spaceborne platforms).

Table 2. Total Remote Sensing Data and GIS Software Market Revenues by Major Segment (World), 1998 [Source: Frost & Sullivan]

Market Segment	1998 Revenues ($ Millions)
Satellite Imaging	139
Airborne Imaging	2,174
GIS Software	976

Major barriers to growth in the airborne segment include:

- Market is highly fragmented;
- End-user education remains an industry hurdle;
- Delivery time is often lengthy (although this has been improving rapidly);
- Profitability in commercial and consumer markets has yet to be proven.

As stated by Frost & Sullivan, base-mapping data such as panchromatic orthophotography will increasingly become the foundation upon which companies build visual records of geographic data. Increased availability from a growing number of space-based and aerial-imaging companies will continue to create downward pressure on the pricing of these products. Furthermore, the greater affordability of these GIS base layers such as digital orthophotos, digital elevation models (DEMs) and roadway network data will enable more frequent purchases and will potentially free up resources for more specialized attribute data collection.

The effects of both natural and man-made catastrophes have emphasized the need for developing a broader view of many natural processes. A GIS approach that takes advantage of a computer's ability to store and process large volumes of data can contribute significantly to the development of a method to obtain, process, and display spatial information in a timely and cost-effective way. It makes it possible to update, retrieve, and derive cartographic models by combining, the various layers of information in the database.

Fig. 9. Landsat image of Liberty, Ellis and Governors Islands, NY acquired on August 22, 1999. This sub-scene uses Landsat 7's 15-meter/pixel resolution panchromatic channel (band 8). [Image courtesy: USGS].

3.2 Optical Systems

Existing sources of optical data include SPOT, Landsat, and the more recently launched Indian Remote Sensing (IRS) satellite. Over the next 2 to 5 years, a number of high-resolution panchromatic, multispectral, and hyperspectral optical systems will be launched. Data from these platforms, along with high-resolution digital aerial photography, will result in the ability to find optical images of desired areas at spatial resolutions of ~1 meter (~4 meter multispectral) with little difficulty.

SPOT High Resolution Visible (HRV) consists of three spectral channels that singly, and in combination, can be used to infer the properties of the reflecting surfaces:

- Channel 1 (500 to 590 nm, visible green) senses the relative high reflectance of water;

- Channel 2 (610 to 680 nm, visible red) senses the relative high reflectance of soil as contrasted with the low reflectance of vegetation;
- Channel 3 (790 to 890 nm, near infrared) senses the high reflectance of vegetation as contrasted to bare soil.

In channel 3, the low reflectance of urban materials such as asphalt and roofing materials are revealed as spatial patterns against other surfaces. Comparisons of pairs of channels, particularly the "joint distribution" of channel 1 vs. channel 3, can be used to generate land cover classes such as water, soil types differing in moisture content, asphalt and concrete, and highly watered vegetation [see 26]. For example, land uses can be inferred from the distribution of classes to identify residential, commercial and industrial regions, and recreational areas such as golf courses.

Current Landsat platforms operate on sun-synchronous, near-polar orbits imaging the same 185-km ground swath every 16 days, and provide for global data between 81 degrees north latitude and 81 degrees south latitude. The characteristics of Landsat Multi-Spectral Scanner (MSS) and TM have been selected to maximize their capabilities for detecting and monitoring different types of Earth resources.

Landsat TM images have been used to contribute to the current national landslide inventory and in hazard mapping programs. Their significance is that they help to identify potential landslide hazards along transportation routes and where protective measures are necessary. For example, retrogressive slope failures on the shale banks of the Saskatchewan River have been conducted using a combination of Landsat TM and SAR images. The spatial resolution of satellite data from TM and SPOT are generally too coarse for landslide characterization unless the image data are re-sampled and merged with other higher resolution images for landslide hazard assessment.

Aerial photography has been used extensively to characterize landslides and to produce landslide inventory maps, particularly because of their stereo viewing capability and high spatial resolution. Air photos have been used to identify steep slopes underlain by weak soils, slopes undercut by rivers and waves, tension cracks, steep hummocky topography, failed surface scarps, anomalous bulges and lumps, terraced slopes, discontinuous bedding planes, drainage-vegetation patterns and elongated ponds on hill slopes [27].

Current satellite imagery (including Landsat and SPOT) is not particularly useful in identifying mass movement phenomenon unless such movement is very large. The use of satellite imagery is currently confined to an examination of the terrain conditions associated with landslides, such as lithology, differences in vegetation and soil humidity. Present available satellite remote sensing is limited as far as it refers to the direct mapping of slope instability features. The spatial resolution dies not allow for the identification of landslide features smaller than 100 m, in conditions of favorable strong contrast between the landslide and the background.

Fig. 10. View of Izmit, Turkey on July 9, 1999 acquired with SPOT "XS" Multispectral Mode. [Image courtesy: Spot Image Corp.].

The use of stereoscopic imagery in slope stability studies is very important in view of the clear and diagnostic morphology, created by mass movements. Features such as scarps, disrupted vegetation cover, and deviations in soil moisture or drainage conditions are generally used in conjunction with morphological features. Considering the size of most landslides, which is of the order of several tens of meters, the most useful photographic scale is around 1:15,000. At this scale, the phenomenon cannot only be identified as a slope instability feature, but a preliminary analysis of the feature is also possible. In fact, analysis and conclusions of the type and causes of landslides can best be determined from scales smaller than 1:25,000 [28].

The need for stereo imagery, for the interpretation of the characteristic and diagnostic morphological features of slope failures, is another limiting point in the applicability of an important part of presently available remote sensing imagery. Photo-interpretation plays a very important role in the creation of a mass movement inventory map.

The visible and infrared bands of the spectrum also allow the detection of the extent of fires generally in both daytime and nighttime conditions with the zone of mass conflagration being delineated very quickly. Aerial optical, as well as infrared, remote sensing is especially important for operational identification of fires in thinly populated areas, which are difficult to access. However, the monitoring of large-scale fires covering several hundred square kilometers and which continue over many weeks is only possible from satellites, and even low-resolution imagery have proven effective in this regard [29].

3.3 Multispectral and Hyperspectral Systems

Multispectral and hyperspectral remote sensing is passive (i.e. the sensor is only a receiver). Spectroscopy is the study of light as a function of wavelength that has been emitted, reflected or scattered from a solid, liquid, or gas. Photons are absorbed in minerals by several processes. The variety of absorption processes and their wavelength dependence allows derivation of the chemistry of a mineral from its reflected scattered or emitted light. Imaging spectroscopy refers to the acquisition of images where for each spatial resolution element in the image a spectrum of the energy arriving at the sensor is measured. These spectra are used to derive information based on the signature of the interaction of matter and energy expressed in the spectrum. Imaging spectroscopy has many names in the remote sensing community, including imaging spectrometry, hyperspectral, and ultra-spectral imaging.

There are four general parameters that describe the capability of a spectrometer: 1) spectral range, 2) spectral bandwidth, 3) spectral sampling, and 4) signal-to-noise ratio (S/N). Spectral range is important to cover enough diagnostic spectral absorption to solve a desired problem. There are general spectral ranges that are in common use; each to first order controlled by detector technology. These are as follows: a) ultraviolet (UV): 0.001 to 0.4 μm, b) visible: 0.4 to 0.7 μm, c) near infrared (NIR): 0.7 to 3.0 μm, d) the mid-infrared (MIR): 3.0 to 30 μm, and d) the far infrared (FIR): 30 μm to 1 mm. The ~0.4 to 1.0-μm wavelength range is sometimes referred to in the remote sensing literature as the VNIR (visible-near-infrared) and the 1.0 to 2.5-μm range is sometimes referred to as the SWIR (short-wave infrared).

Spectral bandwidth is the width of an individual spectral channel in the spectrometer. The narrower the spectral bandwidth, the narrower the absorption feature the spectrometer will accurately measure, if enough adjacent spectral samples are obtained. Some systems have a few broad channels, not contiguously spaced and, thus, are not considered spectrometers. Examples include the Landsat Thematic Mapper (TM) system and the MODerate Resolution Imaging Spectroradiometer (MODIS). Others, like the NASA JPL Airborne Visual and Infrared Imaging Spectrometer (AVIRIS) system have many narrow bandwidths, contiguously spaced.

The first hyperspectral imager to orbit the earth, the 242-band Hyperion built by TRW, launched on November 21, 2000 from Vandenberg AFB, CA (see platform and instrument details see http://eo1.gsfc.nasa.gov/Technology/Hyperion.html). TRW also performs airborne data collection with the TRWIS III with image spatial resolutions spanning from less than 1 meter to more than 11 meters, with spectral coverage from 380 to 2450 nm. Spectral resolution is 5.25 nm in the visible/near infrared (380 - 1000 nm) and 6.25 in the short wave infrared (1000 - 2450 nm).

Remote sensing methods, with their ability to view large areas synoptically, have the potential to improve site condition mapping and slide hazard assessment. Unfortunately, viewing geometry and revisit rate characteristics of the Landsat TM are not adapted for frequent observing of short termed events at a single geographical area. Shortwave infrared or SWIR (1.0 to 3.0 μm) has been shown effective in detecting thermal anomalies less than 30 meters in size at temperatures of 150^{o} C and above can be detected by using the TM SWIR bands [30].

Multispectral TM remote sensing can provide characterizations of soil conditions, degree of slope, bedrock type, rainfall and snow melt conditions, and vegetative cover/indices that provide some level of prediction of soil depths [31]. Remote sensing can map phenologic patterns and, thus indirectly, land forms susceptible to debris flows based on local geomorphic processes. Vegetation maps derived from multispectral TM data show that there is correlation between grass senescence and soil thickness variations on hill slopes; this can be included in debris flow hazard modeling.

Vegetation mapping can be readily accomplished using remotely sensed data and incorporated as a data layer in a multivariate statistical evaluation of landslide susceptibility. Vegetation is considered a potentially relevant factor in cases of shallow sliding such as debris flows. Landsat TM data is well suited to vegetation mapping providing a physical variable and as a predictor of other factors important to hazard assessment, such as soil type. Multispectral data can also be used in some circumstances to identify and map existing landslides obscured by forest canopy.

Remote sensing reveals variations in soil depth on the hill slopes that reflect the local geomorphic processes that are involved in long-term slope evolution. Remote spectral data can further be used to estimate the velocity of an earth flow or define areas within a flow moving at different rates and thus evaluate the internal mechanics of a slide.

Characterization of the earth's surface and atmosphere with hyperspectral remote sensing began with airborne mineral mapping in the late 1970s. Significant advancements in imaging spectroscopy came about with the introduction of the NASA AVIRIS.

Interpretation of hyperspectral data is further complicated by the variation of water vapor and haze in the atmosphere. Water vapor is the most variable component in the atmosphere and it's attenuation affects atmospheric transmission even in the so-called window regions between the prominent water-absorption lines at 940, 1140, 1400 and 1900 nm. This can be corrected for, provided however, that spectral measurements across the water bands are acquired.

Atmospheric haze does not possess particularly strong spectral signatures and methods to correct for such attenuation include the use of ground-based calibration panels, ground-based measurements of the solar aureole (the halo of scattered light about the solar disk), and estimates of propagation codes. Atmospheric haze is usually negligible for wavelengths greater than 1000 nm.

Spectral-mixture analysis and variants thereof, used in conjunction with multi- and hyperspectral data sets, can detect target materials smaller than the sensor's ground instantaneous field of view. Sub-pixel detection has applicability in fields as diverse as geology, environmental remediation (through the detection of contaminated soils), and support for military operations (for the detection of man-made materials).

3.4 Thermal Infrared

Thermal anomalies of ground surfaces, recorded by infrared space images, can sometimes be an important indicator of earthquakes. Satellite images over a number of regions over China have been used not only to identify many active tectonic faults but also to establish a high correlation with the orientation of groups of earthquake epicenters. Thermal anomalies were identified in the regions of development of large earthquakes. Temperature anomalies of the ground surface have been detected, formed on the day before earthquakes were identified from both satellite observations and ground data. Phenomena preceding earthquakes may include the simultaneous development of thermal anomalies (on time scales from 2 to 10 days) and the accumulation of frontal cloud fields (appearing over 1 to 2 days).

Thermal phenomena potentially preceding earthquakes include gaseous emissions rising to the surface through faults and fractures. For example, it has been shown that a ring of clouds (of the smoke ring type) sometimes forms over seismically active regions during the few days before earthquakes. Such formations have been recorded over Central Asia in the Gazla region on the day before two powerful earthquakes in April and May of 1976 [32].

Volcanic eruptions are very dangerous and disruptive natural disasters, especially when they occur in densely populated regions. Thermal IR data have provided information as to the extent, direction and temperature of volcanic plumes, and can be used to estimate the energy of an eruption. The beginning of the explosive eruption of Mount St. Helens volcano (18 May 1980) was recorded by a spectrometer in the infrared band of the spectrum from USAF satellites. Observations of the aerosol cloud, which appeared a minute after the underground shock of the volcanic eruption, were taken simultaneously from two satellites, which made it possible to perform triangulation measurements. In this

way, it was possible to track successive stages in the development of the eruption. Furthermore, integration and analysis of thermal IR with optical and SAR data can not only identify recent but ancient lava fields as well, an important knowledge base when assessing the risk to populated areas adjacent to volcanoes.

Landsat TM classification has contributed to the generation of land cover maps, which separate the vegetation into homogenous species areas and/or delineate zones of different associations (e.g., conifer stands, chaparral, shrub, etc.). Integration of these maps with topographic data sets that reveal slope, elevation, aspect, soils and insolation, provide rapid assessments of fire-damaged areas. Additionally, the inclusion of other factors as moisture, water availability, wind speed and direction, potential sources of ignition, and fire history allowed the analysis and production of effective fire hazard maps and risk zones [33].

The TIROS-NOAA-9 weather satellite sensor was initially designed for day and night cloud imagery. Because of the thermal atmospheric sounder capability to correct data and taking into account the atmospheric absorption, the temperature of a hot pixel of 14 degrees over an area of 1 km x 1 km could be detected. The Advanced Very High Resolution Radiometer (AVHRR) is one of the instrument systems on board NOAA-9.

AVHRR NOAA satellites consist of a scanning radiometer with five spectral bands centered at 620 nm (band 1), 910 nm (band 2), 374 nm (band 3), 1080 nm (band 4) and 1200 nm (band 5, on NOAA-7 and NOAA-9). Ground resolution (pixel size) on the earth varies from 1.1x1.1 km^2 below the satellite to 1.5x4.0 km^2 at the edge of the 3,000-km swath. The satellites are at an altitude of 800 km in near-polar sun-synchronous orbits and pass in view of any point on the earth twice daily.

Nighttime scenes are easy to study with AVHRR infrared channels. One must take into account only the thermal radiance of viewed objects. Although the pixel resolution of the NOAA-9 AVHRR is 1.1 km x 1.1 km, it has been demonstrated that it's 3.7 μm channel can be used for power plant stress monitoring, as in the case of the Chernobyl nuclear accident [34]. Landsat TM is only of use if AVHRR channels 11 μm and 12 μm are used simultaneously using the split window technique to correct for atmospheric absorption.

The increased frequency of data acquisition by AVHRR, as well as its more attractive cost-accuracy relationship, makes AVHRR a good alternative to Landsat, especially when information is required over large areas. Combined analyses of AVHRR and aerial scanner data have proven useful for the study of critical variables of a forest fire in near- real-time [35].

Analysis of AVHRR sensor data was able to detect fires of subpixel size during the Los Angeles riots on April 29, 1992 [36]. Studies cited in [12] document the sensitivity of AVHRR for different types of fires, from forest and agricultural to industrial fires, including localized urban fires following the 1989 Loma Prieta, CA, earthquake.

Image processing of these data requires modeling to correct for variations in surface emissivities and atmospheric absorption due to water vapor and aerosols. The absorption is mainly due to smoke, the properties of which also differ according to the source of combustion, such as wood, plastic or other materials that may be typical of commercial or in-

dustrial construction materials). For example, different thermal behaviors are associated with flaming combustion of cellulosic fuels, glowing combustion, and the smoldering of roofing materials.

Real-time AVHRR imagery can provide a synoptic view of a disaster, using simple models of atmospheric absorption and surface emissivities. Such imagery could be of value to coordinate response efforts over larger geographic extents.

Fig. 11. This image of the city of Tokyo was acquired on March 22, 2000 with the ASTER Terra instrument; the image scene covers an area 13.5 by 19 km. The image displays three bands of the reflected visible and infrared wavelength region, with a spatial resolution of 15 m. It shows part of the Tokyo metropolitan area extending south to Yokohama. Included are the Ginza District, Haneda Airport and the Imperial Palace. [Image credits: NASA/GSFC/MITI/ERSDAC/JAROS, and U.S./Japan ASTER Science Team].

ASTER (Advanced Spaceborne Thermal Emission and Reflection Radiometer) is an imaging instrument that is flying on Terra, a satellite launched in December 1999 as part of NASA's Earth Observing System (EOS). ASTER will be used to obtain detailed maps of land surface temperature, emissivity, reflectance and elevation. The ASTER instrument was built in Japan for the Ministry of International Trade and Industry. A Joint US/Japan Science Team is responsible for instrument design, calibration, and validation. The primary objective for the ASTER mission is to obtain high spatial resolution global, regional and local images of the Earth in 14 colors (spectral bands). Resolution is 15 meter in visible to near infrared, 30 m in shortwave infrared, and 90 m in thermal infrared bands.

3.5 LiDAR

Light Detection and Ranging (LIDAR or lidar) uses the same principles as RADAR. A lidar instrument transmits light to a target. The light that is reflected/scattered back to the

instrument indicates properties of the target, while the time for the light to travel to the target and back is used to determine the range.

Lidar, laser radar, optical radar and ladar are all names used for "radar" systems utilizing electromagnetic radiation at optical frequencies. Wavelengths are 10,000 to 100,000 times shorter than those used by conventional radar. Laser radar can be continuous-wave (CW) or pulsed, focused or collimated.

CW laser radar is used when the signal may be integrated over long time periods and/or the target is nearby. Pulsed lidar are usually used for long-range remote sensing and when long signal integration is impractical. Pulsed laser radar use much higher power levels during the laser pulse than can be maintained with a CW laser.

There are three general types of lidar: range finders, DIAL and Doppler lidar. Range finders are simply used to measure range or distance to a target. Differential Absorption Lidar (DIAL) is used to measure chemical concentrations in the atmosphere (such as of ozone, water vapor, and airborne pollutants). Two laser wavelengths are used, where the molecule of interest absorbs one wavelength. The difference in intensity between the two return signals yields an indication of the concentration of the target molecule. Doppler lidar is used to measure the velocity of a target, including that of the wind (though the reflecting and scattering of dust and aerosol particles), following the well-known behavior of Doppler shifting.

Lidar *mapping* is an emerging tool in the airborne survey field that uses lidar to rapidly generate high-density, accurate, digital geo-referenced elevation data. Lidar mapping is also referred to as laser scanning, laser profiling, lidar scanning, lidar mapping, laser altimetry, laser swath mapping. The adjective "imaging" - as in *imaging laser altimetry* - usually refers to the simultaneous capture of intensity (reflectance) data with the elevation data.

Lidar is an excellent source of XYZ ASCII data for rapid digital terrain model (DTM) generation. Various ground-truth comparisons and evaluations of airborne laser-derived data by groups such as the USGS, US Army Corps of Engineers, FEMA and similar European groups confirm that the absolute accuracy of the Z (elevation) data is 15 cm. The absolute accuracy of the XY (planimetric) data is dependent on the particular operating parameters of the instrument but is approximately tens of centimeters to one meter.

Elevation data is generated at 10,000s of points per second, resulting in elevation point densities significantly greater than traditional ground survey methods. Commercial systems operate between 5,000 and 25,000 sample points per second. Grid spacing can be one meter or less resulting in data sets with high spatial resolution.

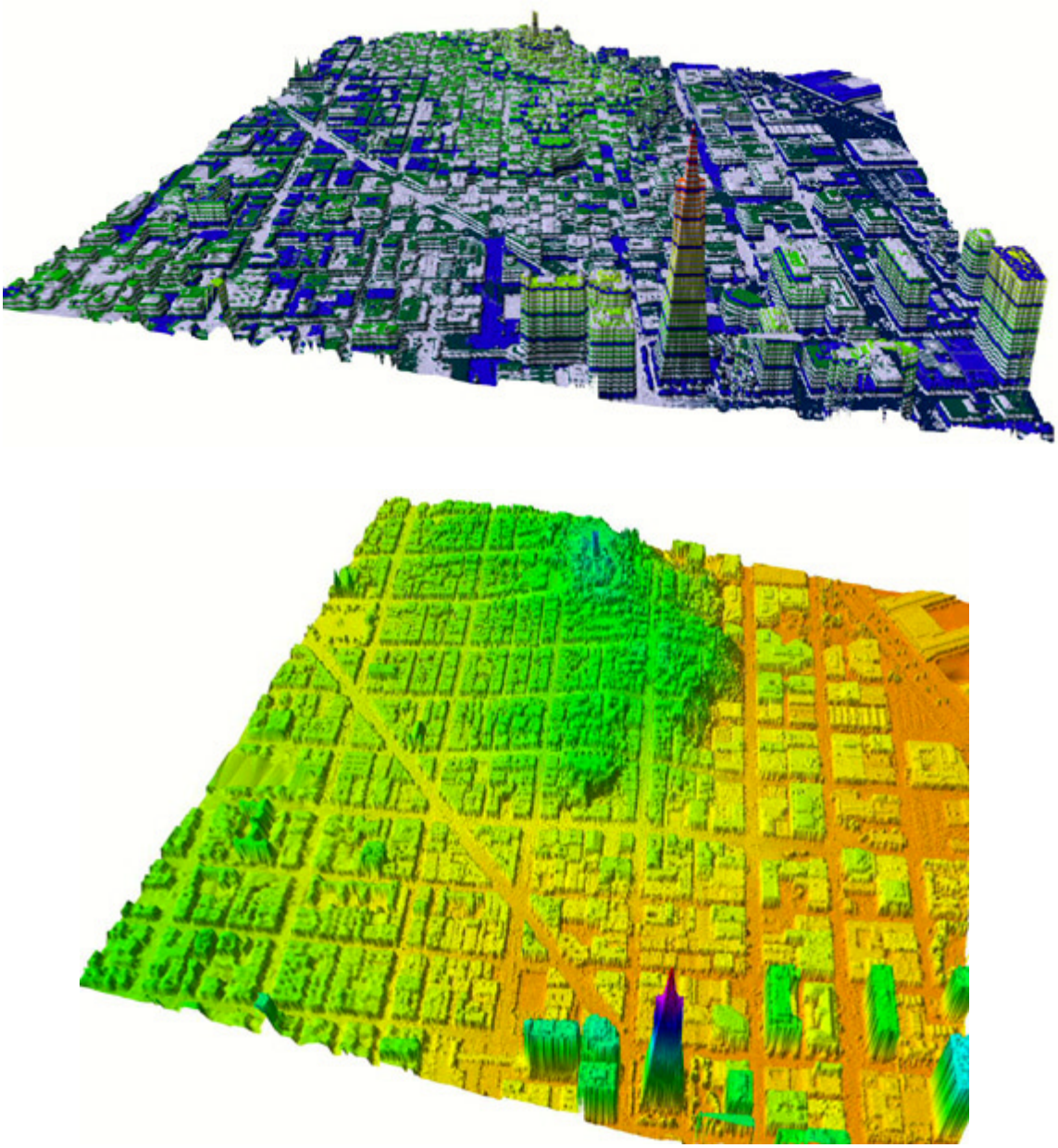

Fig. 12. LiDAR (laser) terrain mapping of San Francisco, CA, depicting two different contouring schemes by contour internal and color to indicate structures in detail or broader topographic features. Average point spacing is less than 1 meter and maximum RMS error is a few centimeters (see http://www.airborne1.com for more details of this and other DTM acquisitions in urban and vegetated areas).

Lidar mapping has faster turn-around times compared to conventional survey techniques due to rapid post-processing – of the order of tens of hours compared to tends of days for traditional methods. For example, one thousand square kilometers of hilly, forested terrain can be surveyed in less than 12 hours, with the geo-referenced DTM data available within 24 hours of the flight. A 500-km linear corridor, such as a section of coastline or a power line corridor can be surveyed in the course of a morning, with results available the next day (see http://www.airborne1.com for examples of lidar, projects and performance).

Lidar data acquired in the urban environment can be used for rapid terrain visualization in emergency planning and response, including line-of sight mapping for wireless communications systems and to map the extent of potential flooding. Further related applications include the mapping of access routes for emergency relief after a disaster, aircraft drop zones for relief supplies and other tactical decision support during response exercises, all relying on the real-time and interferometric capabilities of laser mapping.

As an example of the resolution provided by Lidar, a fly-through of a 1-m DEM collected over the City of Baltimore, MD, using the Optech ALTM airborne laser terrain mapping system flown by Airborne-l Corp. is contained in elevation and intensity files. Airborne laser mapping is described in more detail in a paper by Martin Flood , entitled "Airborne Laser Mapping."

NOAA's Coastal Services Center is using lidar technology, in partnership with NASA and the USGS, to document topographic changes along shorelines. Lidar mapping is used to collect topographic data along US coastlines to help scientists and coastal managers understand long-term erosion trends.

Awareness and adoption of lidar data as a standard deliverable is accelerating among end-user clients and contracting agencies but still not commonplace. Current users include a cross-section of private and public organizations covering a great variety of applications. The American Society of Photogrammetry and Remote Sensing (ASPRS) has established a LiDAR subcommittee of the Photogrammetric Applications Division (see http://www.asprs.org). Standards and independent calibration and verification guidelines are already under development. FEMA contractor guidelines are already published.

Capital costs to acquire an instrument, custom or commercial, currently range from $850,000 to $1,500,000 US with the commercial instruments at the higher end of this scale. Leasing and fractional ownership options are now becoming available. Service providers generally quote on a per project basis with substantial variation in pricing. A general rule is between $1 - $5 (U.S.) per acre.

The website http://www.airbornelasermapping.com provides a reference covering all aspects of the emerging technology of airborne laser mapping.

3.6 Synthetic Aperture Radar (SAR)

Spaceborne radar systems are classified as imagers, altimeters and scatterometers/spectrometers. Imaging radar are used to acquire high-resolution large-scale images

SAR Amplitude

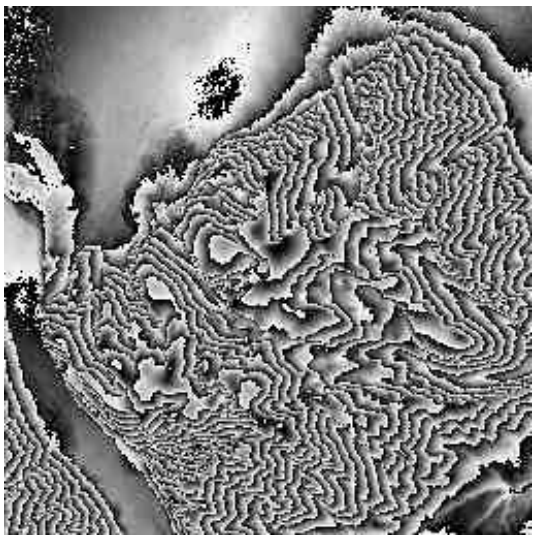

Phase Difference

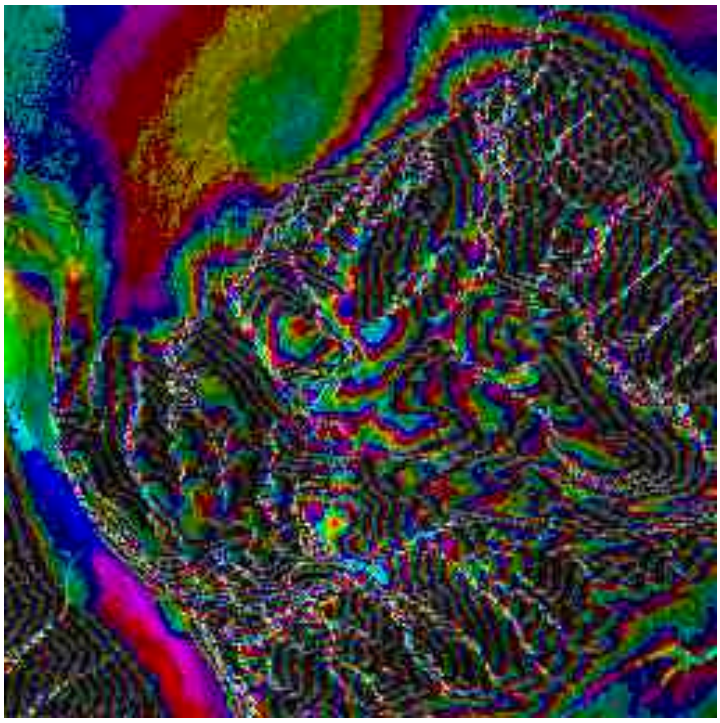

Interferogram

Fig. 13. Representation of the interferogram concept. Interferograms show differences in phase. By subtracting two signals, an interference pattern is generated. By subtracting the phases of two co-registered SAR images, an interferogram is generated. This phase difference is the result of a path length difference; elevation difference, motion or deformation can cause the path length difference. Hence, interferograms can be used to derive accurate elevation maps, monitor small motions, and detect tiny deformations. Often, interferograms are displayed by showing the phase difference as color, and the SAR amplitude as brightness. The phase of the above interferogram shows the topography of the imaged mountain. The phase can be converted into elevation if the two satellites have some distance, or spatial baseline between them.

of the earth's surface. Altimeters are used for surface height measurements, of both land and ocean, along the satellite track. Scatterometers and spectrometers are used to measure very accurately the surface reflectivity as a function of the frequency, polarization and illumination of the sensing signals and are used to characterize surface roughness [37].

Imaging radar provide synoptic images of the surface that are very similar to visible and infrared imagery. However, radar wave interactions with the surface are mainly driven by the physical properties such as slope, morphology, roughness and inhomogeneities, and by the electrical properties such as dielectric constant, absorption and conductivity of the surface, near subsurface and the surface cover.In order to achieve better range resolution on the ground, the imaging geometry of airborne or spaceborne radar antenna is such that it illuminates a surface strip to one side of the nadir track. In other words, a continuous strip of swath width S is mapped on the ground along the flight line. The swath width S is given by

$$S = \lambda h/W \cos^2 \Theta \quad (1)$$

where h is the platform height W is the width of the antenna (e.g. the dimension on the plane perpendicular to the platform track), and Θ is the look angle measured from nadir to the center of the radar beam). This equation is simplified and does not take into account the earth's curvature.

The range resolution corresponds to the minimum distance between two points on the surface that are separated by a distance X_r. Their respective radar echoes will be separated by a time difference Δt given by

$$\Delta t = (2 X_r /c) \sin \Theta. \quad (2)$$

A signal of bandwidth B yields a smallest discriminable time difference equal to 1/B. Therefore, if Δt is set equal to 1/B, the range resolution is shown to be inversely proportional to the signal bandwidth

$$X_r = c/2B \sin \Theta. \quad (3)$$

For example, radar with 20-degree look angle and 20 MHz bandwidth will yield a range resolution of 22 meters.

The azimuth resolution corresponds to the two nearest separable points along an azimuth line. Since this is also along a constant delay line, the azimuth resolution is equal to the antenna footprint and is given by

$$X_a = \lambda h/L \cos \Theta. \quad (4)$$

where L is the length of the antenna (e.g. the dimension on the place parallel to the platform track). For a spaceborne radar, for example, if λ is 3 cm, h is 800 km, L is 10 m and 20 degree, then X_a is 2.5 km.

Real aperture imaging leads an azimuth resolution that is linearly proportional to the distance between the sensor and the surface. A synthetic aperture technique therefore is used for higher resolution imaging. Real aperture imaging, however, is commonly used for scaterrometry and altimetry.

The signal-to-noise ratio (SNR) for a pixel element in the image determines the quality of the imagery acquired. It is directly proportional to the total power collected by the antenna and inversely proportional to the signal bandwidth and system noise temperature. A simple way of characterizing an imaging radar sensor is to determine the surface backscatter cross section that gives an SNR equal to one; the smaller this noise equivalent backscatter cross section, the more improved the SNR.

3.6.1 Synthetic Arrays

An array of antennae is equivalent to a single antenna moving along the array line provided that the received signals are recorded coherently (i.e. in amplitude and phase using an onboard stable oscillator) and then added. Assume that a radar sensor is moving at a velocity v and has an antenna length L. The length of the antenna main beam footprint on the ground in the azimuth direction is equal to

$$L = 2\lambda h/L. \quad (5)$$

The synthesized array will have a beam width equal to $\Theta_a = \lambda / L = L/2h$ and the resulting array footprint on the ground is $X_a = L/2$. This has significant implications:

- The higher the altitude of the sensor, the larger the footprint on the ground and thus the longer the synthetic array, given by L, and a therefore a finer synthetic beam.
- Similarly, the smaller the antenna L, the larger the footprint on the ground and thus the longer the synthetic array, given by L, and a therefore a finer synthetic beam.

3.6.2 Measuring Topography

Measuring surface topography is usually achieved by stereo imaging, basically requiring that two images of the same surface area be acquired from two different locations. Topographic imaging from stereo images must be done on a pixel by pixel basis, and leads to the generation of a contour map or a digital topographic map or database.

Consider a sensor platform at altitude H, and a point on the surface at height (i.e. topography) h. Let r_1 represent the range from point h to the sensor at time t_1 and r_2 the range from point h to the sensor at time t_2. Let X represent the horizontal distance from point h to the nadir projection of the sensor at t_1. The two range measurements to the same surface feature is simply a system of two equations and two unknowns, namely the quantities X and h.

Existing satellite-based SAR systems lack the spatial and height resolution for urban applications, although their capabilities for ground deformation monitoring have been demonstrated and are ongoing in certain geographic areas. Over the next two-to-five years, planned systems will provide high-resolution data commercially. Outside of the US, commercial airborne SAR systems are planned for Japan, Europe, and elsewhere, although not all of them will be capable of interferometry.

Sources of airborne interferometric synthetic aperture (InSAR) data are marginally adequate for assessing the capabilities of InSAR for urban applications. TOPSAR data, for

example, are available over the Los Angeles Basin at a 5 m posting and are well understood; software for processing and analysis readily available. Additional higher resolution data sets are available for other locations from the Environmental Research Institute of Michigan (ERIM) and Sandia National Laboratory.

An airborne InSAR system can collect imagery and elevation data at a rate of 100 km^2 per minute and produces digital terrain models (DTMs) at near-real time with better than 3 meter accuracy on a 2.5 meter grid. Higher accuracy can be generated with limited supplementary ground control [38]. An InSAR forms two images simultaneously from two antennae slightly separated in cross track. Images are accurately registered and phase differences between corresponding pixels measured to create the 3-D data model. Other cartographic products, such as contours, may be generated from the DTM and imagery.

Urban change detection requires repeat passes by aircraft or spacecraft over the time interval of interest. High-resolution, low-amplitude deformation can be monitored using repeat pass interferometry (RPI) from spacecraft (an analysis of a demonstration of RPI from airborne SAR is given in [39]). L-band is required to reduce decorrelation due to vegetation. Larger amplitude changes, such as due to building construction or post-disaster building damage could be assessed by comparing pre- and post- event InSAR imagery. Co-registered panchromatic multispectral data are useful for verifying the areal extent of buildings and, in some cases, their heights.

Table 3 summarizes the capabilities of InSAR for urban applications. Accurate spatial and height resolution of man-made structures and the ability to distinguish structures from ground clutter (trees, vegetation, etc.) and image noise are of primary importance. Current airborne cross-track interferometric (XTI) SAR systems can resolve features at the 2-15 meter level, depending on the system frequency, bandwidth, and desired signal-to-noise ratio, with height accuracy of less than one meter and up to several meters. Horizontal resolution is inversely proportional to bandwidth, while vertical resolution is a function of noise (thus frequency) and other factors, such as incidence angle. Higher bandwidth, higher frequency systems are preferable for urban studies, although many other factors contribute to the final resolution capabilities.

Capabilities exist for broad land use characterization [40]. Based on relative building heights and their spatial distribution, regional land use classifications can be segmented into distinct regional structure classes. Land use is a key link between image interpretation and physically characterizing risk. Each classification will represent a comprehensive urban land use describable by its physical properties and remote sensing attributes.

Building material investigations are at a much more preliminary stage; additional theoretical work, as well as data collection and analysis, are required. SAR techniques could yield data on the physical properties of building surfaces, such as their roughness and reflectivity (e.g., brightness as a function of azimuth angle). SAR combined with optical techniques could provide information about the small-scale construction details of buildings, or the thermal inertia of buildings and their retention of rainwater on surfaces. Multispectral and hyperspectral optical and infrared sensors could help to identify the building materials themselves, or, at the least, to broadly classify building construction types.

Table 3. Urban Studies and Change Monitoring Radar

Feature	Horiz. Res. (m)	Precision / Accuracy (w/ units)	Instruments and Techniques
Building Shapes			
Height	1 - 10	<1 - 3 m	XTI InSAR (X or C band), > 40-80 MHz
Area	1 - 10	10 sq m	InSAR (X or C band), optical
Volume	1 - 10	30 cu m	InSAR
Base topography	50 - 500	1 - 5 m	Dual frequency InSAR (X/C, L- and P-band)
Classification			
Regional Usage	100 - 1000	5-10 classes, 95%	InSAR, PolSAR, optical
Regional structures	50 - 500	10-15 classes, 80%	InSAR, PolSAR, optical
Individual structures	5 - 50	>20 classes, 75%	InSAR, optical
Change Detection			
Construction and demolition	1 - 50	1 - 5 m	Difference InSAR, optical images
Ground deformation	10 - 1000	0.1 - 5 cm	L band, short baseline repeat-pass interferometry (RPI)
Erosion	50 - 500	1 - 50 cm	L band, short baseline RPI
Post-disaster	10 - 500	10 classes, 95%	Difference InSAR, L-band RPI
Surface Materials			
Physical	1 - 5	5-10 classes, 70%	Multi-frequency SAR, PolSAR, optical/IR
Chemical/Spectral	1 - 5	5-10 classes, 70%	Multispectral optical/IR

One of the most important features of any interferometric radar is its ability to acquire range and phase data of sufficient accuracy to be used in the production of digital terrain products. The accuracy of these products is largely a result of being able to precisely determine the position and length of the antennae baseline. Systems that rely on two aircraft or multiple satellite passes have difficulty controlling and determining this baseline.

For example, RADARSAT (http://www.rsi.ca) must either employ two orbits or use two points on a single orbit to form SAR images from which to extract height data either using interferometric techniques or SAR stereo photogrammetry. Since these data sets are separated in time by minutes or hours, scene decorrelation occurs and the baseline is not accurately known. These error sources mean that the data from two pass systems will not be as accurate as with a single pass system. Also the elevation accuracy of two pass data will be variable due to uncontrollable baseline changes, random scene decorrelation and observation variations.

4. Remote Sensing of the Urban Environment

Various airborne and spaceborne remote sensing sensors are currently in operation or planned for the near future. Each offers different advantages and capabilities. For applications in loss estimation, remote sensing must be capable of addressing the specific information needs for risk assessment and vulnerability analyses associated with the built or urban environment. These needs are the focal point of this report and are considered in detail in this Section.

Remote sensing of urban areas can be undertaken with optical, multispectral and hyperspectral sensors, laser imaging radar (LIDAR), and synthetic aperture radar (SAR) systems. Recent research points out the need for multi-band data registration and fusion using various sensors and ancillary data sources, such as census data and thematic maps. Spatial resolution of less than 5 meters is required for the extraction of urban geometrical patterns [41]. Otherwise, imagery does not provide value in terms of quantitative information extraction and thus are of little marginal benefit in risk assessment, mitigation and response planning activities.

No one is currently developing quantitative databases of the built environment by extracting information from remote sensing imagery. Aerial photography was incorporated into the inventory process in a study of Boston, Mass. [42] and Wichita, Kansas [43]. Satellite images, low-level aerial photos and street-level photos were used in a wind modeling study of Sacramento, CA [44]. Landsat TM and SPOT image data were used in conjunction with ERS-1 SAR image data to improve land use classification and feature identification over a mixed urban and rural area [45]. SPOT image data also were used to determine the heights of forty tall urban buildings by measuring length geometrically [46].

4.1 InSAR and the Urban Landscape

InSAR data are processed to produce three data layers [47]: radar intensity image of the scene, corresponding correlation, and height map. The production of urban height layers is carried out in two steps:

1. Production of an InSAR-derived background topography layer;
2. Production of a residual height distribution layer (InSAR reported height layer minus the topography layer).

Interpretation of the InSAR measurements over urban areas is complicated by the interaction of the radar signal with the urban environment. The returned radar is, in general, a coherent sum of direct returned signal plus signals which have undergone a number of reflections from the neighboring structures. The characteristics of returned signals are dependent on the radar frequency, polarization, and the scattering nature of the areas illuminated. In addition, for urban areas, the scattered radar signal is dependent on the geometry and the material properties of the buildings and the neighboring environment.

As an example, consider the situation of a hypothetical flat-topped building as an isolated target object.

- Shadows are created at the trailing edge of the building, wherein at 45- degree incidence angle the shadow length is the approximate height of the building.
- The unrectified shadow interface with the building is displaced toward the radar.
- Layover (i.e. the region on the ground where the building first interacts with the radar incident wave front) would probably cause elevation information to be lost, depending on the relative magnitudes of the scattering cross-sections of the foreground, near-side and top near-side of the building. At 45-degree incidence angle, the horizontal uncertainty is approximately equal to twice the height of the building.

Noise-reduction filters normally smooth the phase and have the effect of averaging over step function height discontinuities, and the phase unwrapping in response to step-function phase changes will impact derived elevations.

By modeling the interaction of radar signals with a realistic urban environment, one could investigate the possibility of discriminating the building materials directly from the InSAR radar intensity layer and correlation layer. For example, modeling, based on well known high frequency electromagnetic methodology [48; see also 49] can be directed towards the segmentation of trees from buildings of similar size in order to produce building shapes by employing a template matching filter to the residual height map.

Table 4 lists GIS layers that would be produced by the automated InSAR and multispectral processor. Spatial requirements to be specified are the areal coverage of contiguous scenes, pixel spacing and resolution, height resolution, scene dimensions and ground track separation. The accuracy of classification is dependent on radar incidence angle, frequency, polarization, and the orientation of urban features with respect to the imaging radar. For aircraft systems, the radar incidence angle variation can be as large as 40 degrees, which significantly affects the scattering properties of the geometrical structures, and adds to the complexity of the classification of urban areas.

The radar incidence angle for a space platform is limited due to higher altitude with respect to the area of coverage. For example, aircraft InSAR platforms are operated at 10 km altitude as opposed to 800 km for ERS-1 and 570 km for JERS-1) and the incident angle variation is about 6 degrees so that scattering sensitivity is greatly resolved.

Airborne hyperspectral data also can provide valuable information for InSAR DEM interpretation. An important aspect of sensor fusion is the spatial resolution. Both radar reflectance and interferometric characteristics can be used to formulate decision rules for categorizing pixels unclassed by the hyperspectral analysis.

A model for the InSAR measurements over urban areas must be developed for interpreting the intensity, correlation, and height maps data layers. Modeling would also consider the possibility of discriminating building material from InSAR measurements, higher resolution building discrimination and separation of manmade structures from trees of similar size.

Table 4: Select Product Layers and Processing Applications

GIS Product Layer	*Processing Application*
Multispectral imagery	
Vegetation cover mask	Classification and InSAR filter
Building pattern (2D), transportation routes	Radar masking, urban mapping
InSAR imagery	
Height error	(Automated processor sub-layer)
Radar brightness and correlation	Discrimination of building materials
Background topography, surface gradients	Digital terrain mapping
Vegetation cover	Classification, moisture content, fire risk
Pattern/shape recognition (2-D)	Usage and occupancy type
Pixel height sub-layer	Maximum building height estimate
Height distribution sub-layer, resid. heights	Imaging extent of structures, codification
Co-registered InSAR and optical/near-IR	
Built environment classification	Vulnerability analysis
Aggregate material properties (e.g. roof types)	Risk assessment and valuation
Surface roughness and dielectric properties	Material and construction type modeling

Table 5. Select Urban Applications of Radar Remote Sensing [50]

Feature	*Horiz. Resolution (m)*	*Precision / Accuracy*	*Instruments and Techniques*
Height	1 - 10	<1 - 3 m	XTI InSAR (X, C band), > 40-80 MHz
Area	1 - 10	10 sq. m	InSAR (X, C band), multispectral
Volume	1 - 10	30 cu m	InSAR
Base topography	50 - 500	1 - 5 m	Dual frequency InSAR (X/C, L/P band)
Regional Usage	100 - 1000	5-10 classes, 95%	InSAR, PolSAR [51], multispectral
Regional structures	50 - 500	10-15 classes, 80%	InSAR, PolSAR, multispectral
Individual structures	5 - 50	>20 classes, 75%	InSAR, multispectral
Physical properties	1 - 5	5-10 classes, 70%	Multi-freq. SAR, PolSAR, optical/NIR
Chemical/Spectral	1 - 5	5-10 classes, 70%	Multi-frequency, multispectral/IR

Development and demonstration of an automated InSAR and multispectral processor for urban land use classification would help to:

- Improve the information content of databases for inferring aggregate valuation of building inventories;
- Assess the exposure of the built environment to natural hazards.

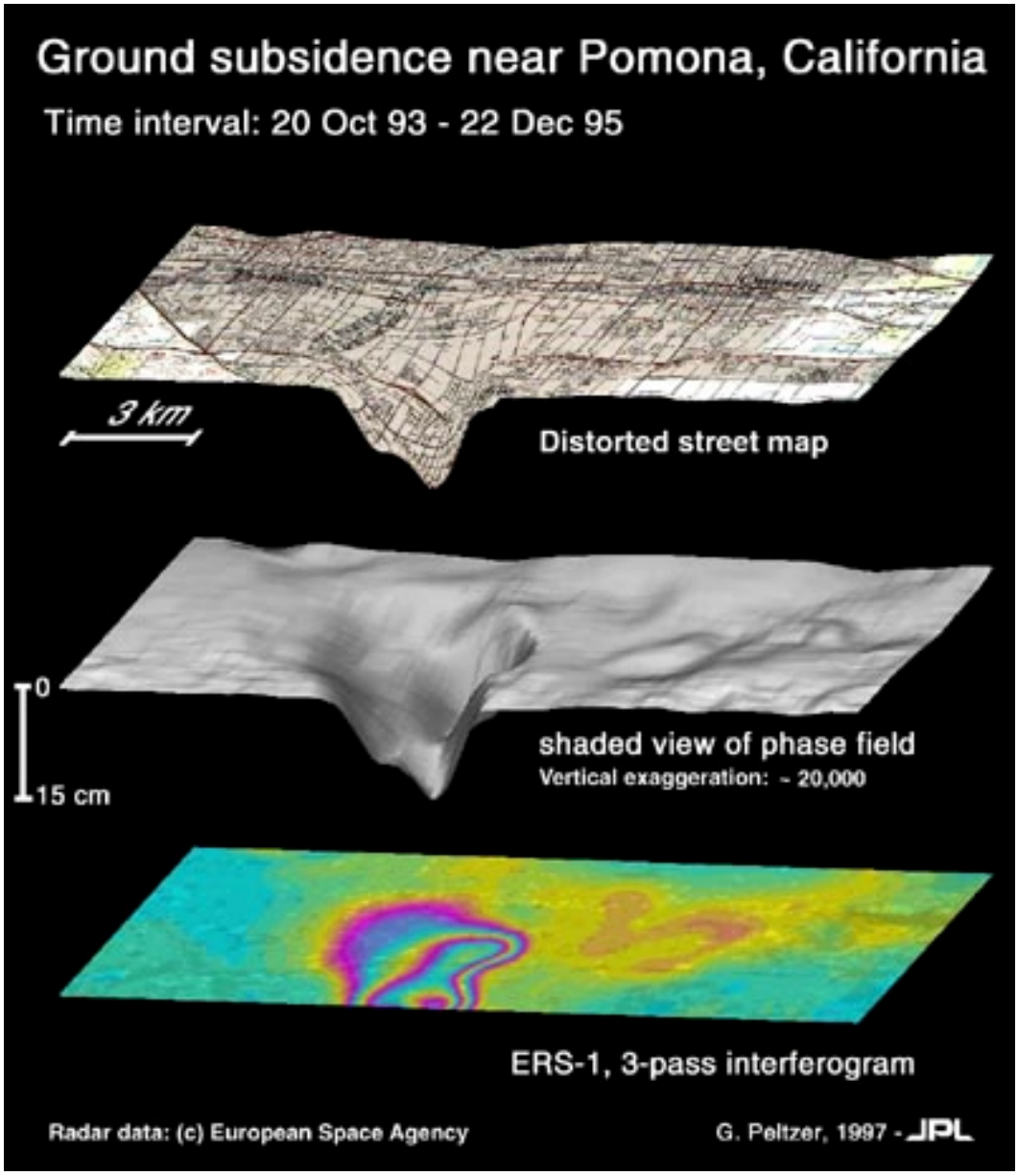

Fig. 14. Ground subsidence in the Pomona, Los Angeles Count area. Bottom: Bird's eye view of a detail of the ERS-1, 3-pass interferogram shown above. The colors depict the displacement of the ground along the radar line of sight (23 degrees off vertical) having occurred between October 20, 1993 and December 22, 1995. One color cycle represents 5.6 cm of range displacement. Center: Shaded view of the radar phase field displayed with 20,000 vertical exaggeration. Top: Distorted USGS street map wrapped on phase field. Ground subsidence in the Los Angeles basin is usually associated with oil or water withdrawal. This particular example shows the surface effect of a deficit in water over a two-year period in a densely populated area.

Technical objectives that would have to be addressed include:

- Advancing electromagnetic scattering model capabilities to improve building height measurements;
- Developing building height information extraction algorithms from InSAR data;
- Using multispectral data to improve radar-based characterization of the urban environment;
- Developing building material classification layers from remotely sensed multispectral data.

The InSAR-derived height map layer contains the overall elevation information for the radar-illuminated areas. The heights are reported with respect to a reference elevation plane at the aircraft nadir. The reported heights are dependent on the ground geometry. Roof top heights are reported as the building heights, and ground level heights are reported for open fields, parking lots, parks, etc. Heights reported for trees can vary from the top canopy height to the ground level de-pending on the operating frequency, polarization, and tree density, and structure.

The objective of background topography removal is to provide an elevation map layer of the covered area without the presence of manmade objects in addition to the treetops. The corresponding algorithm should minimize the number of computations to reduce the processing time and computer resource requirements because the amount of height data that are processed for a typical radar scene is very large. This background topography layer can be used for a number of applications such as urban planning, geologic hazard assessment and hydrology studies (see example in Fig. 14).

The information contained in the residual height layer is pixel-based as well as spatial. For example, each pixel representing a building is surrounded by pixels of similar vertical height. This is a spatial attribute that can be used to distinguish the pixels representing buildings from isolated pixels with large vertical heights that might represent trees, electric posts, or interpolation artifacts.

An important consideration in computing the urban height layer is the size of the area over which the height distribution is produced. Segmentation should be sensitive to the variations of the urban environment such as the differences between a residential and a commercial area. Larger areas, of the order of several square kilometers, typically consist of a mixture of a number of urban classes. Small areas, of the order of 100 square meters, are too small to provide a statistically robust distribution of urban classes and will be very sensitive to the boundaries.

4.2 Integration of Radar with Optical and Hyperspectral Data

Preliminary studies with currently available sensors suggest that the best characterization of the built environment from remote sensing product layers will be achieved by integrated analysis of both radar and hyperspectral visible-to-near IR data (VNIR). Radar provides the ability to measure the height of buildings, and the subjacent general topography, in greater detail than any other remote method over a wide geographic area. However, the radar method can be confounded by the presence of trees, and also by unusual

building configurations. Both of these problems can be addressed through judicious analysis of multispectral image data.

Radar is especially sensitive to the topography, roughness, and electrical properties of the surface imaged. Used interferometrically, radar can provide very high-resolution information on surface heights. It may be possible to extract electrical properties of imaged materials in this fashion as well. Conversely, visible and near infrared sensors principally are sensitive to material reflectivity and composition. Since radar and multispectral sensors measure very different physical phenomena, using both portions of the electromagnetic spectrum provides substantial additional information.

In the case of currently available satellite image data, such as Landsat Thematic Mapper (TM) or SPOT, many classes of surface cover types can be extracted. More detailed analysis can disclose the distribution, character, and health of vegetation, producing a class of vegetative cover layers. Many material types can be discriminated (as opposed to directly identified) in this type of data. Discrimination may not be much of a handicap in an urban environment as the number of material classes is relatively restricted. Combination of the material discrimination capabilities of the multispectral data with the potential electrical properties extraction from radar data may be a powerful technique for characterizing buildings and inferring corresponding material and construction types.

The key to successful identification of pixels containing significant vegetation lies in capitalizing on the highly reflective nature of green vegetation. This reflectivity is higher in the near-infrared portion of the electromagnetic spectrum compared to the visible red portion. Previous work that indicates the potential of analyses of this sort includes the following. Weydahl et. al. [52] used Landsat TM and SPOT image data in conjunction with ERS-1 SAR image data to improve land use classification and feature identification over a mixed urban and rural area. They indicate that the combination of multispectral and SAR data resulted in:

- Improved ability to identify the nature of the land use;
- Ability to identify particular features;
- Inference of certain different roofing material types.

Information on imaging spectroscopy for classification of materials can be obtained at the USGS Spectroscopy Laboratory website http://speclab.cr.usgs.gov/.

Burkhart et al. [53] indicate the need for "tree recognition and extraction" in order to construct proper digital elevation maps (DEMs) from SAR data. The strong signature of green vegetation in multispectral data would seem to be an obvious way to address this problem.

Cheng and Thiel used SPOT image data to determine the heights of forty tall buildings in an urban environment by measuring the length of geometrically [54]. The process was not automated, and also does not appear to be readily amenable to automation since precise identification of a shadow is easy for a human interpreter, but very difficult to do algorithmically. However, the ability to produce building outlines, and other feature out-

lines, is obviously of great advantage in a system which incorporates both multispectral and SAR data.

Two additional benefits that are afforded by the multispectral data sources are global availability and long-term temporal coverage. The SPOT and Landsat satellites fly in near polar orbits, so the entire world is available for imaging. Although the resolution is inadequate for identification of buildings, basic classification of the urban environment is possible from Landsat Thematic Mapper (TM) data, which is available from 1982 to the present. SPOT (http://www.spot.com) also now provides a product called "LandClass" which discriminates and identifies up to 18 different land cover categories (but not building height). SPOT data are available from 1986 on, in both the high-resolution panchromatic mode (10 m) and the multispectral (20 m) mode. Individual buildings can often be discerned in SPOT data, particularly in merges of the panchromatic 10-meter data with the 20-meter multispectral data.

Capabilities already exist for broad land-use characterization with radar [55]. Based on the relative building heights (measured height minus ground height) and their spatial distribution, these regional land-use classifications can be broken down into more distinct regional structure classes. Polarimetric SAR and multispectral data could provide additional classification parameters.

Production of an urban change detection layer requires repeat passes interferometry (RPI) by aircraft or spacecraft over the time interval of interest. High-resolution, low-amplitude deformation (e.g., seismically induced ground motions) can be monitored RPI from spacecraft. L-band is required to reduce decorrelation due to vegetation. Larger amplitude changes, such as building construction or post-disaster building damage could be assessed by comparing pre- and post-event InSAR imagery.

The 1995 Hyogoken-Nanbu earthquake damaged large parts of urban Kobe, Ashiya and Nishinomiya cities. ERS-1 intensity maps from before the earthquake indicated urban structure. This was not the case with images after the event. Norm type correlation coefficients of data pairs between the before and after indicated decorrelation at damaged urban areas. The areas where the backscatter correlation changed significantly before and after the earthquake correspond to damaged built-up areas observed by aerial photographs [56].

Satellite receiving and processing systems are becoming more portable and affordable. The launch of high-resolution optical sensors, the growing interest in commercial radar satellites, and the growth of the value-added sector are creating demand for lower cost yet capable ground station systems. A ground station provides for direct data acquisition through satellite downlink privileges, and processed image products such as orthorectified (creating map-registered output images with the geometric distortions removed), stereo (such as a SAR processor generating a digital terrain height model from a pair of images) and interferometric images.

5. Integration of Remote Sensing with GPS

In recent years, InSAR has demonstrated significant potential to map crustal strain. However, the small movements involved (e.g. 1-2 mm/year) are often outside the system's spatial or displacement resolution. Furthermore, subtle changes in the land surface, even changes in foliage or soil, can result in decorrelation particularly at short microwave wavelengths. For this reason, L-band SAR (at 10 m resolution or better) is preferable, though lengthening the wavelength degrades displacement resolution accordingly.

Significant challenges need to be overcome before reliable deformation measurements can be made on a routine or operational basis. One promising approach is to use ground GPS surveys in combination with InSAR not only such that the techniques complement each other but so that GPS can "calibrate" out errors in InSAR. There have been recent developments, and experiments are ongoing, in methods to overcome these shortcomings of InSAR, particularly through the use of both man-made and natural reflectors. Such reflectors would remain "coherent" over many years, allowing detection of the correspondingly large displacements.

Continuous GPS data can be used to reduce two error sources in determining ground displacements with InSAR:

- "Baseline" or orbital errors – by placing radar reflectors and transponders at GPS sites. The SAR data covering these points will correspond to a precisely located point and could be used to provide three-dimensional control on the spacecraft orbit and improve the accuracy of the ground displacement measurements.
- Tropospheric propagation errors – GPS stations can be used with mesoscale models to map the spatial and temporal distribution of water vapor. Temporal variations in the horizontal gradients of line-of-sight integrated water vapor, if not properly calibrated, can produce artifacts in the radar displacement fields with magnitudes of ~ 1 cm.

A 20% spatial or temporal change in relative humidity is estimated to cause between 80 and 290 m of topographic error for baseline between 400 and 100 m [57].

Regional atmospheric effects corresponding to long-wavelength ionospheric perturbations, and differences in the hydrostatic component of the troposphere manifest themselves as a planar phase trend in an interferogram [58]. If these regional effects are not removed, they will produce a constant offset in the phase gradient map that could be interpreted as a regional tilt [59].

Topographic phase-corrected interferograms may contain atmospheric error artifacts. Short-wavelength atmospheric artifacts could be confused with small-scale tectonic deformations. These artifacts have typical length scales of the order of 5-10 km and can cause as much as 10 cm of excess two-way path length (three interferogram fringes) [60, 61, 62].

There are two approaches to reducing DEM errors due to atmospheric changes [63]. One approach is simply to select interferometric pairs that yield the smallest atmospheric ef-

fects, by comparing interferometric heights to a lower resolution DEM or by comparing interferometric DEMS themselves. The second approach is to average several interferometric datasets, at the unwrapped phase stage if they are from the same track or at the geocoded DEM stage if they are from different tracks.

Height above sea level is the usual reference used for topographic height information. The continuation of sea level below the land mass provides a surface called the geoid. The geoid is the proper reference surface for heights above sea level (i.e. orthometric heights) and is the basis for topographic maps. Heights determined by GPS, on the other hand, refer to the surface of an ellipsoid. The reference ellipsoid (e.g. WGS85) is a geometric rather than s physical surface. While the ellipsoid is a good approximation to the geoid on a global scale, deviations may reach 100 m. Differences between a reference ellipsoid and the geoid are called geoid undulations, which are sufficiently small to ignore over small test areas.

DEMs generated by InSAR that uses DGPS for system positioning refer to ellipsoidal heights. Knowledge of the geoid in the image area is therefore required in order to provide mapping products in an orthometric height systems.

InSAR data can be combined with gas, oil and waterhole extraction records, and borehole water level measurements to estimate the rates and spatial extent of human-induced motion. Other parameters that can be modeled to separate tectonic from human-induced movement include porosity, elasticity and compaction of soil.

GPS measurements and InSAR images can be combined to help constrain significant postseismic rebound in both horizontal and vertical directions. Both data can be used to study whether rebound is due to continuous time-dependent afterslip at depth or due to viscoelastic flow below seismogenic depths.

For three to five years following the 1989 Loma Prieta earthquake, surface creep slowed or ceased on much of the southern Hayward fault [64]. The long-term slip rate in the southern section is along 9 mm/yr. Available geodetic data do not provide the resolution needed to discriminate between models of uniform creep and a partially locked fault. Not knowing the extent of creep and locked portions of the Hayward fault yields uncertainty about the potential for future earthquakes, their magnitudes and probabilities.

Field observations [creepmeter and alignment array measurements] only measure horizontal strike slip. These observations of strike-slip faulting along the Hayward were combined with InSAR measurements to identify an accompanying vertical slip component, as follows. A sharp phase offset was noted along the trace of the actively creeping Hayward fault that suggested a component of surface fault displacement in the satellite range direction. However, a fault scarp could produce such a range change in the interferogram if topographic effects are not carefully removed [65].

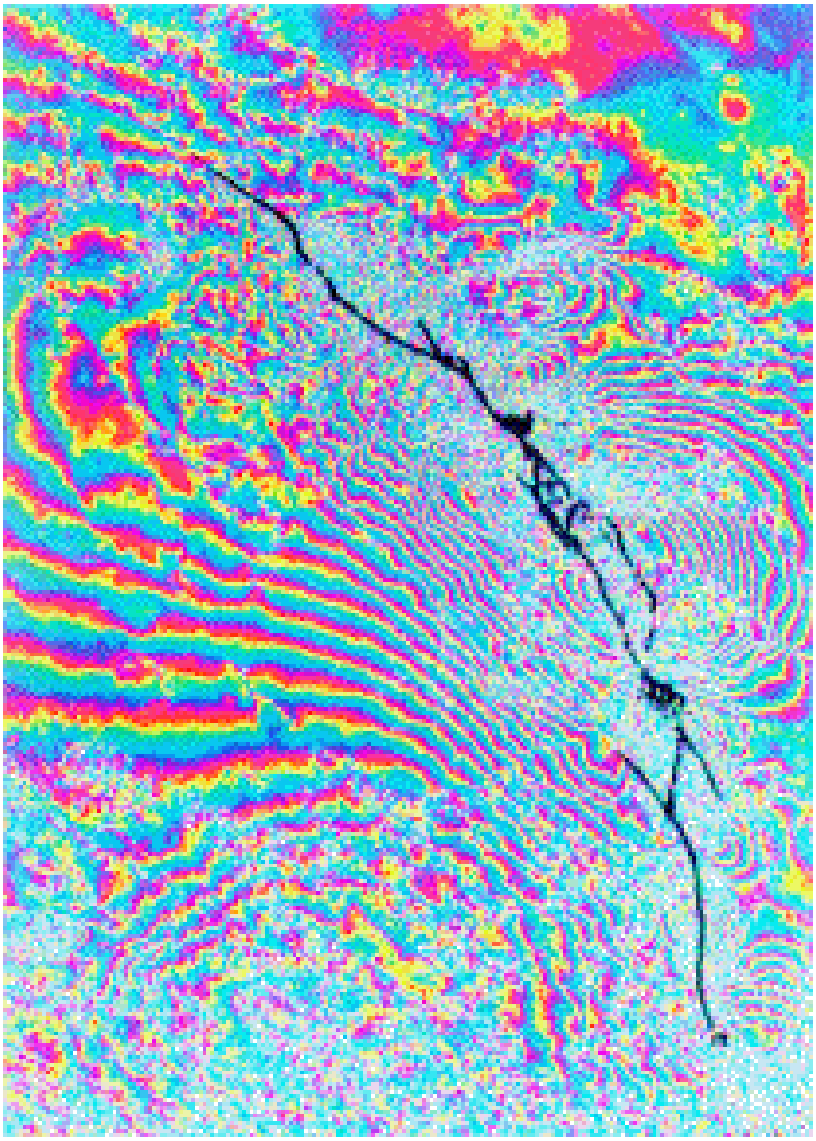

Fig. 15. Differential interferometry can be astonishing in its precision, as is illustrated by measurement of the coseismic displacements caused by the Landers earthquake in California (Massonnet et al., 1993). Development of an ability to measure pre-cursors to significant seismic events is a principal aim of SAR interferometry; this would have important implications for earthquake prediction.[66].

Repeat-pass interferometric SAR can not accurately measure interferometric phase differences in:

- Areas that are decorrelated because of steep topography;
- Areas where motion has exceeded one phase cycle across a single pixel (using ERS-1 data, one phase cycle in the interferogram corresponds to 28 mm of apparent range change between the satellite and the earth's surface);
- Areas where significant changes have occurred in surface properties (i.e., changes in vegetation, structures).

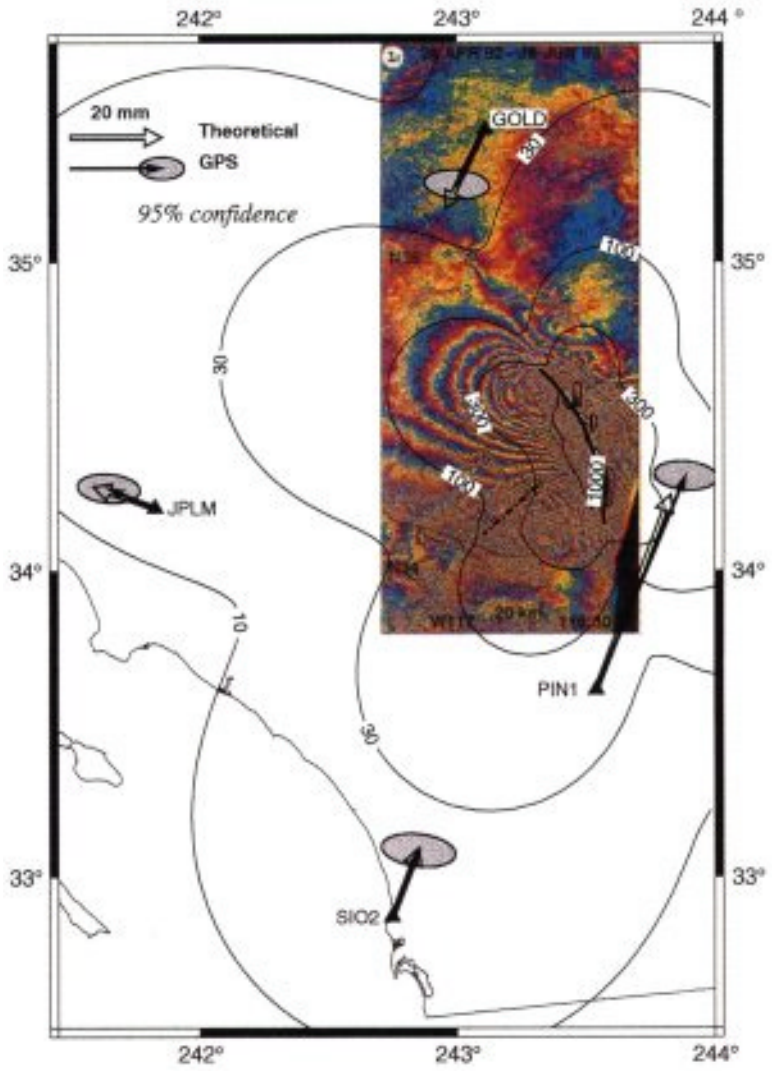

Fig. 16. Comparison of GPS-determined vector displacements and InSAR.

Slip rates estimated from InSAR were compared, in this case with field measurements of horizontal offset perpendicular to the fault trace, and corresponding to the InSAR observation period, thus identifying a vertical slip component.

Without such complementary field observations, the InSAR data could very easily be misinterpreted as indicating very high strike-slip rates. Transient (geologic long term dip-slip estimates are much smaller along the southern Hayward fault) vertical-slip of 2-3 mm/year was identified, with the northeast up (thus the enhanced offset in the radar range direction of the interferogram.

Analysis of two JERS-1 SAR images collected 1.5 years apart, before and after the January 17, 1997 Kobe earthquake indicate about 58.8 cm displacement of the area around Kobe in a direction towards the satellite and about 105.8 cm displacement away from the satellite at Awaji Island [67].

The tradeoff between viscosity and afterslip in a weak layer of the fault plane at depth is nearly linear. For example, GPS measurements following the 1992 Landers earthquake suggested lower viscosities and thinner weak zones than InSAR images.

Similarly, GPS measurements obtained after the January 17, 1994, Northridge earthquake indicated significant aseismic deformation, with an estimated 22% of the mainshock moment release. An analysis of InSAR data the spanned the earthquake and two years of postseismic deformation was then studied. A synthetic phase field was removed based on inversion results performed by Wald and Heaton (1996). Clearly, the residual between GPS and InSAR includes mismodelled coseismic motion in addition to the postseismic deformation. Preliminary comparison between the range change observed at GPS stations by both data sets showed excellent agreements. However, the deformation (estimated from seismic moment release) summed over several aftershocks accounts for only a small percentage of the geodetically observed deformation. This suggests significant aseismic deformation over the observation period.

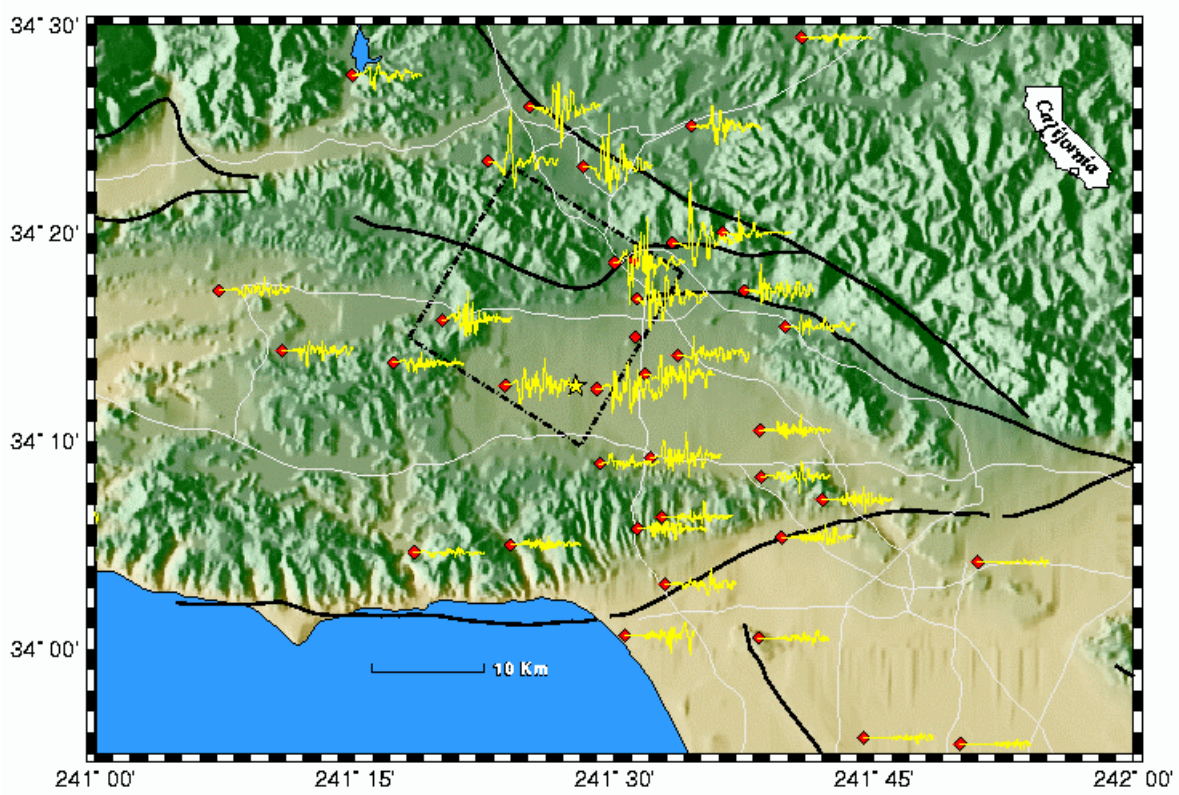

Fig. 17. Map view of Northridge fault plane (dashed rectangle) projected to the surface. Yellow lines are recorded ground velocities at the recording site (red diamonds). All seismograms are on the same scale. Epicenter is shown with a yellow star. [Image courtesy: USGS].

InSAR-GPS integration was first suggested [in print, at least] in 1997 [68], wherein InSAR, GPS and results of dislocation modeling of the 1992 Landers earthquake were superimposed.

A quasi-observation approach to joint inversion of InSAR and GPS is presented in [69]. Firstly, various types of geodetic data were analyzed to form the loosely constrained quasi-observations. Secondly, a Kalman filter was used to combine these loosely constrained, quasi-observations to obtain a loosely constrained, global solution within a uniform reference frame. Thirdly, *a priori* knowledge was utilized to impose constraints on this solution to derive more reliable estimates of the deformation field. Coseismic and postseismic deformations were either estimated explicitly or treated as stochastic perturbations. An iterative approach was used to obtain the optimal separation of the secular motion, coseismic and postseismic deformation.

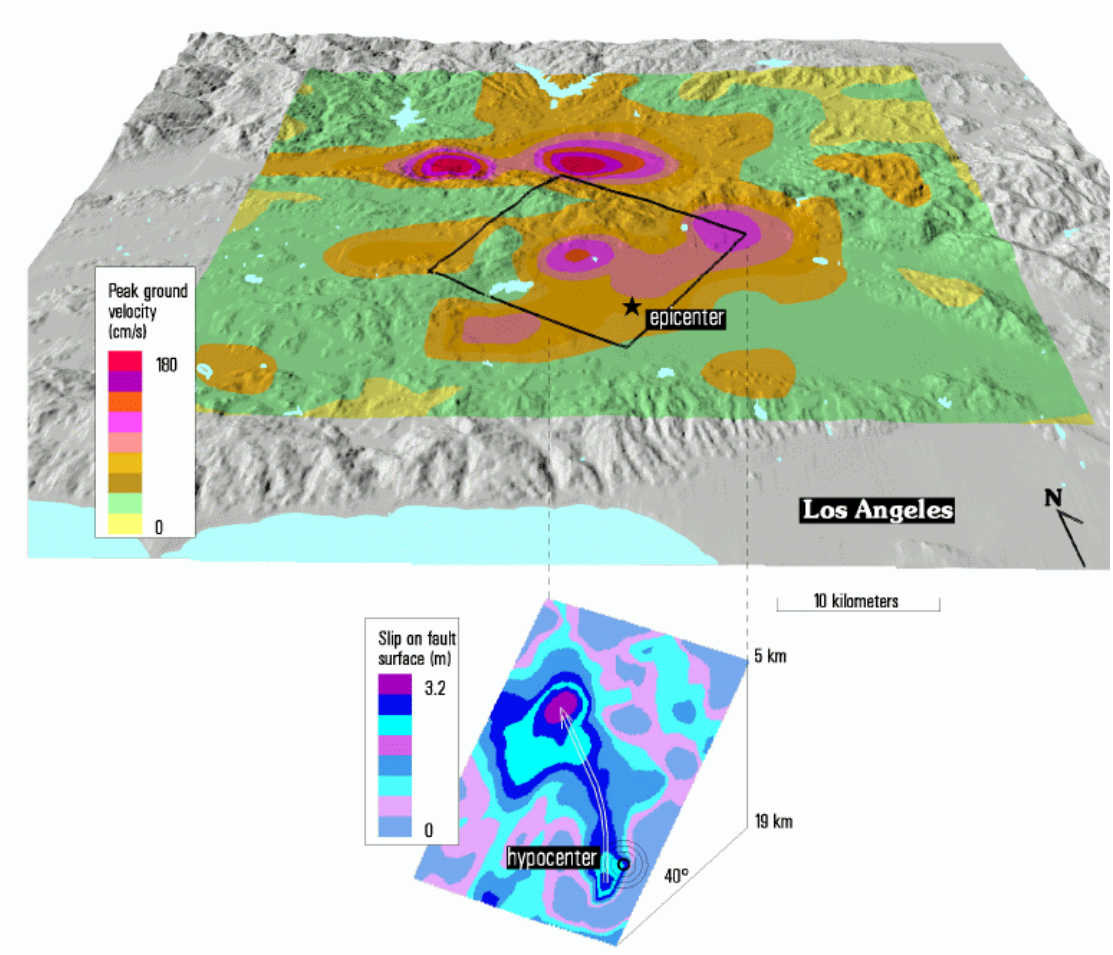

Fig. 18. Image of Northridge slip distribution in perspective 3-D view. The rupture began at the hypocenter near the lower right corner of the fault, propagated upward to the north, and focused energy in the northward direction as seen by the predicted ground velocity shown draped on the topography.

A research group at the University of New South Wales [J. Trinder, S. Han and C. Rizos] is pursuing a project that incorporates InSAR and GPS for terrain mapping. The approach suggested for InSAR-GPS integration is double interpolation and double prediction

(DIDP) [70]. The DIDP technique is being tested using CGPS and SAR data from Japan. In the DIDP approach, the steps are:

1. Derive both tropospheric and ionospheric corrections to InSAR from CGPS.
2. Remove or mitigate the SAR satellite orbit errors by using GPS results as constraints. Metal corner reflectors can be collocated with, or tied precisely to, GPS receiver sites. SAR data covering each of these GPS sites will thus correspond to a precisely located point, and so can be used to provide 3-D corrections to the nominal spacecraft orbit, and hence aid in improving the accuracy of the ground displacement measurement.
3. CGPS observations, separated by one or several InSAR repeat cycles within the SAR image, are densified in the form of a grid by interpolation in the spatial domain based on the GPS-corrected InSAR results. The densified grid observations are then interpolated in the time domain based on the daily, hourly, or even 30 second sampling rate of the CGPS series.
4. Based on the double interpolation result, forward filtering is used to predict the crustal deformation at all points on the grid (in fact a double prediction in both the temporal and spatial domains).

In a study of the Landers, CA, earthquake the results of forward modeling of the large-scale ground displacement field near earthquakes agree qualitatively with InSAR fringe maps [71]. Interferometric fringes form a map of one component of the displacement (i.e. along the line from the ground to the SAR platform) field with dense spatial sampling of greater than 100 pixels/km^2. Previous studies compared the coseismic deformation signatures obtained from InSAR with those measured by GPS [72, 73]. The authors in [57] found interferometric displacement estimates to agree with GPS displacement measurements within 3.4 cm RMS. The correlation of GPS displacements with those obtained from the interferometric method was 0.958 [58].

The RNGCHN program, described with the relevant equations in [74], uses the dislocation formulation given in closed form [75]. The dislocation may be a point source or a rectangular fault patch of finite dimension. The line-of-sight between the point on the ground and the radar satellite in the sky defines two angles, the radar incidence angle and the azimuth of the satellite ground track. Defining the corresponding unit direction vector, RNGCHN calculates the associated change in range along this line-of-sight direction.

Studies at the Berkeley Seismological Laboratory are utilizing surface creep rates established over several decades using traditional geodetic techniques, GPS measurements spanning about four years, and ERS-1/ERS-2 InSAR data spanning a 5-year period from June 1992 to September 1997. Preliminary results find that the current GPS data set provides little added constraint to the shallow slip on the Hayward fault. However, the GPS data allow an improved representation and integration of the deeply seated regional strain accumulation. A denser GPS network will help towards optimizing the resolution of slip potential.

6. Loss Estimation Methodology

Hazard analysis methods are deterministic, empirical/statistical or probabilistic. Deterministic methods rely on realistic calculations of ground model and structural response. Setting values to different model variables required detailed knowledge of the given scenario. A parametric analysis is based on setting minimum and maximum parameter values, or a range of values to analyze sensitivity. A statistical model is based on the behavior exhibited by a sample data set, whereas a probabilistic approach is based on a likely distribution of parameter values.

In this section, these different analysis methods are considered with the intent of addressing the application of advanced technologies. For example in deterministic approaches, remote sensing can provide a basis for validation of model ground displacements. On the other hand, in statistical or probabilistic approaches, remote sensing can provide constraints on ground displacements and structural damage. There is an increasing trend to integrate geospatial information products with GIS-based loss estimation tools (see http://www.hazus.org, http://www.fema.gov/hazus/ and http://www.nibs.org for recent developments in loss models and standards therein).

Modeling losses requires the determination of the assets at risk, either individually or geographically aggregated, including factors such as daytime and nighttime occupancies, structural types and construction methods. The hazard is modeled based on historical data, such as frequency of occurrence, (i.e. statistical model based on empirical data), or on scientific information such as mathematical representations of ground motion due to a slip dislocation on a fault (i.e. analytical model). Attenuation relationships are used to model the hazard intensity (i.e. ground shaking in seismic risk) at distances away from the source location (i.e. hypocenter along with rupture characteristics such as length, orientation and directionality). The relationships are based on statistical analyses and the physical characterization of the propagation medium and subject site (e.g. soil type, depth and topography). Most loss estimation models use the Modified Mercalli Intensity (MMI) scale for characterizing ground shaking.

At a given site (i.e. geo-location of a structure at risk) the intensity is used to estimate induced damage to a structure using a vulnerability function for the given type of structure (e.g. wood frame, reinforced concrete shear wall, unreinforced masonry, etc.) and method of construction (see http://www.atcouncil.org/). The damage represents replacement costs of the structure and contents (for example, see http://www.marshallswift.com). Casualties are determined from the occupancies. For further information, see also http://www.ibhs.org.

Losses are then computed based on the amount of damage. Results are typically quoted as a "probable maximum loss (PML)" or an "expected annual loss (EAL)" due to the inherent uncertainties in the modeling. The PML scenario is a worst case analysis, while the EAL is a probabilistic annualized analysis. Loss estimates can be computed for a given "scenario event" (e.g. *deterministically*, such as a repeat of a significant past event, a historically based maximum possible event without consideration of its probability of

occurrence, or *probabilistically* such as an event with a certain probability of occurrence). Uncertainties in deterministic methods concern the recurrence of a historical maximum event or speculation that an even larger event may occur. The loss estimate thus corresponds to a "predetermined" event. Loss estimates also can be obtained for a distribution of possible events (i.e. varying magnitudes from a suite or system of faults) in a given time period (for example, one year), wherein a hazard curve provides the probability of exceedance of a selected intensity within the specified time period. The scenario event is defined through the selection of a probability of exceedance to be used in the loss estimate. In this latter case, the loss estimates for each event are aggregated in a *probabilistic* manner to yield an annualized loss estimate and uncertainty.

In each of these loss modeling steps – identification of assets at risk, hazard modeling, propagation medium characterization, and structural vulnerability assessment – the advanced technologies that are the subject of this document have varying applicability. In earthquake hazard modeling, seismic and more recently joint seismic and GPS data inversions provide a good understanding of fault rupture and patterns of ground motion. However, the probability of earthquake occurrence is still a weak link in loss models.

Characterization of the propagation medium, particularly through the development of digital soil maps and digital elevation models (DEMs) (for example, see the California Department of Conservation, Division of Mines and Geology website at http://www.consrv.ca.gov/dmg/). Interferometric remote sensing techniques and detailed topographic imaging may shed new light on the distribution of ground motions due to rupture and propagation effects. Multispectral and hyperspectral imaging can provide land cover maps to supplement the detailed ground-based data.

Finally, the knowledge base on structural vulnerability to ground shaking is empirical. While sensors can be deployed on structures in the field and in the laboratory, remote sensing methods can offer only a limited perspective. For example, it is possible to image structures with InSAR and lidar, including footprints, heights and land cover layouts. With the integration of some multispectral bands, it is possible to infer structural types by roof-top compositions**.**

Structural characteristics cannot be inferred directly with remote sensing, however a limited number of structural classes could be inferred, particularly by differentiating commercial, industrial and residential areas. A rigorous assessment of the error budget in GIS-based loss estimation tools may suggest interesting tradeoffs that may allow remote sensing to be a cost-effective alternative to more detailed structural inventory developments. The number of structural classes and vulnerability models required would be dictated by the variability in area of interest. Classification with remote sensing could provide quicker loss model development in new geographic regions at the expense of some accuracy, but this tradeoff should be weighed against an understanding of the overall error budget. The websites of leading loss estimation firms are http://www.eqe.com, http://www.riskinc.com and http://www.air-boston.com.

6.1 The Inventory of Structures and Lifelines

One of the three principal elements of loss estimation consists of the vulnerability analyses (the other elements being assessing the potential for the occurrence of an event and quantifying the financial and casualty exposure). Property and casualty losses are estimated by modeling the number and distribution of structures and lifeline systems and their responses to ground motion, or other forcing functions, related to the particular natural hazard.

The preparation of an inventory of the built environment is usually the most time-consuming and costly element of a loss study. Based on NOAA, US Geological Survey, and Applied Technology Council (funded under the Federal Emergency Management Agency) reports, panel experts recommend the inputs of experienced civil and structural engineers, locally knowledgeable real estate consultants, architects and building department officials in the development and assessment of inventory methodologies [76].

Built environment inventories typically are generated from (digital, if available) databases of county tax assessor data. However, the accuracy and reliability of tax assessor's data can be hampered by mixed availability, lack of standardization, gaps in data collection, and politics surrounding ad-valorem taxation. Databases also can be developed from an insurer's policy portfolio if provided, but because such information is proprietary to the insurer/client, aggregate exposure analyses are hampered by the unavailability of data across the industry. State Departments of Insurance, similarly, may make some data available.

Discussions with public and private stakeholders (e.g. engineering firms, emergency management, property and casualty insurers, financial institutions) point out inadequacies of current modeling methodologies, and particularly the inability to export capabilities to regions and cities other than those for which they were developed. Data collection is time consuming and labor intensive. Current databases are in disparate formats, unreliable and incomplete.

As a specific example, consider that the Los Angeles metropolitan area covers an area of about 1,200 sq. km. In 1991, a replacement value estimate for the commercial building stock in California alone was $427 billion, and now exceeds $600 billion in total inventory, based on the ATC-13 procedure for using census ZIP and SIC data. The predominance of low-rise, single-family residential structures in Los Angeles County suggests that an urban land use classification for aggregate residential square footage is a sensible information product complement to identification of medium- and high-rise detached and close-set structures (see Table 6).

Table 6. Number of buildings by height and material type (Source: Los Angeles County Tax Assessor's Data)

# stories	Wood-frame	Steel-frame	Concrete	Brick/concrete block/other	Total	% Total
0-3	1,677,971	746	896	52,397	1,731,990	99.95
4-7	0	136	127	175	438	0.027
8+	0	190	121	56	367	0.023
Subtotals	1,677,951	1,072	1,144	52,628	1,732,795	100
% Total	96.83	0.06	0.07	3.04		

6.2 Statistical Approach

An alternative and statistical approach to assessing exposure to natural hazards risk is proposed in [77], noting the inadequacies in the traditional methods: unavailability and inconsistency of data; difficult or inaccessible data; and regional differences in the classifications of facilities as to their structural types and occupancies. The proposed methodology uses social wealth, represented by Gross Domestic Product (GDP), as the macroscopic indicator with which to estimate earthquake loss. The fundamental assumption is that the number of man-made facilities is directly proportional to GDP.

GDP is compiled on a regular basis by various agencies and institutions, such as the World Bank, World Resources Institute and the United Nations. Increasingly these data, represented at the national level, is becoming available in digital form as a database file or in GIS format. Studies and reports by the World Bank indicate that population density and economic exposure are closely related (references cited in Chen et al., 1997). Thus, the GDP per unit geographic area can be estimated in proportion to population densities. World population data were obtained from a 5-minute by 5-minute grid.

Table 7. Comparison of Expected Losses Calculated by Macroscopic Indicator Method and Scenario-based Ground Motion, Vulnerability and Exposure Model

Scenario Event	Expected Loss Macroscopic Indicator Method	Expected Loss Risk Management Solutions, Inc.
San Francisco (1906, M8.3, MMI:XI)	$126.7 billion	$110 billion
Kanto (1923, M7.9, MMI:X)	$330.6 billion	$1,050 billion

Traditional loss estimation models incorporate the number of buildings and their structural types, and damage functions for a given ground shaking intensity and building type. By using the GDP macroscopic indicator method, expected physical loss instead is estimated from the probability of a given intensity level, a mean damage factor or hazard-exposure-loss relation, and the GDP function. The GDP function scales the number of facilities according to social wealth (e.g. the higher the percent of the GDP attributed to a region, the greater the scaling factor). Intensity levels for a given location and distance

from a scenario event follows a simple attenuation relation and isoseismals. Results of the study are indicated in Table 7.

The large discrepancy for the Kanto scenario is attributed to poor granularity of population densities, inappropriate intensity attenuation and hazard-exposure-loss relationships, and effects of soil site conditions. Nevertheless, the point is that improvements in seismic parameterizations would be straightforward compared to improving structural databases. This is a particularly interesting approach when the development of inventory databases is limited by the lack of available parcel data.

6.3 Methodologies Based on Remote Sensing

Developing an inventory of structures and lifelines is a critical element in loss estimation methodologies, and one that high-resolution three-dimensional remote sensing imaging is able to address. The robustness of generating an inventory remotely must be assessed through continued research and validation studies that rely on ground truth data to assess the accuracy and efficacy of a remote sensing methodology. Furthermore, trade-offs in cost and uncertainty must be considered.

The application of remote sensing technology to real-time damage assessment will require a comprehensive research program. Several issues must be addressed; the most important of which is how to model remote sensing images to quantitatively separate the effects of surface displacement from building or infrastructure damage. Massonnet et al. [78] and Ozawa [79] attempted to address this problem.

6.3.1 Example: Hyogoken-Nanbu Earthquake of 1995

Several earth observation satellites observed the Kobe area in Japan before and after the 1995 Hyogoken-Nanbu earthquake. Detection of damaged built-up areas by the Hyogoken-Nanbu earthquake using SAR intensity images has been reported [80]. Since a part of the damage survey results of this earthquake was maintained as GIS data, a quantitative analysis of the surface changes in damaged areas was possible. Spectral characteristics of the area damaged by the earthquake were investigated using Landsat and SPOT satellite optical images taken before and after the earthquake, for examining the possibility of extracting the earthquake damage distribution by satellite remote sensing [81]. Multispectral characteristics were different between images of the liquefied areas and burned areas taken by airborne remote sensing just after the earthquake occurred [82]. Other studies had previously suggested the possibility of interpreting the damaged area based on the spectral pattern changes between satellite images taken before and after the earthquake [83, 84].

The building damage data was based on detailed survey results compiled by AIJ (the Architectural Institute of Japan) and CPIJ (the City Planning Institute of Japan), and digitized by BRI (Building Research Institute, Ministry of Construction). In the corresponding GIS data, the building damage level was classified into the five categories: damage by fire, severe structural damage, moderate damage, slight damage and no damage, and the numbers of damaged buildings were totaled for each block in cities [85].

SPOT/HRV and Landsat/TM observed the area of interest on January 20, and January 24, 1995, respectively. Images taken on March 22, 1990 by SPOT and on August 17, 1994 by Landsat were used for data before the earthquake. Since the digitized values in the satellite images were different depending on the observation situation and the surface conditions, the digital number (DN) correction was required before starting the study. Cloud-cover and vegetation index corrections also were performed. For DN correction, pixels in non-liquefied and non-damaged areas were selected, considered to be the areas in which there was no change of the surface after the earthquake.

The pixels that represent the area of liquefaction, burning, heavy damage, slight damage and no damage of buildings were selected from the images to examine the characteristics of the DN in the earthquake-damage area. Specifically, the DN are larger for all Landsat/TM bands, other than band 6, in the liquefied area in comparison with the non-damaged area [86]. The DN of the burned area is smaller than that of the non-damaged area. The DN of the heavy damage area is similar to that of the non-damaged area. These results are in good agreement with the damage survey performed by airborne multispectral scanner remote sensing [87].

The changes of the DN in earthquake damage areas for SPOT showed the same pattern as that in the Landsat images; the DN became high in the liquefied area. However, the changes of the DN in the burned or building damage area did not show such great differences compared with the non-damaged area. This coincides with results of previous research [88].

Finally, damage distribution was extracted by a "minimum distance classification" discriminant analysis using the DN after the earthquake and the differences in DN before and after the earthquake as the representative variables, using Landsat data. The extracted damage distribution agreed with damage survey results.

Aoki et al. [89] also attempted quantitative evaluation of the damage area due to the Hyogoken-Nanbu earthquake. The satellite SAR images used in their analysis are those taken from the ERS-1 on October 12, 1994 (before the earthquake) and May 23, 1995 (after the earthquake). In each recorded image, one pixel is equivalent to a ground distance of 12.5-m [see 90]. The same comprehensive building damage survey was used as in the previous study above. The data set contains the total number and the number of damaged buildings per each block of city district. The damage ratios evaluated for each block were used as the reference data.

The analytical procedure consists of the following steps:

- Geometric correction: A geometrically corrected image is generated through a process that uses control points on the ground having high correlation before and after the earthquake. The correlation coefficient is calculated by dividing the covariance of the two images by the dispersion of each image, and is expressed as

$$r = E(a, b) / E(a)\, E(b) \qquad (6)$$

  where *a* and b indicate the back-scattering coefficients of pixels before and after the earthquake.

- Transformation to back-scattering: A pixel value of satellite SAR images is transformed into the back-scattering coefficient, which is the basic physical value of the quantitative comparison of images at two time instants.
- Correlation image: The correlation coefficient is used as a characteristic value of satellite SAR images at two different time instants. The correlation image is generated using a pixel value of the average correlation coefficient within a 5 by 5 pixel window.
- Difference image: The difference of the back-scattering coefficients is also considered as a characteristic value. This difference image is generated using a pixel value of the average difference of back-scattering coefficients before and after the earthquake within a 5 by 5 pixel window.

The difference before and after the earthquake is considered to reflect the changes to the land cover. The correlation image and the difference image are compared with the damage ratio of buildings evaluated from the field survey data. The severe damage ratio is defined as the ratio of the number of seriously damaged buildings to the total number of buildings within a district block.

The results show that the difference of the back-scattering coefficients becomes high and negative and the correlation coefficient becomes low in the area of a high severe damage. On the other hand, in the area of a low severe damage ratio, the difference of the back-scattering coefficients becomes high and positive and the correlation coefficient becomes high. However, since the standard deviations of the above two values are quite large, a large amount of randomness is included in the damage identification based on the method using the two values.

Generally, artificial structures show comparatively large reflection because of the specular characteristics of the structure and the ground. Open space yields comparatively small reflection because of its smooth surface. Following the earthquake, structures were destroyed and removed leaving the plain exposed. Therefore, it is considered that the back-scattering intensity taken after the earthquake is smaller in comparison with that taken before the earthquake. It is desirable that the difference of the backscattering coefficients of the non-damaged area become zero.

The relationship between the building damage area by the field survey and the satellite SAR images revealed the trend regarding the severe damage ratio. The trend in the area of a high severe damage ratio was obtained when the difference of the backscattering coefficients becomes high and the correlation coefficient becomes low.

6.4 Concept for a Methodology Integrating Remote Sensing and GPS

An approach conceptualized herein is to rely on remote sensing images as the primary data source, as others have done previously, but add to this information other independent data such as GPS observations and ground motions produced by real-time earthquake monitoring networks, like TriNet [see http://www.trinet.org].

A SAR interferogram, *I*, will represent the observable changes to the earth and to the built environment after an earthquake has occurred. This interferogram can be characterized by

$$I = \mathrm{f}\,(\phi_{\Delta}, \phi_{\mathrm{scatt(A)}}) \tag{7}$$

where ϕ_{Δ} is the phase difference caused by a change in the line-of-sight rage between the sensor platform and the earth's surface, and $\phi_{\mathrm{scatt(A)}}$ is the phase difference caused by a change in the scattering properties from the earth's surface. *A* represents the average effects over an area. Using an interferogram, the amount of change is measured by the strength of the correlation between the pre- and post-earthquake images. In general, the correlation is a function of $\phi_{\mathrm{scatt(A)}}$. A correlation of one indicates absolute correlation, whereas a correlation of zero, or significantly less than one, indicates that the pre- and post-earthquake images show a change over the observation span.

Images of urban areas generally remain stable for long periods of time. Since these areas consist of man-made surfaces such as buildings and roadways, the scattering properties show little variation with time. Trees and vegetation, on the other hand, can show significant changes in scattering properties over time. Furthermore, image changes can be quantitatively related to physical measurements or states. For example, a careful ground-based validation of imaged areas could result in quantitative models that relate image changes to surficial changes. This would be crucial if post-event damage levels are to be related to SAR image changes. In the case of surface changes due to an earthquake, possible reasons for low correlation would include aseismic motions, coseismic ground displacements, and building and lifeline damage.

Consideration of the equation (7) suggests that if high correlation is observed, scattering effects are low and the change in line-of-sight range is measurable. This would correspond to no building damage and small surface displacements. If the correlation is marginal, change has occurred but the source of this change is difficult to identify. Such change could be due to the slight tilting of a building or a result of large, lateral displacements that can mis-register an image. If the correlation is low, it is most likely due to large scattering variations. The condition that most closely matches this situation would be widespread building and infrastructure damage. Validation and verification of this would be based on select interferograms that show a range of correlation, and an attempt to ground-truth these images with actual surface displacement and building damage data.

In order to relate SAR image changes to building damage, algorithms will have to be developed that effectively "filter" these varied effects. One potential means of characterizing the change in scattering properties is through independent measurements, such as comparison of displacement vectors calculated using GPS data. Ground surface displacement maps can be generated or estimated from GPS network measurements using inverse dislocation modeling techniques. If this GPS information is transformed so that displacements in the line-of-sight are determined, such as using the RNGCHN algorithm, a one-to-one comparison can be made between displacements inferred by SAR interferogram data and those recorded by a GPS network.

If we define a term, α, as the residual displacement between these two displacement measurement techniques (still along the line-of-sight between the ground and SAR sensor platform), then one can associate ground-based information such as building damage with this term. Generally, for example, one would expect building or infrastructure damage to vary proportionally with α. When low correlation is observed in the SAR image comparisons, one would expect the trend to be inversely proportional. When correlation is high, these parameters would be directly proportional.

For further elaboration, consider the following scenarios. Low correlation means that a comparison of the pre- and post-earthquake SAR images shows little similarity between images. By subtracting the measured displacements, as yielded by GPS, a low α would be consistent with high building damage since the differences can only be explained by changes in the built environment. An example would be the Santa Monica area of Los Angeles following the Northridge earthquake, where most of the damage was caused by poor construction (i.e. unreinforced masonry building damage). A high α would be consistent with low building damage since major lateral movement of the earth's surface could explain the variation in the images.

High correlation means that a comparison of pre- and post-earthquake images shows strong similarities between images. If α is small, it would imply that the strong correlation could be explained in large part by the observed displacements. A large α would suggest that the only way to explain the high correlation is that damage has occurred without significant ground disruption. An example would be the mid-story collapse of the Kobe City Government Building after the 1995 earthquake.

6.5 Model Inputs to Catastrophe Risk Financing

The insurance and financial communities are market-testing the packaging of catastrophe risk as securities that insurers and investors can buy and sell in the capital markets. This process, called securitization, allows insurers and reinsurers to share catastrophe risk with investors, and is an alternative form of financing catastrophe losses. For example, there are two sources of capital to finance large catastrophe risks – the federal government and the capital markets. The latter, through the emergence of capital market solutions, has been witnessed in the recent interest in the securitization of catastrophe risk. The principal forms of securitization include catastrophe or "act of God" bonds, contingent surplus notes, exchange-traded catastrophe options, and catastrophe equity puts. The growth of catastrophe risk securitization will depend on these products providing insurers a cost-effective means of spreading risk and providing investors an alternative for enhancing the performance of their portfolios.

Catastrophe bonds are corporate bonds that require the bondholders to forgive or defer some or all payments of interest or principal if actual catastrophe losses surpass a specified amount or trigger. When that happens, an insurer or reinsurer that issued catastrophe bonds can pay claims with the funds that would otherwise have gone to the bondholders. Contingent surplus notes are surplus notes that an insurer has purchased the right to issue in the future to investors at preset terms in exchange for cash or liquid assets. The right

to issue the surplus notes may be contingent on specified catastrophe events taking place. Exchange-traded catastrophe options are standardized contracts that give the purchaser the right to a cash payment if a specified index of catastrophe losses for a specific period reaches a specified level – the strike price. Catastrophe options are a form of securitization that allows for the hedging of catastrophe risk. Catastrophe equity puts are put options that enable stock insurers to sell shares of their stock to investors at pre-negotiated prices when catastrophe losses exceed the levels specified in the options. Some insurers have also used swaps to spread their catastrophe risk. In a catastrophe swap, an insurer agrees to make periodic payments to another party, and the other party agrees to make payments to the insurer that are based on a measure of catastrophe losses. Further information can be obtained at the Insurance Services Office website at http://www.iso.com and at http://www.eqecat.com and http://www.guycarp.com, for example.

The improving capabilities of catastrophe modeling to provide estimates of potential losses, quantify potential losses by geographic regions, and provide scenarios for managing risk from natural disasters have placed modeling into a critical role in the issuance of catastrophe bonds and the development of other risk transfer mechanisms. Originally used for gauging an insurance company's probable maximum loss from natural hazards, catastrophe modeling is now a critical tool for the development of pricing, underwriting, and risk-transfer strategies leading to overall portfolio optimization and integrated risk management. As the insurance and capital markets continue to merge, catastrophe modeling will play an increasingly important role in these new alternatives to traditional reinsurance [91].

A few examples can be cited. In 1997, Residential Re sold $477 million in catastrophe bonds and used the proceeds to provide reinsurance to the United Services Automobile Association (USAA). Also in 1997, SR Earthquake Fund, Ltd., issued $137 million in catastrophe bonds and provided reinsurance for California earthquake losses to Swiss Re Company. In 1998, special-purpose reinsurer Trinity Re, Ltd., issued $83.6 million in catastrophe bonds and sold reinsurance to Centre Solutions (Bermuda) Ltd., also a reinsurer. Also in 1998, Residential Re sold another $450 million in catastrophe bonds to again reinsure USAA [92].

Bond rating (by one of the four US rating agencies) is typically required to place large multi-year risk transactions. Catastrophe risk models assist the rating process by presenting the risk analytically and allowing for sensitivity analyses (i.e. "stress testing").

In March 2000, Risk Management Solutions (RMS) for example announced that it provided the risk analysis to support Lehman Re Ltd., the reinsurance subsidiary of Lehman Brothers Holdings Inc., in a $150 million securitization of California earthquake risk. The 22-month transaction transfers to investors the risk associated with certain levels of insurance industry losses in California from earthquakes and resulting fires. Securities were offered to investors by special-purpose Cayman Islands company Seismic Limited, which in turn entered into a swap agreement with Lehman Re. Moody's Investors Service and Standard & Poor's both reviewed the transaction and the RMS modeling and assigned ratings to the notes.

Through Seismic Ltd., investors are providing Lehman Re with coverage for aggregate industry losses from all covered earthquake events that occur during the 22-month period [93]. To assist potential investors and rating agencies in evaluating the securities, RMS provided estimates of overall loss probabilities, key scenario losses and regional contributions to the risk. RMS developed its estimates from a stochastic simulation of insurance industry losses for thousands of possible earthquake events using proprietary earthquake models and an exposure database that provides a detailed representation of earthquake and fire insurance exposures throughout California

6.6 Emergency Management

Emergency management decisions made in the minutes and hours following a major event are based on limited field reconnaissance. Necessary parameters include:

- Accurate and reliable data on earthquake magnitude and location
- Distribution maps for peak accelerations and shaking intensity
- Loss estimates inferred from damage and population distributions

It is the intent suggested herein to be able to contribute to each parameter with the rapid acquisition of remote sensing data, in addition to broadband seismic network data and the increasing utilization of permanent GPS geodetic networks.

The various data modalities discussed in the previous sections must be integrated in order to provide the most beneficial input to loss estimation methodologies. Singly and jointly, these information products and risk assessment tools can be part of an advanced global disaster information management system. The infrastructure for data retrieval, distribution, value-added processing, storage and dissemination to users in public and private sectors is enabled by the continuing growth of the telecommunications, information technologies and in systems sectors.

The Pacific Disaster Center (http://www.pdc.org/), for example, is a federal information processing facility that supports emergency managers in the Pacific and Indian Ocean Regions. In operation since February of 1996, the PDC works closely with federal, state, local and regional entities involved in emergency management to provide timely, accurate information using state-of-the-art technology. See also the Global Disaster Information Network at http://www.gdin.org.

A Global Disaster Observation Satellite (GDOS) System has been proposed to provide images and data of disaster stricken areas for transmission to relevant organizations on an international basis [94]. Elements of the multi-hazard system would include:

- Frequent, if not daily, observations of any point on the earth's surface;
- High ground resolution of under 5 m;
- All weather capability
- The ability to provide full views of the disaster region within hours of the event and maintain highly frequent subsequent observations.

Databases of variable resolution maps would be created for post-disaster use, to identify areas of highest multi-hazard risk.

The technical, operational, organizational, management, political and financial aspects of such an enterprise are complex. An overview of the system architecture and its applicability is given in [94]. While some level of coordination would be desirable with commercial remote sensing efforts, the GDOS concept is more of an international and governmental nature. Further advances in this direction of global disaster observation, management and response are promoted in the form of international cooperative research among government organizations.

GDOS would consist of four satellites in each of six sun-synchronous planes, and data relay satellites positioned in geostationary orbits at 60 degree intervals; ground stations, control stations and multiple local user stations. The satellite types and their distributions would be according to the onboard sensor.

The following recommendations are obtained from a report of the current and projected utilization of Earth Observation (EO) space technology applied to the management of earthquake disaster. The study is part of the Disaster Management Support Project of the Integrated Global Observing Strategy [http://www.ceos.noaa.gov].

Table 8. Remote sensing sensors that provide various levels of spatial resolution with potential for disaster management applications.

Sensor Type	Resolution	Observation Width
Visible and near infrared radiometer for high resolution stereoscopic color images	2 m	40 km
Visible and near infrared radiometer for medium resolution stereoscopic color images	15 m	180 km
Shortwave infrared radiometer	15 m	180 km
Visible thermal infrared radiometer to monitor surface temperatures	40 m	40 km
Synthetic aperture radar to monitor vertical changes in the surface	5 m	40 km
Microwave radiometer for monitoring of water vapor and sea surface temperatures	5-60 km with 1° K temperature resolution	500 km
Scatterometer for observation of wind directions and speeds	50 km 2m/s, 20°	1,200 km

There have been recent efforts by some space agencies to acquire and disseminate data relating to certain disasters. When these services are offered, they are not coordinate or integrated with other services, and are not widely accessible to, or for that matter understood by, for the earthquake disaster management community. With the availability of very high-resolution data, such as IKONOS-2, coordination of such efforts will be necessary to ensure a benefit for disaster management.

Several recommendations are offered, that include:

- Expand existing global database of seismic risk zones, and coincide with population distribution, seismic history, relevant geology, known strain (i.e. as from GPS networks), estimated InSAR coherence level and optical very-high resolution base maps.
- Begin to develop an archived database of multi-year InSAR-derived strain over seismic regions.
- Support research efforts into "point sample" InSAR (i.e. differencing signal phase against point targets).

Consider that after the February 20, 1998 Afghanistan earthquake, for example, it took two weeks to locate settlements that might be damaged, as there were no accessible, up-to-date maps of the region. High-resolution, e.g. SPOT panchromatic, and very-high resolution optical data (i.e. IKONOS-2) data could play a significant role in base-mapping of all regions in the developing world in zones of high seismic risk.

Non-near-real-time damage mapping using image differencing is operational. However, near-real-time damage mapping is in a developmental stage. Until the recent successful commissioning of IKONOS-2, the best spatial resolution generally available was SPOT panchromatic data at 10 m. There is no near-real-time access to 5.8 m IRS data. A single acquisition (i.e. non-differencing) of data at this resolution precludes the reliable identification of even major damage (e.g. building collapse).

In an investigation performed by NASA, these data could not be used to detect major damage in villages following the Spitak, Armenia earthquake of December 7, 1988. Aircraft imagery of damage at Kobe, acquired at 1-m resolution and degraded step-wise to 10 m indicates that 2 m or better resolution is generally needed to reliable detect major damage with single acquisitions. However, temporal resolution is still a concern (i.e. the ability to image a damage region within a sufficient time to impact disaster management). Also, the impact of possible cloud cover on optical systems must be considered.

Primary considerations, in addition to sensor resolution, include operational ease, suitability for meeting critical and priority requirements, cost-effectiveness, and address the following:

- Formats and compatibility with existing data, architectures and decision support tools;
- Volume management, including temporal and spatial sampling requirements and integration of different sensor types for land use and land cover classification and information extraction; data storage and mining, real-time vs. store-and-forward approaches, and advanced visualization;
- Staff training and interpretive skills requirements, and the corresponding education requirements to nurture the growth of a geospatial knowledge-based workforce in public and commercial sectors;
- Data acquisition and update costs;
- Opportunities for resource pooling at the State and local levels.

The types of information layers (i.e. inputs to geographic information system (GIS) architecture) that must be extracted from remotely sensed imagery are varied. These in-

clude elevation, slope, aspect, hydrologic modeling (e.g. for run-off and non-point-source pollution studies) from vegetation and impervious surface classification and DEMs, and proximity to features in the built environment, building footprints and heights, roadway networks, critical facilities and lifelines.

Recent research of the urban environment by the remote sensing community points towards the need for data fusion using various sensors and ancillary data (e.g. geologic maps of soil types and conditions). This is necessary in order to define detailed three-dimensional geometry and provide classification of complex land use and land cover. Available sensors and/or data types that typically are considered include:

- Digital orthophotography quadrangles (DOQs) – A digital orthophoto is a digital image of an aerial photograph in which displacements caused by the camera and the terrain have been removed. It combines the image characteristics of a photograph with the geometric qualities of a map. The standard digital orhthophoto produced by the USGS, for example, is a black-and-white, or color infrared, 1-meter ground resolution quarter quadrangle (DOQQ) image (see http://edc.usgs.gov). The accuracy and quality of USGS digital orthophotos must meet National Map Accuracy Standards at 1:12,000 scale for 3.75-minute quadrangles and at 1:24,000-scale for 7.5-minute quadrangles. See http://www.fgdc.gov/nsdi/nsdi.html for information on the National Space Data Infrastructure. Utmost resolution of 2 to 3 cm can provide a comprehensive layout of roads, property boundaries, right-of-ways and easements. Composite maps with parcel land bases can be generated to include property attributes such as assessor's records, parcel records, legal documents and aerial photography.

- Radar-derived, high detail/accuracy Digital Elevation Models (DEMs) available from Intermap Technologies, Inc. using their STAR-3i airborne X-band interferometric synthetic aperture radar (InSAR), for example. Typical accuracy is about 1.5-m root mean square error (RMSE) in vertical and horizontal with 2.5-m posting. (For further information, see http://www.intermaptechnologies.com, http://www.globalterrain.com/ and http://www.erim-int.com).

- Digital Elevation Models (DEMs) meeting a 1-m RMSE in the horizontal and 15-cm RMSE in vertical; and digital panchromatic geo-referenced or ortho-rectified images (ORIs) (i.e. for planimetric feature information) with 0.3 m resolution per pixel. These products are available from EagleScan Inc., for example, using their Digital Airborne Topographical Imaging System comprised of a lidar (see http://www.airborne1.com and http://www.airbornelasermapping.com). Only one ground control point is required for most applications, reducing costs and time compared to photogrammetric methods. DEMs and ORIs provide the base layers of a GIS (see http://www.isprs.org for photogrammetry and remote sensing).

- IKONOS - High-resolution panchromatic 1 to 2.5 meters and multispectral to 4 meters. IKONOS, launched by Space Imaging on September 24, 1999, is the first 1-meter satellite for high-resolution, high-accuracy panchromatic digital earth information. IKONOS simultaneously collects 4-meter multispectral data (see http://www.spaceimaging.com and also EarthWatch at http://www.digitalglobe.com).

- Landsat - Broad aerial coverage with panchromatic resolutions of 5 to 15 meters, and multispectral data resolution of 10 meters. Landsat-7 acquires over 400 scenes in the US every 16 days. Landsat-7 provides repetitive, synoptic coverage of continental surfaces with absolute radiometric calibration. The V/IR bands have 30-m resolution, the thermal IR bands have 60-m resolution, and the panchromatic band has 15-m resolution. See the USGS EROS Data Center for Landsat 5 and Landsat 7 products at http://edc.usgs.gov or http://edcwww.cr.usgs.gov/.

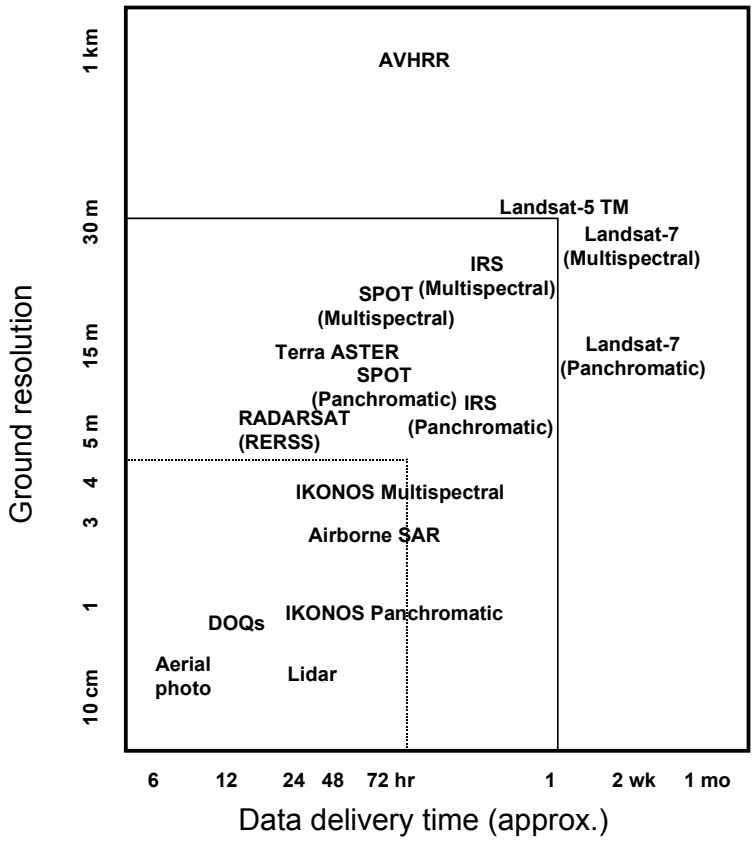

Fig. 19. Overview of various selected operational remote sensing systems shown with respect to ground resolution and approximate data delivery time.

- SPOT High Resolution Visible/IR, 10-m panchromatic (i.e. black and white) data for fine geometrical detail, and 20-m multispectral data for color composites (see http://www.spot.com).
- OrbView-2 - Hyperspectral, up to 300 bands, in the optical/near infrared with resolution of 8 to 30 meters. OrbView-2, launched by Orbital Sciences Corporation in August 1997, has 6 channels in the visible and 2 in the near infrared with spatial resolution of 1.1 km (http://www.orbimage.com).

- RADARSAT - C-band SAR with six different operating modes and 24-day repeat cycle. Fine resolution mode provides a 10-m resolution with a 45-km swath (see http://www.rsi.ca).

Table 9. The websites of the various remote sensing systems represented in Fig. 19.

Remote Sensing System	Website
Airborne SAR	http://www.intermaptechnologies.com http://www.globalterrain.com/ http://www.erim-int.com http://www.calgis.com
AVHRR	http://edc.usgs.gov http://www.ngdc.noaa.gov
Digital Orthophotos (DOQs)	http://edc.usgs.gov http://www.fgdc.gov/nsdi/nsdi.html
IKONOS	http://www.spaceimaging.com (see also http://www.digitalglobe.com, http://www.orbimage.com)
IRS	http://www.ipdpg.gov.in
Landsat	http://edcwww.cr.usgs.gov/
Lidar	http://www.airborne1.com http://www.airbornelasermapping.com
Radarsat	http://www.rsi.ca
SPOT	http://www.spot.com
Terra ASTER	http://eos-am.gsfc.nasa.gov/

Advanced NASA sensors include (1) GeoSAR – A public-private airborne radar project developed by JPL through DARPA and operated by Calgis, Inc. (see http://www.calgis.com). GeoSAR consists of X-band and polarimetric P-band sensors that yield 0.5-1.2 m and 1-3 m relative DEM height accuracy, respectively. (2) Shuttle Radar Topography Mission (SRTM): C-band and X-band InSARs to produce DTM products. These meet Interferometric Terrain Height Data (ITHD)-2 specifications (30 m x 30 m spatial sampling with 16-m absolute vertical height accuracy, 10-m relative vertical height accuracy and 20-m absolute horizontal circular accuracy). (3) Recent algorithm advances include the integration of hyperspectral imagery with radar using AVIRIS and AirSAR; and fusion of polarimetric C-, L- and P-band AirSAR data with interferometric C-band TOPSAR data and Landsat TM data. These types of studies provide for improved differentiation and classification of the complex textures of the urban environment.

7. Recommendations

The benefits that can be derived from the application of new technological capabilities to the analysis of seismic risk and vulnerability of buildings and lifeline systems include:

- Innovative and cost-effective procedures for assessing the seismic hazard potential of large urban regions;
- Alternative approaches for developing regional damage or vulnerability models for buildings and lifelines;
- Cost-effective procedures for creating building and lifeline inventories;
- Rapid loss estimation and model calibration methodologies for post-earthquake damage assessment.

Each of these benefits would rely on the utilization of geographic information systems (GIS) to provide the architecture with which various layers of geospatial information products can be integrated to support decision-making.

Three technologies have been reviewed in this document: seismological systems, the Global Positioning System (GPS) and remote sensing. Continuous GPS-based ground deformation monitoring networks, in addition to seismological networks and wireless communications systems for real-time response provide critical measurements for understanding the earthquake process and its impact on the built environment. Continued deployment of GPS monitoring networks will lead to:

- Better definition of off-fault surface deformation,
- Timely detection of diagnostic changes in the fault environment
- Constraints on the extent of surficial fault creep and its significance to potentially significant earthquakes,
- Accurate estimates of the distribution of potentially damaging ground motions from such earthquakes to enable ground motion modeling, structural design planning and risk assessment.

Real-time seismological monitoring systems can be used to calculate the likelihood of subsequent, probabilistically related events. Seismological networks that are used for early warning and rapid response rely on the ability to perform real-time waveform inversions in order to provide earthquake parameters during the actual rupture process. These networks also contribute to the reduction of recovery times after a major earthquake, and help to allow a more rapid determination of the resources that will be needed for post-disaster rebuilding and recovery.

The emergence of airborne and spaceborne remote sensing systems, from optical to microwave spectral bands, has created arguably the most significant opportunity for improving loss estimation methodologies. When fully operational for natural hazards risk management applications sometime in the next decade, these systems and attendant data visualization technologies will provide enhanced measurement accuracy, near-real-time

capability, greater geographic coverage and hold the promise of reduced operational cost. The continued demonstration, validation and adoption of remote sensing in disaster management and other applications, plus greater competition among data and service providers, and increasingly better defined civil and private user requirements for data and information products will lead to stable data rights, licensing and pricing options. This will engender the growth of the industry in a manner that can support routine operational capacity in disaster management and response and other equally time-sensitive applications.

The assessment of these advanced technologies for loss estimation as reported in this document lead to the following set of recommendations. These recommendations must be recognized to be dependent on the state-of-the-art of the technology, as represented herein, and are subject to review and updating as the technology industry continues to undergo rapid changes and advancements.

Recommendation 1: Seismic information obtained from dense broadband networks should be complemented with maps and geospatial information products derived from remotely sensed imagery that are integrated into a common geographic information system (GIS) architecture.

Digital map products can provide regularly updated information on regional geomorphology, urban topography, structures, roadway networks and vegetation. Remote sensing imagery provides a complementary layer in a multidisciplined approach to understanding risk and vulnerability.

Recommendation 2: Applied research should continue in validating and demonstrating the capability to image man-made structures and lifelines with remote sensing.

This geospatial information layer of the built environment can be superimposed on the various layers that characterize the terrain. In so doing, in a GIS, geocoded surficial effects could be integrated with the vulnerability models of structures and lifelines and used for developing map-based loss estimates with granularities, or geospatial grid resolutions (i.e. counties, zip codes, blocks) required by disaster management and insurance and financial applications. The loss model outputs, in turn, could be reviewed against a backdrop of actual digital imagery products of the impacted area.

Recommendation 3: The development of an operational capability to integrate GPS network data with seismic data should continue and expand into different tectonic and urban settings in order to help distinguish the effects of wave propagation from those of earthquake rupture.

Geodetic and seismic data are necessary in order to understand the source-rupture process and thus infer the resultant patterns of damage. The correlation of seismicity with regional tectonics is an important element of the overall seismic hazard assessment. GPS measurements provide an extension to the long-period end of the seismic spectrum and valuable constraints on seismic inversions for fault rupture characteristics.

Recommendation 4: There is a distinct need for continued research and development into a multidisciplinary approach to the theoretical and practical integration

of remote sensing data products with measurements provided by dense seismographic and GPS networks.

The geospatial information that can be extracted from remotely sensed imagery is relevant not only to assessing the potential for risk, but towards better defining the state of vulnerability, and thus the exposure to loss, within a given geographic region. For example, development of automated interferometric synthetic aperture radar (InSAR) and multispectral processors for urban land use classification would help to:

- Improve the information content of databases for inferring aggregate valuation of building inventories;
- Assess the exposure of the built environment to natural hazards.

While it is recognized that structural characteristics cannot be inferred directly with remote sensing, a limited number of structural classes could be inferred, particularly in differentiating commercial, industrial and residential areas. A rigorous assessment of the error budget in GIS-based loss estimation tools may suggest interesting tradeoffs that may allow remote sensing to be a cost-effective alternative to more detailed structural inventory developments. The number of structural classes and vulnerability models required would be dictated by the variability in area of interest. Classification with remote sensing could provide quicker loss model development in new geographic regions at the expense of some accuracy, but this tradeoff should be weighed against an understanding of the overall error budget.

<u>Recommendation 5</u>: Continued applied research and demonstration projects should target technical objectives that include:

- **Advancing electromagnetic scattering model capabilities to improve building height measurements;**
- **Developing building height information extraction algorithms from InSAR and lidar data;**
- **Using multispectral data to improve radar- and lidar-based characterization of the urban environment;**
- **Developing building material classification layers from remotely sensed multispectral data.**

Applications of remote sensing technologies to the urban environment are receiving increased attention in areas such as urban planning, infrastructure and transportation. Continued work in land use and land cover classification and mapping will help the infusion of these geospatial information products into loss estimation discipline. Further research is likely to compare the results of InSAR with those of lidar. There are other, non-performance factors that must be considered, such as the all-weather capability of radar and the decreasing operational costs of lidar.

Recommendation 6: The development of high-resolution sensors, with a resolution of 1-meter or better, is necessary.

Existing satellite-based InSAR systems lack the spatial and height resolution for urban applications, although their capabilities for ground deformation monitoring have been demonstrated. In order to increase the adoption of these technologies in urban applications, the resolution must "compete" with traditional photogrammetric approaches that yield very high-resolution (sub-meter) digital orthophotogrammetric products. Sources of airborne InSAR data are marginally adequate for assessing their capabilities for urban applications. Recent research in remote sensing of urban areas points out the need for multi-band data registration and fusion using various sensors and ancillary data sources, such as census data and thematic maps. Spatial resolution of less than 5 meters is required for the extraction of urban geometrical patterns. Resolution of 1 meter is generally needed to reliably detect major damage with single acquisitions. Lidar is providing an increasing interesting alternative to high-resolution imaging.

Recommendation 7: Further research and remote sensing demonstration projects are necessary in order to assess the development of inventories of structures and lifelines for GIS-based loss estimation models.

No one is currently developing quantitative databases of the built environment by extracting information from remote sensing imagery. The robustness of generating an inventory remotely must be assessed through continued research and validation studies that rely on ground truth data to assess the accuracy and efficacy of a remote sensing methodology. Trade-off in cost and uncertainty must be considered. At the same time, the potential benefits of using remote sensing must be considered in light of the error budget of loss model outputs. Rather than use remote sensing to replace the current approach to database development, geospatial information products will likely call for a different interface to loss estimation models. Furthermore, remote sensing would be used to infer [a fewer number of] structural classes based on recognized patterns of urban development and zoning. Individual or aggregate structures would be geocoded for integration with other geospatial data. While the inventory *per se* may no longer look like a database file, rather a map of inferred structural classes with attribute data.

Recommendation 8: Research efforts should be augmented to focus on the joint analysis of GPS and InSAR measurements.

GPS measurements and InSAR images can be combined to help constrain significant postseismic rebound in both horizontal and vertical directions. However, significant challenges need to be overcome before reliable deformation measurements can be made on a routine or operational basis with InSAR. Research results to-date have demonstrated the InSAR is a valuable tool in observing surface deformation over relatively large geographic areas, surface conditions permitting. Lidar measurements are also providing detailed maps of fault rupture topography. While the capabilities of systems overlap, it is important to realize that the specific problem at hand dictates which technologies to integrate towards a solution that addresses performance, costs and data delivery requirements.

Recommendation 9: The application of remote sensing technology to real-time damage assessment will require a comprehensive research program.

Several issues must be addressed; the most important of which is how to model remote sensing data to quantitatively separate the effects of surface displacement from building or infrastructure damage. An approach may be to rely on remote sensing as the primary data source, but to add independent data such as GPS observations and ground motions from real-time earthquake monitoring networks in order to separate decorrelation due to damage to the built environment from that due to ground displacements**.** While this is theoretically sound, the reduction to practice is subject to data availability and sampling limitations, in addition to further research and development. Furthermore, the adoption rate of remote sensing will continue to depend on educating potential users on GIS.

Recommendation 10: Remote sensing should be encouraged to be an increasingly utilized contributor to catastrophic risk modeling and emergency management.

Decisions made in the minutes and hours following a major event are based on limited field reconnaissance. The improving capabilities of catastrophe modeling to provide estimates of potential losses, quantify these losses by geographic regions, and provide scenarios for managing risk from natural disasters have placed modeling into a critical role in the issuance of catastrophe bonds and the development of other risk transfer mechanisms. As the insurance and capital markets continue to merge, catastrophe modeling will play an increasingly important role in these new alternatives to traditional reinsurance. Remote sensing can provide decision-makers not only information for model inputs, but also an actual image reference for comparison of disaster scenarios with digital orthophotos, high-resolution topography, land use and land cover classification maps of projected affected areas.

8. Notes

[1] NPA Data Services, Inc., established in 1985, is an economic research, forecasting and data development firm located in Washington, DC. The company specializes in developing and maintaining geographic databases for counties, metropolitan statistical areas, states, economic areas, regions and the U.S. The databases contain historical data and detailed projected of economic, demographic, construction and real estate variables.

[2] Luscome, B. W., and H. M. Hassan, (1993), Applying remote sensing technologies to natural disaster risk management: Implications for developmental investments (The World Bank), *Acta Astronomica*, **29**, 871-876.

[3] "Research needs emerging from recent earthquakes," recommendations from a workshop organized by the Earthquake Engineering Research Institute for the National Science Foundation, Oct. 25-26, 1999.

[4] Eguchi, R., B. Houshmand, M. Shinozuka and D. M. Tralli, MCEER Project Title: Estimation, Development of Damage Functions using Remote Sensing and Real-time Decision Support Systems, SUNY at Buffalo.

[5] Gamba, P. and F. Casciati, (1998), GIS and image understanding for near-real-time earthquake damage assessment, *Photo. Eng. and Rem. Sens.,* 64, 987-994.

[6] Accepted methods for generating the C/A-code and P-code are set forth in the document GPS Interface Control Document ICD-GPS-200, published by Rockwell International Corporation, Satellite Systems Division, Revision B-PR, 3 July 1991.

[7] A discussion of the GPS and techniques for obtaining position information from the satellite signals is found in Tom Logsdon, "The NAVSTAR Global Positioning System," Van Nostrand Reinhold, New York, 1992, pp. 1-90.

[8] Effective May 1, 2000, the Executive Office made the decision to discontinue Selective Availability as part of an ongoing effort to make GPS more responsive to civil and commercial users worldwide. The increased performance in civilian GPS is also expected to accelerate its acceptance and use by businesses, governments, and private individuals in the U.S. and around the world, as noted in http://www.igeb.gov.

Selective Availability (SA) is the deliberate introduction of error to the precise timekeeping of the GPS satellites, thereby reducing both positioning and timing accuracy for civilian users. It was designed to provide U.S. and Allied military forces with a navigational advantage in times of crisis or conflict. With SA activated, civilians are only guaranteed to be within a 100-meter radius of where their GPS receivers say they are. The removal of SA will give civilian users a predicted error of approximately 20 meters. Depending upon the circumstances, some real-world users will experience far better accuracy.

There are more than 4 million GPS users worldwide, and the market for GPS applications is expected to double in the next three years, from $8 billion to over $16 billion. Some of these applications include: air, road, rail, and marine navigation, precision agriculture and mining, oil exploration, environmental research and management, telecommunications, electronic data transfer, construction, recreation and emergency response. Relief agencies such as the Federal Emergency Management Agency

(FEMA) will be able to use basic, standalone GPS receivers to map out geographical features such as flood plain boundaries, levees, and drainage ditches - a task that previously required expensive and labor intensive GPS augmentation techniques.

Even with SA turned off, GPS alone will not meet all users needs. For users with higher accuracy, availability, and integrity requirements - such as commercial airlines, ships navigating within harbors, railroads performing precise train control, precision farmers and miners, and surveyors - GPS will still need to be augmented locally with high-fidelity error correction systems based on differential GPS (DGPS) technology. The U.S. is also adding two new civilian signals to future GPS satellites to further improve accuracy and reliability on a global basis. But for the many other users listed above, the elimination of SA will enable the most inexpensive, standalone GPS receivers to meet their needs.

[9] Blewitt, G., M. B. Heflin, K. J. Hurst, D. C. Jefferson, F. H. Webb, and J. F. Zumberge, (1993), Absolute far-field displacements from the 28 June 1992 Landers earthquake sequence, *Nature*, **361**, 337-340.

[10] Bock, Y., et al., (1993), Detection of crustal deformation from the Landers earthquake sequence using continuous geodetic measurements, *Nature*, **361**, 337-340.

[11] King, N. E., J. L. Svarc, E. B. Fogelman, W. K. Gross, K. W. Clark, G. D. Hamilton, C. H. Stiffler and J. M. Sutton, (1995), Continuous GPS observations across the Hayward fault, California, 1991-1994*, J. Geophys. Res*., **100**, 20,271-20,283.

[12] Shimada, S., and Y. Bock, (1992), Crustal deformation measurements of central Japan determined by a Global Positioning System fixed point network, *J. Geophys. Res*., **97**, 12,437-12,455.

[13] Miyazaki, S., H. Tsuji, Y. Hatanaka, Y. Abe, A. Yoshimura, K. Kamada, K. Kobayashi, H. Morishita, and Y. Iimura, (1996), Establishment of the nationwide GPS array (GRAPES) and its initial results on the crustal deformation of Japan, *Bull. Geog. Surv. Inst. Jpn*, **42**, 27-41.

[14] Fundamental Seismic Survey and Observation Plan, Headquarters for Earthquake Research Promotion, Prime Minister's Office, Government of Japan, August 29, 1997.

[15] Segall, P., and M. Matthews, (1997), Time dependent inversion of geodetic data, *J. Geophys. Res*., **102**, B10, 22,391-22,409.

[16] Savage, J. and R. W. Simpson, (1997), Surface strain accumulation and the seismic moment tensor*, Bull. Seism. Soc. Am*., **87**, 1345-1353.

[17] Kagan, Y. Y., (197), Are earthquakes predictable? *Geophys. J. Int.*, **131**, 505-525.

[18] Kanamori, H., E. Hauksson and T. Heaton, (1997), Real-time seismology and earthquake hazard mitigation, *Nature*, **390**, 461-464.

[19] "Research needs emerging from recent earthquakes," Recommendations from a workshop organized by the Earthquake Engineering Research Institute for the National Science Foundation, October 25 and 26, 1999.

[20] Hartzell, S., E. Cranswick, A. Frankel, D. Carver and M. Meremonte, (1997), Variability of site response in the Los Angeles urban area, *Bull. Seism. Soc. Am*., **87**, 1377-1400.

[21] Behr, J. A., K. W. Hudnut and N. E. King, Monitoring Structural Deformation at Pacoima Dam, California Using Continuous GPS, April, 1999.

[22] Teague, E. H., J. P . How, L. G. Lawson and B. W. Parkinson, GPS as a structural deformation sensor, In *Proceedings of the AIAA Guidance, Navigation and Control Conference*, Baltimore, MD, August 1995.

[23] Teague, E. H., J. P. How, L. G. Lawson, M. Boerjes, and B. W. Parkinson, Techniques for real-time control of flexible structures using GPS, *AAS 96-047*, Stanford University.

[24] Wald, D. J. and T. H. Heaton (1994). Spatial and temporal distribution of slip for the 1992 Landers, California, earthquake, *Bull. Seism. Soc. Am*., 84, 668-691.

[25] M. L. Zoback, R. C. Jachens and J. A. Olson (1999), Abrupt along-strike change in tectonic style; San Andreas fault zone, San Francisco Peninsula. *J. Geophys. Res.,* B, Solid Earth and Planets. **104**, 5, 10,719-10,742.

[26] Dousset, B., Surface temperature statistics over Los Angeles: the influence of land use, *Proceed. IGARSS91*, IEEE, 367-371, Helsinki, 1991.

[27] V. Singhroy, K.E. Matar and A.L. Gray, (1998), Landslide characterization in Canada using Interferometric SAR and combined SAR and TM images, *Advanced Space Research*, **21**, 3, 465-476.

[28] Franco Mantovani, R. Soeters, C.J. Van Weston, (1996), Remote Sensing Techniques for Landslide Studies and Hazard Zonation in Europe, *Geomorphology,* 15, 213-225.

[29] A.A. Grogor'ev and K.Ya.Kondrat'ev, (1997), Satellite Monitoring of Natural and Anthropogenic Disasters, *Earth Obs. Rem. Sens.,* **14**.

[30] V. Jayaraman et al, Managing the Natural Disasters from Space Technology Inputs*, Acta Astronautica*, 40**,** No. 2-8.

[31] J. McKean, S. Buechel, L. Gaydos, Remote Sensing and Landslide Hazard Assessment, *Photogrammetric Engineering & Remote Sensing*, 57, No. 9.

[32] A.A. Grogor'ev and K.Ya.Kondrat'ev, (1997), Satellite Monitoring of Natural and Anthropogenic Disasters, *Earth Obs. Rem. Sens.,* **14**.

[33] Emilio Chuvieco and Russell Congalton, (1989), Application of Remote Sensing and Geographic Information Systems to forest Fire Hazard Mapping, *Remote Sensing Environment*, **29**, 147-159.

[34] J.R. Givri, Satellite Remote Sensing Data on Industrial Hazards, *Advanced Space Research*, **15**, No. 11.

[35] Emilio Chuvieco and Russell Congalton, (1989), Application of Remote Sensing and Geographic Information Systems to forest Fire Hazard Mapping, *Remote Sensing Environment*, **29**, 147-159.

[36] Dousset, B., P. Flament (1993), Los Angeles Fires Seen from Space, *EOS Trans. Am. Geophys. U*., **74,** 33.

[37] Elachi, C., (1988), Spaceborne radar remote sensing: applications and techniques, Institute of Electrical and Electronics Engineers, Inc., New York, 252 pp.

[38] Adams, G. F., D. A. Ausherman, S. L. Crippen, G.T. Sos, B. P. Williams and R. Heidelbach, The ERIM Interferometric SAR: IFSARE, *IEEE AES Systems Magazine*, December 1996.

[39] Gray, A. L. and P. J. Farris-Manning, (1993), Repeat-pass interferometry with airborne synthetic aperture radar, *IEEE, Trans. Geosc. and Remote Sensing*, **31**, 180-191.

[40] Rodriguez, E., T. R. Michel, J. M. Martin and B. Houshmand, (1996), Automated map generation using C-band IFSAR data, *IEEE Trans. Geosci. Remote Sensing*. Comparison of classification results in a number of areas in California and Oregon with collected ground truth showed an accuracy of more than 80% for four land cover classes, namely tree-covered areas, open fields, urban areas and bodies of water.

[41] According to studies sponsored by the European Commission - DG XIII- Application of Remote Sensing to Urban Areas, cited in: Casciati, F., P. Gamba, F. Giorgi and Alessandro Mecocci, (1997), "Planning a RADATT extension," GIS and Applications of Remote Sensing to Damage Management Conference, Greenbelt, MD, Jan. 13-15.

[42] Gauchat, U. P. and D. L. Schodek, 1984. "Patterns of housing type and density: a basis for analyzing earthquake resistance," Department of Architecture, Harvard University.

[43] Jones, B., D. M. Mason, C. M. Hotchkiss, M. J. Savonis and K. A. Johnson, 1986. "Estimating building stocks and their characteristics," EPA Material Distribution Workshop, Sept. 8-11, Hanover, New Hampshire.

[44] Cionco, R. M., and R. Ellefsen, (1998), High resolution urban morphology data for urban wind flow modeling, *Atmos. Environ*., **32**, 7-17. A morphological database of vegetative canopies and urban structures was generated, with 17 urban terrain zones identified that encompassed attached, commercial high-rise buildings, to detached close-set and open-set buildings with a commercial, residential and industrial classification. The database was constructed on an hectare (100 m by 100 m) grid, providing building densities as percentages, building orientations, reflectivity and canopy properties, and heights to 3-meter stories.

[45] Weydahl, D. J., X. Becquey and T. Tollefsen, (1995), Combining ERS-1 SAR With Optical Satellite Data Over Urban Areas, *IGARSS '95* , Firenze, Italy, 10-14 July 1995, IEEE, pp. 2161-2163. Combination of multispectral and SAR data resulted in the abilities to identify the nature of the land use; identify particular features; and infer certain roofing material types.

[46] Cheng, F. and K. H. Thiel, (1995), Delimiting the Building Heights in a City From the Shadow in a Panchromatic Spot-Image Test of 42 Buildings*, International Journal of Remote Sensing*, **16**, 3, 409-415.

[47] Madsen, S. N., H. A. Zebker, and J. Martin, (1993), Topographic Mapping Using Radar Interferometry: Processing Techniques, *IEEE Trans. Geosci. Remote Sensing*, **31**, 1.

[48] Houshmand, B., (1995), A Geometrical Optics Model For the Interferometric SAR Height Measurements For Urban Areas, in *URSI Proceedings*, July 21.

[49] Taket, N. D., S. M. Howarth and R. E. Burge, (1991), A model for the imaging of urban areas by synthetic aperture radar, *IEEE, Trans. Geosc. Remote Sensing*, 29, 432-433.

[50] Change detection using differential InSAR and L-band short baseline repeat-pass interferometry, for applications such as construction planning, ground deformation and post-disaster monitoring, are not included.

[51] For DEM generation, only single polarization is needed. There is no *conclusive* evidence about which polarization is better for urban sites. A fully polarized system is very expensive operationally.

[52] Weydahl, D. J., X. Becquey and T. Tollefsen, (1995), Combining ERS-1 SAR With Optical Satellite Data Over Urban Areas, *IGARSS '95* , Firenze, Italy, 10-14 July 1995, *IEEE*, 2161-2163.

[53] Burkhart, G. R., Z. Bergen, R. Carande, S. Hensley, D. Bickel and J. R. Fellerhoff, (1996), Elevation Correction and Building Extraction from Interferometric SAR Imagery, *IGARSS'96*, Lincoln, Nebraska, 27-31 May, 1996, 659-661.

[54] Cheng, F. and K. H. Thiel, (1995), Delimiting the Building Heights in a City From the Shadow in a Panchromatic Spot-Image Test of 42 Buildings*, International Journal of Remote Sensing*, **16**, 3, 409-415.

[55] Rodriguez, E., T. R. Michel, J. M. Martin and B. Houshmand, Automated Map Generation Using C-band IFSAR Data, *IEEE Trans. Geosci. Remote Sensing*.

[56] Yonezawa, Chinatsu, Takeuchi and Shoji, (1998), Detection of damaged built-up areas by the 1995 Hyogoken-nanbu earthquake using ERS-1/SAR intensity images, *J. of the Japan Soc. of Photogrammetry and Remote Sensing*, **37**, 4, 57-61.

[57] Zebker, H. A., P. A. Rosen and S. Hensley, (1997), Atmospheric effects in interferometric synthetic aperture radar surface deformation and topographic maps, *J. Geophys. Res*., **102**, 7547-7563.

[58] Tarayre, J., and D. Massonnet, (1996), Atmospheric propagation heterogeneities revealed by ERS-1 interferometry, *Geophys. Res. Lett*., **23**, 989-992.

[59] Price, E. J., and D. T. Sandwell, (1998), Small-scale deformations associated with the 1992 Landers, California, earthquake mapped by synthetic aperture radar interferomtery phase gradients, *J. Geophys. Res.,* **103**, 27,001-27,016.

[60] Massonnet, D., and K. L. Feigl, (1995), Discrimination of geophysical phenomena in satellite radar interferograms *Geophys. Res. Lett*., **22**, 1537-1540.

[61] Rosen, P. A., S. Hensley, H. A. Zebker, F. H. Webb, and E. Fielding, (1996), Surface deformation and coherence measurements of Kilauea Volcano, Hawaii from SIR-C radar interferometry, *J. Geophys. Res.,* **101**, 23,109-12,125.

[62] Zebker, H. A., P. A. Rosen, and S. Hensley, (1997), Atmospheric effects in interferometric synthetic aperture radar surface deformation and topographic maps, *J. Geophys. Res.*, **102**, 7547-7563.

[63] The term DEM refers to the estimated elevation of the scattering surface. The underlying bald-earth elevation model is the DTM (Digital Terrain Model).

[64] Burgmann, R., E. Fielding and J. Sukhatme, (1998), Slip along the Hayward Fault, California, estimated from space-based synthetic aperture radar interferometry, *Geology*, **26**, 559-562.

[65] It is assumed that atmospheric effects, effects due to subsurface water level changes, and tectonic nature are not significant or properly modeled and corrected.

[66] Massonnet, D., M. Rossi, C. Carmona, F. Adragna, G. Peltzer, K. Feigl and T. Rabaute, (1993), The displacement field of the Landers earthquake mapped by radar interferometry, *Nature*, **364**, 138-142.

[67] Ohkura, H., T. Jitsufuchi, T. Matsumoto and Y. Fujinawa, (1997), Application of SAR data to monitoring of earthquake disaster, *Adv. Space Res*., 19, 1429-1436.

[68] Bock, Y., and S. Williams, (1997), Integrated satellite interferometry in southern California*, EOS Trans., AGU*, **78**, 29, p. 293.

[69] Dong, D., et a., Obtaining deformation field from a combination of GPS and terrestrial survey data, Pres. 1997 *Seismological Soc. of Japan*, Fall meeting, 24-26 September, Hirosaki, Japan.

[70] Ge, L. et al., The integration of INSAR and CGPS: a solution to efficient deformation monitoring, Pres*. Int. Symp. on Current Crustal Movement and Hazard Reduction in East Asia and Southeast Asia*, Wuhan, P. R. Chine, 4-7 November, 1997.

[71] Peltzer, G., K. W. Hudnut, and K. L. Feigl, (1994), Analysis of coseismic surface displacement gradients using radar interferometry: New insights into the Landers earthquake, *J. Geophys. Res.,* **99**, 21,971-21,981.

[72] Massonnet, D., M. Rossi, C. Carmona, F. Adragna, G. Peltzer, K. Feigl, and T. Rabaute, (1993), The displacement field of the Landers earthquake mapped by radar interferometry, *Nature*, **364**, 138-142.

[73] Zebker, H. A., P. A. Rosen, R. M. Goldstein, A. Gabriel and C. L. Werner, (1994), On the derivation of coseismic displacement fields using differntial radar interferometry: The Landers earthquake, *J. Geophys. Res.,* **99**, 19,617-19,643.

[74] Feigl., K. L. and E. Dupre, (1999), RNGCHN: a program to calculate displacement components from dislocation in an elastic half-space with applications for modeling geodetic measurements of crustal deformation*, Computers and Geosci*., **25**, 695-704.

[75] Okada, Y., (1985), Surface deformation to shear and tensile faults in a half-space*. Bull. Seism. Soc. Am*., **75**, 4, 1135-1154.

[76] See Applied Technology Council (ATC), (1985), Earthquake damage evaluation data for California (ATC-13). Redwood City, California.

[77] Chen, Q., Y. Chen, J. Liu and L. Chen, (1997), Quick and approximate estimation of earthquake loss based on macroscopic index of exposure and population distribution*, Natural Hazards*, **15**, 217-229.

[78] Massonnet, D., et al., (1993), Image of an earthquake, *Nature*, **364**, 8, July.

[79] Ozawa, D., M. Murakami, S. Fujiwara and M. Tobita, (1997), Synthetic apertura radar interferogram of the 1995 Kobe earthquake and its geodetic inversion, *Geophys. Res. Lett.,* **24**, 18, 2327-2330.

[80] Yonezawa, C. and Takeuchi, S. (1998). Detection of Damaged Built-up Areas by the 1995 Hyogoken Nanbu Earthquake using ERS-1/SAR Intensity Images, Photogrammetric Engineering and Remote Sensing, **37**, 4, 57-61 (in Japanese).

[81] Matsuoka, M. and F. Yamazaki, (1998), Identification of damaged areas due to the 1995 Hyogoken-Nanbu earthquake using satellite optical images, *19th Asian Conf. on Remote Sensing*, Q9, 1-6.

[82] Mitomi, Y. and S. Takeuchi, (1995). Analysis of Spectral Feature of the Damaged Areas by Liquefaction and Fire Using Airborne MSS Data, Proc. of the 18th Japanese Conf. on Remote Sensing, 117-118 (in Japanese).

[83] Inanaga, A., S. Tanaka, S. Takeuchi, K. Takasaki and Y. Suga, (1995). Remote Sensing Data for Investigation of Earthquake Disaster, Proc. of the 21st Annual Conf. of the Remote Sensing Society, 1089-1096.

[84] Yoshie, T. and H. Tsu. (1995). Satellite Data Processing to Delineate the Densely Built-up Areas Damaged Disastrously by 1995 Hyogoken-Nanbu Earthquake, Proc. of the 18th Japanese Conf. on Remote Sensing, 119-122 (in Japanese).

[85] Building Research Institute (1996). Final Report of Damage Survey of the 1995 Hyogoken-Nanbu Earthquake (in Japanese).

[86] The DN in the liquefied area was high in the range from the visible to mid-infrared bands, because of the higher reflectance of sand than the surface of asphalt. Also, it is conceivable that the DN was raised in infrared bands in the heavy damage area due to the exposure of soil under mud walls and roofing tiles upon the collapse of old wooden dwellings.

[87] Mitomi, Y. and S. Takeuchi, (1995). Analysis of Spectral Feature of the Damaged Areas by Liquefaction and Fire Using Airborne MSS Data, *Proc. of the 18th Japanese Conf. on Remote Sensing*, 117-118 (in Japanese).

[88] Hosokawa, M. and S. Zama, (1998). Comparison of Landcover Mapping Method Using Satellite Data for Extracting Area Damaged by 1995 Hyogoken Nanbu Earthquake, Technical Report of National Research Institute of Fire and Disaster, **85**, 10-21 (in Japanese).

[89] Aoki, H., M. Matsuoka and F. Yamazaki, (1998), Characteristics of satellite SAR images in the damaged areas due to the Hyogoken-Nanbu earthquake*, 19th Asian Conference on Remote Sensing*, Q9.

[90] The image that was obtained in the nearest day after the earthquake is that of four months after. Because of this time difference, a direct comparison between the SAR images and the field survey data is not very accurate.

[91] Porter, B., and S. Ming Lee, (1999), Catastrophe modeling from risk assessment to risk management and transfer, *Catastrophe Modeling*, July/August, 264-269.

[92] Financial Catastrophe Risk: Capital Market Solutions, January 1999. Insurance Services Office, Inc., 7 World Trade Center, New York, NY 10048-1122, (212) 898-6000.

[93] The transaction marks the first foray into the capital markets by Lehman Re, which was established in Bermuda in 1998 and currently has a capital base of over $500 million. Lehman Re will receive payments from Seismic Ltd. if losses exceed $22.5 billion and will receive the full $150 million if losses equal or exceed $31.5 billion. Industry losses from individual events will be determined by Property Claims Services (PCS), a unit of Insurance Services Office.

[94] Kuroda, T., T. Orii, and S. Koizumi, (1997), Concept of Global Disaster Observation Satellite System (GDOS) and Measures to be Taken for its Realization, *Acta Astron*., **41**, 537-549.